The Dissertation Committee for Jittima Weerachayaphorn certifies that this is the approved version of the following dissertation:

MOLECULAR TRANSPORT PROPERTIES OF SODIUM/DICARBOXYLATE COTRANSPORTERS

Committee:

Ana M. Pajor, Ph.D., Supervisor

Robert A. Davey, Ph.D.

David W. Good, Ph.D.

Simon A. Lewis, Ph.D.

John B. Pritchard, Ph.D.

Dean, Graduate School

MOLECULAR TRANSPORT PROPERTIES OF SODIUM/DICARBOXYLATE COTRANSPORTERS

By

Jittima Weerachayaphorn, M.Sc.

Dissertation

Presented to the Faculty of the Graduate School of Biomedical Sciences

The University of Texas Medical Branch

in Partial Fulfillment

of the Requirements

for the Degree of

Doctor of Philosophy

The University of Texas Medical Branch

August 2007

To my dearest family

ACKNOWLEDGEMENTS

I would like to express my deepest gratitude and sincere appreciation to my wonderful mentor, Dr. Ana M. Pajor for her guidance, valuable advice, supervision, excellent encouragement, enthusiasm and enormous patience throughout my Ph.D. study. She has never been lacking in kindness and support. She encouraged my interest in molecular biology. She has been training me to be a critical thinker as well as to be professional. She is intelligent and a very talented scientist. With her efforts and tutelage, I have gained invaluable knowledge and skills. Without her virtue, this work could never have been accomplished. I am eternally grateful for my time with her.

My cordial gratitude is also expressed to all the members of my dissertation committee, Dr. Simon A. Lewis, Dr. David W. Good, my committee members from the graduate program of Cellular Physiology and Molecular Biophysics, Dr. Robert A. Davey, my outside program committee member, and Dr. John B. Pritchard, my outside campus committee member from National Institute of Environmental Health Sciences (NIEHS). I thank them for providing critical discussions and invaluable advice on experiment design, data interpretation and my education.

Special thanks are given to Naomi Oshiro, Sheri M. Foltz, Dr. Jason A. Hall, Jamie R. Lewis, Dr. Aileen K. Ritchie, Dr. Nancy K.Wills, Cynthia Cheatham and all staff members of the Department of Physiology, for their willingness to help with anything, kindness, sincerity and also friendship. I am particularly indebted to my Master Professor, Dr. Pawinee Piyachaturawat and Dr. Varanuj Chatsudthipong, who had a huge influence on my chosen profession as well as friends Kathleen M. Randolph and Aditya D. Joshi. Thanks for friendship, millions of interesting conversations and for doing me lots of favors throughout my four years here. My life as a graduate student at UTMB would not have been as pleasurable, memorable or meaningful without them.

Lastly, I wish to express my profound and infinite gratitude and appreciation to my dearest mother, father, sister, and my brothers for their encouragement, kindness, unconditional, everlasting love and understanding throughout my life. They deserve to be mentioned as a part of my success.

MOLECULAR TRANSPORT PROPERTIES OF SODIUM/DICARBOXYLATE COTRANSPORTERS

Publication No._____

Jittima Weerachayaphorn, M.Sc., Ph.D.

The University of Texas Medical Branch, August 2007

Supervisor: Ana M. Pajor

The Na^+/dicarboxylate cotransporter (NaDC1) plays important roles in absorption of citric acid cycle intermediates from the intestinal and renal tubular lumen. NaDC1 influences the homeostasis of citrate, which may be associated with the formation of kidney stones. The studies in this dissertation focused on two aspects of NaDC1: the transport pathway of di-and tricarboxylates in the small intestine and structure-function studies of NaDC1.

The transport pathways of di-and tricarboxylates in the intestine have not been clearly identified; thus, the identification of intestinal di-and tricarboxylate transport pathway was investigated in human Caco-2 cell line. The results show that these cells contain at least three distinct transporters, including the Na^+-dependent di- and tricarboxylate transporters, NaDC1 and NaCT, and a sodium-independent pathway, possibly an organic anion transporter. Most of the succinate transport is mediated by sodium-dependent pathways, predominantly NaDC1. In contrast, citrate transport in Caco-2 cells occurs by a combination of sodium-independent pathways, possibly mediated by an organic anion transporter, and sodium-dependent mechanisms.

The amino-terminal half of the protein in NaDC1, in particular transmembrane helix (TM) 3, appears to be important in determining substrate specificity and affinity; therefore, the investigation of the permeation pathway in NaDC1 was examined. The extracellular half of TM3 in NaDC1 was studied using the substituted-cysteine accessibility method and the transport specificity ratio (TSR). The TSR analysis provides evidence that TM3 contains determinants for substrate specificity and catalytic efficiency. All of the mutants were tested for sensitivity to the membrane-impermeant cysteine-specific reagent (2-sulfonatoethyl) methanethiosulfonate (MTSES), but only K84C was sensitive to MTSES inhibition.

Pre-exposure of K84C to succinate results in protection from MTSES inhibition. The mechanism of substrate protection appears to be steric hindrance, rather than large-scale conformational change. The data suggest that TM3 may be located in the permeation pathway and also point to a new location for Lys-84.

The interaction between TM7, 10 and 11 of NaDC1 contribute to the differences in substrate and cation affinity between rabbit (rb) and human (h) NaDC1. However, the important residues responsible for the differences have not been identified. The identification of residues was focused in the TM 10 region. Four mutants were made in which the rabbit sequence was substituted for that of the human NaDC1. The human-T509S mutant transporter exhibits the cation and substrate affinity and specificity of the R10 chimera, hNaDC1 with a substitution of TM10 and associated loop from rbNaDC1. The rabbit-S512T mutation made in rbNaDC1 at the equivalent position has properties similar to those of human NaDC1. It appears that a serine or threonine at position 509 (in human NaDC1) or 512 (in rabbit NaDC1) determines functional differences between NaDC1 orthologs in both substrate and cation transport.

NaDC1 is implicated in many physiological processes, it is essential to understand its structure and function. These studies have provided new fundamental structural-function relationship information on the transport mechanism of NaDC1. As membrane proteins are one of the key components for drug designing and targeting, this knowledge will provide information in the development of novel therapies with NaDC1 as a target.

TABLE OF CONTENTS

LIST OF TABLES

LIST OF FIGURES

LIST OF ABBREVIATIONS

cDNA	complementary deoxyribonucleic acid
2, 2-DMS	2, 2-Dimethylsuccinate
f	Prefix, flounder
h	Prefix, human
HEPES	N-2-Hydroxyethylpiperazine-n-2'-ethanesulfonic acid
Indy	Na^+-independent dicarboxylate transporter from *Drosophila*
IgG	Immunoglobin G
kDa	kilodalton
kb	kilobase
m	Prefix, mouse
MTSEA	2-aminoethylmethane thiosulfonate
MTSES	2-sulfonatoethylmethane thiosulfonate
MTSET	2-trimethylammonieothylmethane thiosulfonate
NaDC1	Low-affinity Na^+/dicarboxylate cotransporter
NaDC3	High-affinity Na^+/dicarboxylate cotransporter
NaCT	Na^+-coupled citrate transporter
NaS	Na^+/sulfate cotransporter
o	Prefix, opossum
OAT	Organic anion transporter
PBS	Phosphate-buffered-saline
PCR	Polymerase chain reaction

LIST OF ABBREVIATIONS (CONT.)

PMSF	Phenylmethanesulfonyl fluoride
r	Prefix, rat
rb	Prefix, rabbit
RT-PCR	Reverse transcription-polymerase chain reaction
SLC	Solute carrier gene family
SDS-PAGE	Sodium dodecyl sulfate polyacrylamide gel electrophoresis
Sulfo-NHS-LC-Biotin	Sulfosuccinimidyl-6-(biotinamido) hexanoate
TM	Transmembrane helix
TSR	Transport specificity ratio
x	Prefix, *xenopus laevis*

CHAPTER 1: INTRODUCTION

This dissertation describes the studies aimed at understanding structural and functional aspects of the Na^+/dicarboxylate cotransporter, NaDC1, at the molecular level. In the first study (Chapter 2), the transport pathways of di-and tricarboxylates were identified in the human colonic carcinoma cell line, Caco-2. In the second (Chapter 3) and third (Chapter 4) studies, the relationship between structure and function of NaDC1 were investigated in transfected cell lines with NaDC1 and NaDC1 mutants. The following introduction will begin with general information about membrane transport proteins and subsequently focus on the Na^+/dicarboxylate cotransporter and the SLC13 family.

MEMBRANE TRANSPORT PROTEIN

Membrane transport proteins are important pathways for transporting various substances into and out of the cells. Membrane transporters are integral protein molecules embedded in the lipid bilayer (Van Winkle *et al.*, 1999). Integral proteins have one or more membrane-spanning segments and most segments are believed to be α-helices oriented more or less perpendicularly to the plane of the membrane (Van Winkle *et al.*, 1999). In some cases, some of the helices may be tilted and may even be paralleled to the membrane (Persson & Argos, 1996). In 1999 and updated in 2002, a novel classification system of the transport proteins, called the Transporter Classification system, was proposed (Saier, Jr., 1999; Saier, Jr., 2000; Busch & Saier, Jr., 2002). According to the transporter classification system, the membrane transport

proteins are classified into two major types, channel and carrier proteins (Figure 1.1). Channel proteins form tiny hydrophilic pores, and their binding sites for the solutes to be transported are accessible from both sides of the membrane at the same time (Oh & Amidon, 1999). Channels selectively allow ions to move down their electrochemical gradients (Hille, 1986; Decoursey, 2003). Basically, ion channels have two conformations: open and closed. The channel opens and closes via a gating mechanism. The flow of the ions is governed by the probability of the channels being open and the single channel conductance (Hediger *et al.*, 2004). Carrier proteins, also known as transporters, comprise polypeptide chains that crisscross back and forth across the bilayer multiple times forming a continuous protein-lined pathway. Transporters bind a solute at one side of the membrane and deliver it to the other side, and require a conformational change during the process of solute translocation across the membrane (Oh & Amidon, 1999). Carriers typically have a fixed stoichiometry of ion/solute movement per translocation cycle (Hediger *et al.*, 2004).

Based on the nature of the transport proteins, mode of transport and energy coupling mechanism, carrier proteins can be classifed into three subtypes: facilitated diffusion carriers or uniporters, primary active transporters and secondary active transporters (Figure 1.1) (Busch & Saier, Jr., 2002; Petzinger & Geyer, 2006). The movement of molecules or ions through the membrane via uniporter is the movement of molecules downhill following the electrochemical gradient (Petzinger & Geyer, 2006). The primary active transporters use the energy from hydrolysis of adenosine triphosphate (ATP) directly to drive transport of solutes against their electrochemical gradient. Primary active, ATP-dependent transporters include members of the ATP-binding cassette (ABC) transporters and ion pumps (ATPase). The secondary active

transporters transport solutes using an electrochemical gradient generated by the primary active transport process. There are two major subtypes: cotransporters (symporters) and exchangers (antiporters), which transport solutes and couple in the same and opposite directions, respectively.

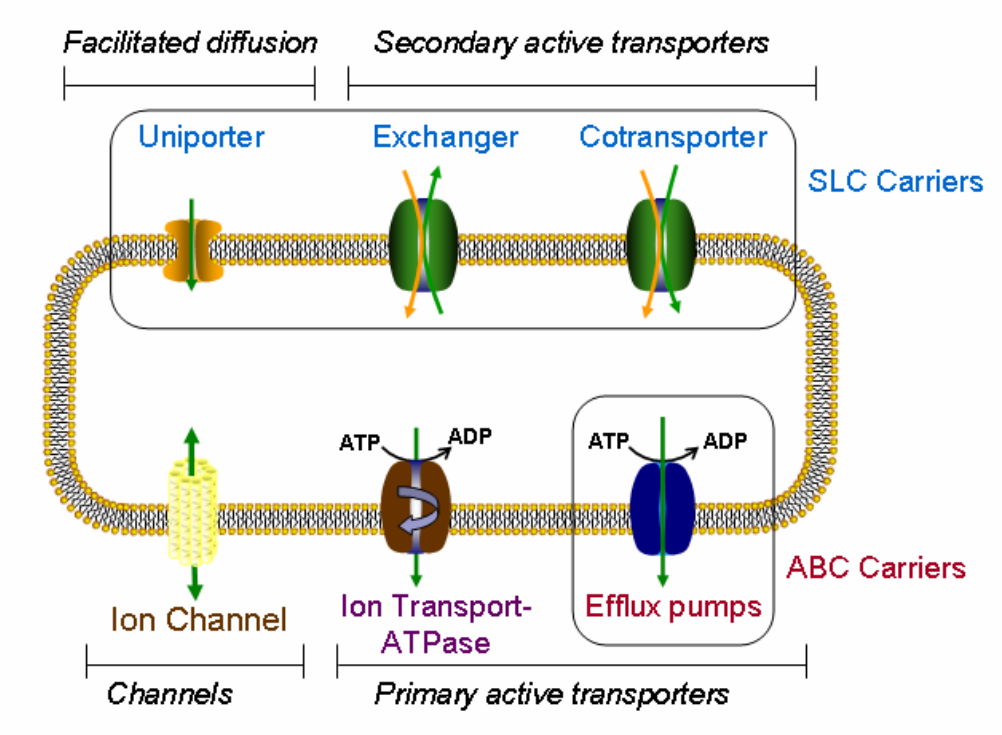

Figure 1.1 General classification of membrane transport proteins. Transport proteins can be classified into two major types: channel proteins and carrier proteins. Carriers or transporters can be further sub-classified into three types: uniporters, primary active transporters and secondary active transporters. SLC: solute carriers, ABC: ATP-binding cassette carriers. (Figure modified from Petzinger and Geyer, 2006)

A majority of the driving forces of secondary active transporters are sodium- and proton-electrochemical gradients (Petzinger & Geyer, 2006). An example of an exchange type of secondary active transporter is the Na^+/Ca^+ exchanger. The

Na^+/Ca^+ exchanger uses the energy stored in the sodium gradient, which is generated from the Na^+/K^+-ATPase, to transport two sodium ions into the cell and one calcium ion out of the cell. An example of the cotransport type of secondary active transporter is the Na^+/dicarboxylate cotransporter (NaDC1). NaDC1 uses the energy stored in the sodium gradient to transport three sodium ions and one dicarboxylate ion into the cell. NaDC1 contains binding sites for sodium and substrate. Once all of the cations and substrate bind, the carrier protein changes its conformation and the sodium ions and substrate are transported together to the inside of the cell.

THE SOLUTE CARRIER 13 GENE FAMILY

This dissertation focuses on Na^+/dicarboxylate cotransporters, called NaDC. The genes encoding human NaDCs are part of the solute carrier family 13 (SLC13 family) (Markovich & Murer, 2004). This gene family comprises five members in humans (Table 1.1). Proteins encoded by these genes are divided into two functionally unrelated groups: the Na^+-sulfate cotransporters and the Na^+/di-and tricarboxylate cotransporters (Markovich & Murer, 2004). Members of the SLC13 family include the low-affinity Na^+/dicarboxylate cotransporter (NaDC1), the high-affinity Na^+/dicarboxylate cotransporter (NaDC3), renal Na^+-dependent inorganic sulfate transporter-1, (NaS1), the sulfate transporter (NaS2) and the Na^+-coupled citrate transporter (NaCT). Their genes are designated as SLC13A2, SLC13A3, SLC13A1, SLC13A4 and SLC13A5, respectively (Table 1.1). All of members in this gene family are approximately 40% - 50% identical in protein sequence (Pajor, 2006). The general characteristics of the SLC13 proteins are Na^+-coupled transporters with 11-13 predicted transmembrane helices. The members of the SLC13 family have a

wide tissue distribution, most are expressed in the epithelial cells of the kidney and the gastrointestinal tract (Markovich & Murer, 2004).

Table 1.1 Characteristics of human members of the SLC13 family (Pajor, 2006)

Human Gene (Protein)	***Substrate***	***Tissue distribution***	***Orthologs***	***Reference***
SLC13A1 (NaS1)	Sulfate K_m 400 μM	Kidney, intestine	Human (h) Rat (r) Mouse (m) *Xenopus laevis* (x)	(Lee *et al.*, 2000) (Markovich *et al.*, 1993) (Beck & Markovich, 2000) (Nakada *et al.*, 2005)
SLC13A2 (NaDC1)	Dicarboxylates: succinate, citrate K_m 800 μM (succinate)	Kidney, intestine	Human Rabbit (rb) Rat Mouse Opossum (o) *Xenopus laevis*	(Pajor, 1996) (Pajor, 1995) (Sekine *et al.*, 1998a) (Pajor & Sun, 2000) (Aruga *et al.*, 2004) (Bai & Pajor, 1997)
SLC13A3 (NaDC3)	Dicarboxylates: succinate, α-ketoglutarate K_m 20 μM (succinate)	Kidney, brain, liver, placenta	Human Rat Mouse *Xenopus laevis* Flounder (f)	(Wang *et al.*, 2000) (Kekuda *et al.*, 1999) (Pajor *et al.*, 2001) (Oshiro & Pajor, 2005) (Steffgen *et al.*, 1999)
SLC13A4 (NaS2)	Sulfate K_m 400 μM	Brain, liver, endothelial venules, testis	Human	(Girard *et al.*, 1999; Markovich *et al.*, 2005)
SLC13A5 (NaCT)	Citrate, dicarboxylates K_m 600 μM (citrate)	Brain, liver, testis	Human Rat Mouse	(Inoue *et al.*, 2002a) (Inoue *et al.*, 2002b) (Inoue *et al.*, 2004)

THE LOW AFFINITY Na^+/DICARBOXYLATE COTRANSPORTER, NaDC1

NaDC1 is the best studied Na^+/dicarboxylate cotransporter. The first NaDC1 was originally cloned in 1995 by Pajor from rabbit kidney using the expression cloning method in *Xenopus* oocytes (Pajor, 1995). NaDC1 cDNA is approximately 2.3 kb in length and codes for a protein of 593 amino acids. NaDC1 orthologs have subsequently been cloned from human, *Xenopus*, rat, mouse and opossum (Pajor, 1996; Bai & Pajor, 1997; Sekine *et al.*, 1998a; Pajor & Sun, 2000; Aruga *et al.*, 2004) displaying from 67 to 78% identity with rbNaDC1. The amino acid sequence of hNaDC1 is 78% identical to rbNaDC1 (Pajor, 1996). The gene for human NaDC1 has been mapped to chromosome 17 (*p*11.1-*q*11.1) (Mann *et al.*, 1999).

Functional characterization of NaDC1

The functional characterictics of NaDC1 have been studied in several heterologous expression systems, mostly in *Xenopus* oocytes by either radiotracer uptake assays or the use of two-electrode voltage clamp (TEVC) (Pajor, 1995; Pajor, 1996; Pajor & Sun, 1996b; Bai & Pajor, 1997; Sekine *et al.*, 1998a; Pajor & Sun, 2000; Yao & Pajor, 2000). The transport of the dicarboxylate, succinate, by NaDC1 expressed in *Xenopus* oocytes exhibits saturable transport of succinate, and is sodium-dependent. In kinetic experiments, the Michaelis-Menten constant (K_m) for succinate varies between 0.3 and 1 mM depending upon the species; NaDC1 is therefore categorized as a low affinity transporter. The half-saturation constant for sodium (K_{Na}) varies between 10 and 80 mM (Pajor, 1996; Bai & Pajor, 1997; Pajor & Sun, 2000; Aruga *et al.*, 2004). There is a difference in the half-saturation constant for

sodium between hNaDC1 and rbNaDC1. The hNaDC1 has a lower apparent affinity for sodium (K_{Na}, 78 mM) than rbNaDC1 (K_{Na}, 41 mM) (Pajor & Sun, 1996b). The Hill coefficient for all of NaDC1 orthologs is between 2 and 3, indicating that a minimum of two highly cooperative sodium binding sites and more than one sodium ions are involved in transport of one divalent (Pajor, 1996; Bai & Pajor, 1997; Pajor *et al.*, 1998a; Pajor & Sun, 2000; Yao & Pajor, 2000; Aruga *et al.*, 2004). The Hill coefficient is consistent with a transport stoichiometry in which three sodium ions are coupled to the transport of single divalent dicarboxylate resulting in a net movement of one positive charge from extracellular to cytoplasmic space (Yao & Pajor, 2000).

Substrate affinity and specificity

The substrate specificity of NaDC1 is broad. NaDC1 recognizes dicarboxylates as its primary substrate and generally transports divalent dicarboxylates, including succinate, malate, fumarate, α-ketoglutarate, glutarate and the divalent form of citrate (Figure 1.2). The transport of succinate by NaDC1 is insensitive to pH, while the transport of citrate is stimulated by acidic pH at 5.5 in which approximately 90% of citrate is in the di-anionic form (Pajor, 1995; Pajor, 1996). The affinity for protonated citrate is very high compared to trivalent citrate (Yao & Pajor, 2000). In hNaDC1 the $K_{0.5}$ of total citrate is 6.8 mM. However when the concentrations of protonated citrate, which is only 7% of the total at pH 7.5, are taken into account, the $K_{0.5}$ of $citrate^{2-}$ is calculated as 88 μM (Yao & Pajor, 2000; Pajor, 2006). Therefore, the preferred substrates of NaDC1 seem to be divalent anions. The rabbit and human NaDC1 have similar affinities for succinate and glutarate with K_m values of about 0.5 - 0.8 mM and 6 - 8 mM, respectively (Pajor &

Sun, 1996b). However, these two transporters differ in their handling of citrate. At pH 7.5, the K_m value for citrate in rbNaDC1 is 0.9 mM and 7 mM in hNaDC1. Although the transport of citrate is sensitive to pH in both transporters, hNaDC1 is more sensitive to pH than rbNaDC1 (Pajor & Sun, 1996b).

Using the two-electrode voltage clamp (TEVC) approach, substrate specificity for rbNaDC1 and hNaDC1 has been studied by measuring currents in the presence of test substrates (Pajor *et al.*, 1998a; Yao & Pajor, 2000). The largest currents in rbNaDC1 are seen with fumarate, succinate, methylsuccinate, citrate and tricarballylate, and the current seen with glutarate is about 50% of succinate-induced currents (Pajor *et al.*, 1998a). In contrast, methylsuccinate, dimethylsuccinate, citrate, and α-ketoglutarate induce less than 50% of succinate-induced currents in hNaDC1, and a small current <20% with glutarate and tricarballylate (Yao & Pajor, 2000). Therefore, the rabbit and human NaDC1 have overlapping substrate specificity but there are some differences in the selectivity profiles between them. Based on their sequences these two NaDC1 orthologs are 78% identical, implying that the differences in selectivity reflect structural differences in their binding sites. These differences could originate from the amino acid composition of the protein (Yao & Pajor, 2000).

Although most functional characteristics of mouse NaDC1 (mNaDC1) are similar to other NaDC1 orthologs, mNaDC1 exhibits functional properties that differ in substrate specificity from rbNaDC1 or hNaDC1. For instance, under the two-electrode voltage clamp, 2,2-dimethylsuccinate (2,2-DMS)-induced currents are about 60% of succinate-induced currents in mNaDC1 compared with only 8% in rbNaDC1 (Pajor *et al.*, 1998a; Pajor & Sun, 2000). In general, mNaDC1 exhibits substrate

selectivity in common with the NaDC3 transporter, including the transport of glutarate and 2,2-DMS (Pajor & Sun, 2000). Thus, there are species differences in preferred substrates among the NaDC1 orthologs.

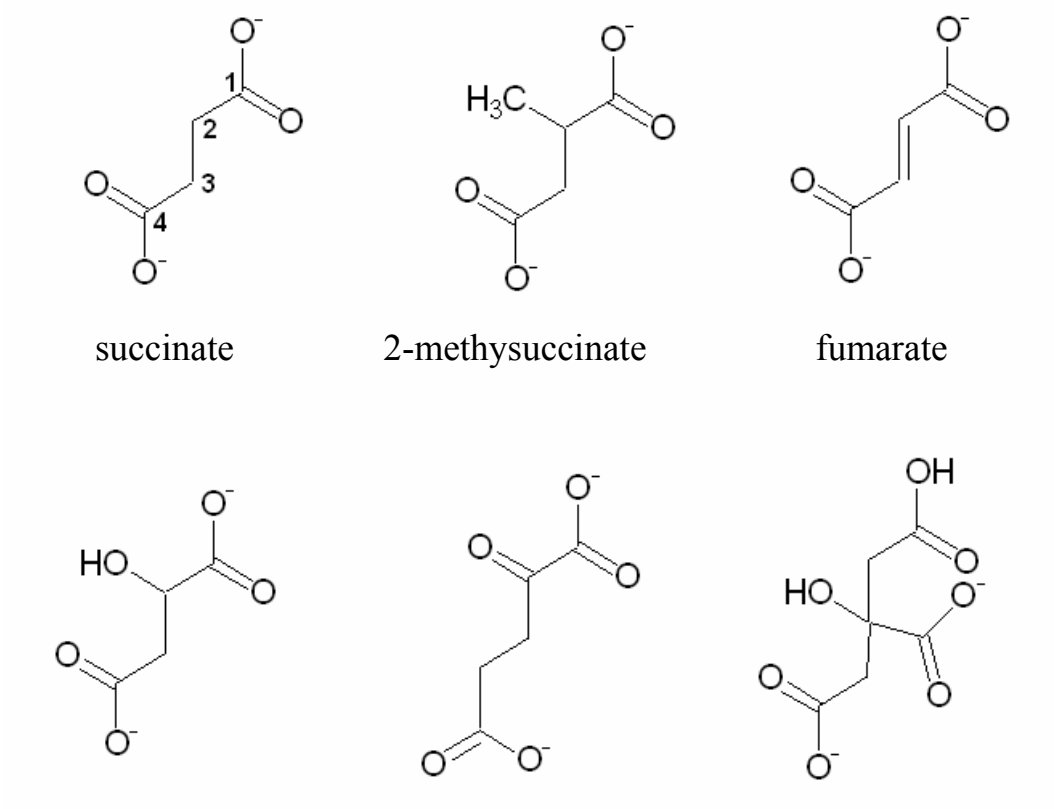

Figure 1.2 Examples of substrates of Na^+/dicarboxylate cotransporters. The numbers of carbons are numbered on the succinate structure consecutively starting from the top. 2,2-dimethylsuccinate (2,2-DMS) (not shown) has two methyl groups located on the C-2 carbon.

Cation and sensitivity to inhibition by lithium

The transport of dicarboxylates by NaDC1 is specific to sodium ions as the replacement of sodium by other cations, except for lithium, abolishes transport (Wright *et al.*, 1982). Sodium acts as an activator of dicarboxylate transport. The K_m for succinate became larger as the concentration of sodium decreased (Wright *et al.*, 1983; Yao & Pajor, 2000). Lithium can substitute for sodium in the transport of succinate partially, but the affinity for succinate in the presence of lithium is approximately ten times as high as in sodium (Pajor *et al.*, 1998a).

The replacement of sodium by lithium, which activates succinate transport, is observed in rabbit, mouse, opossum, and *Xenopus* NaDC1 (Bai & Pajor, 1997; Pajor & Sun, 2000; Aruga *et al.*, 2004). Nevertheless, in the presence of sodium, lithium serves as an inhibitor in NaDC1 mediated transport. In rbNaDC1, at 2.5 mM lithium in the presence of 97.5 mM sodium, succinate transport is inhibited approximately 60% (Pajor & Sun, 1996b; Pajor *et al.*, 1998a). This suggests that lithium can compete with sodium at a minimum of one of the cation binding sites (Pajor & Sun, 1996b; Pajor *et al.*, 1998a). Unlike rbNaDC1, the hNaDC1 is highly specific to sodium as no substrate-induced currents are seen when sodium was replaced by lithium (Yao & Pajor, 2000). Moreover, the hNaDC1 is insensitive to inhibition by lithium and other anion transport inhibitors, such as furosamide and flufenamate compared with rbNaDC1. Thus, the rabbit NaDC1 is much more sensitive to inhibition by lithium and inhibitors than hNaDC1.

Tissue distribution of NaDC1

By Northern blot analysis using the full-length rbNaDC1 cDNA as a probe, positive signals of rbNaDC1 mRNA at the size of 2.8 kb are detected in both kidney and jejunum (Pajor, 1995). The similar expression pattern of NaDC1 transcripts is observed in other species including human, *Xenopus laevis*, and mouse (Pajor, 1996; Bai & Pajor, 1997; Pajor & Sun, 2000). The expression of hNaDC1 is weak in the kidney compared with that in the small intestine (Pajor, 1996). Unlike mammalian NaDC1, *Xenopus* NaDC1 mRNA is only detected in intestine (Bai & Pajor, 1997).

The tissue distribution of rNaDC1 was determined using poly $(A)^+$ RNA obtained from rat in various tissues (Sekine *et al.*, 1998a). Single transcripts of rNaDC1 mRNA at the size of 2.4 kb were detected in the small and large intestine and in the kidney (relative abundance in small intestine > large intestine > kidney). More detailed membrane localization of rNaDC1 in kidney was further identified using polyclonal anti-rNaDC1 antibody to stain rat kidney sections (Sekine *et al.*, 1998a). Immunohistochemistry of rNaDC1 revealed positive staining in the outer stripe of the outer medulla and in cortex. The expression of rNaDC1 was observed and localized to the renal proximal tubule S2 and S3 segments. The rNaDC1 is localized exclusively on the apical membranes of the proximal tubule cells not on the basolateral membranes (Sekine *et al.*, 1998a), suggesting that NaDC1 functions as an entrance pathway for dicarboxylates in renal proximal tubules.

Na^+-coupled transport mechanism of NaDC1

NaDC1 mediates substrate transport with proposed coupling stoichiometry of three sodium ions for each dicarboxylate substrate molecule (Pajor, 1999a; Yao &

Pajor, 2000). Based on the ealier electrophysiological study, oocytes expressing hNaDC1 produce inward currents in the presence of sodium and succinate. A decrease in the sodium concentration leads to a large decrease in succinate-induced currents. The transport process of NaDC1 follows an ordered binding mechanism in which three sodium ions bind prior to a single divalent dicarboxylate as shown in the cartoon model in Figure 1.3 (Yao & Pajor, 2000).

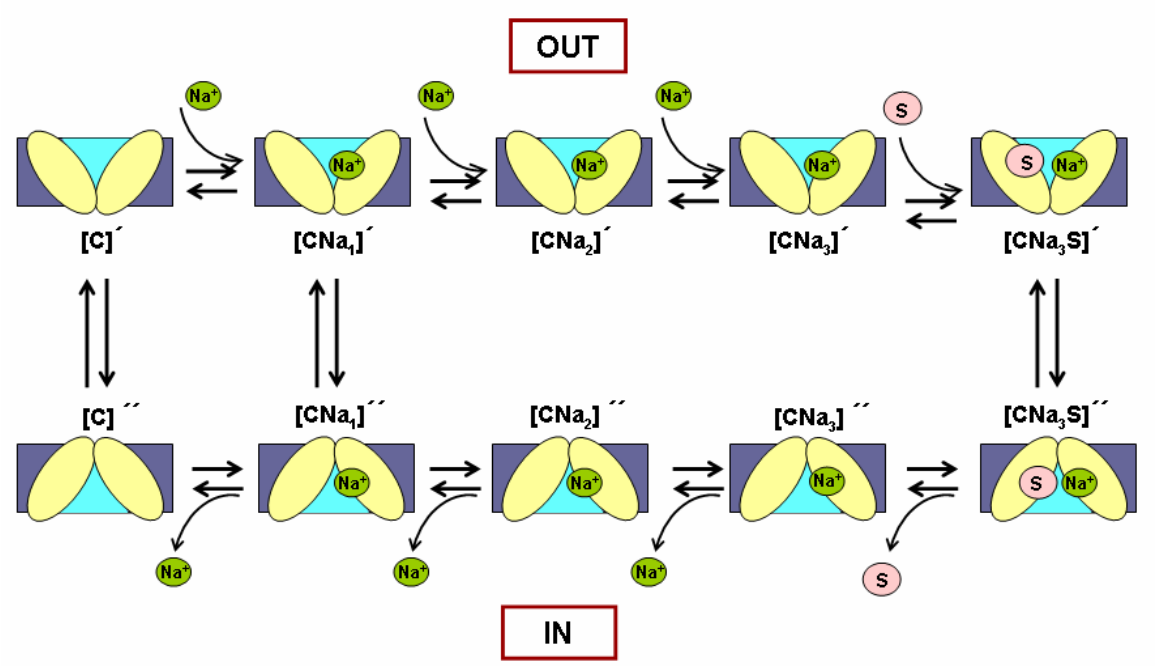

Figure 1.3 Transport model of Na^+/dicarboxylate cotransporter. [C] represents NaDC1, and S represents the dicarboxylate substrate. The ′ refers to the extracellular facing conformation, and ″ refers to intracellular facing conformation. The transport process was proposed based on two types of observed currents: a substrate-dependent current and a sodium-dependent substrate-independent current (sodium leak current). The transport process follows an ordered binding mechanism in which three sodium ions bind to the transporter and trigger a conformational change leading to an increase in the affinity for substrate. One dicarboxylate anion substrate binds to the NaDC1 protein. Once the transporter is fully loaded with sodium and substrate, the substrate and cation binding sites reorient to the inside of the cell. The order of release is not known. After translocation, the transporter reorients the substrate and cation binding sites to the outside. (Figure modified from Yao and Pajor, 2000).

This transport process was proposed based on two types of observed currents: a succinate-dependent current and a sodium-dependent succinate-independent current (sodium leak current). As Pajor and coworkers discussed (Yao & Pajor, 2000), the presence of the sodium leak current indicated that at least one of the sodium ions binds before the substrate, as shown by the Hill coefficient of one for the sodium leak current. In two-electrode voltage clamp experiments with hNaDC1, changes in sodium concentrations affected succinate K_m (Yao & Pajor, 2000). At different sodium concentrations, the I_{max} of succinate was constant. The increase of succinate concentration was able to rise above the effect of decreased sodium concentration. This provided evidence for an ordered binding model in which sodium binds prior to succinate. Therefore, in the model proposed, the first step is the cooperative binding of three sodium ions, which increase the affinity of NaDC1 for the substrate. Then, one divalent anion substrate binds to NaDC1. Once the NaDC1 is fully loaded with sodium and substrate, the transporter undergoes a conformational change that exposes the substrate and sodiums to the inside of the cell. All four molecules are released on the inside of the cell. The order of release is unknown. Then, the empty NaDC1 reorients to face the outside of the cell to initiate another cycle of an ordered binding transport. Thus, one transport cycle moves one net positive charge inside the cell. In addition to the coupled substrate-dependent pathway, there is another pathway for sodium transport, an uncoupled substrate-independent leak pathway (Yao & Pajor, 2000). This leak pathway is an electrophysiological characteristic of NaDC1. Only hNaDC1 and rNaDC1 have been reported to have substrate-uncoupled leak currents (Yao & Pajor, 2000; Chen *et al.*, 1998).

Secondary structure model of NaDC1

The current secondary structure model of rbNaDC1 contains 11 TMs (Figure 1.4) (Pajor & Sun, 1996a). The sequence of NaDC1 contains two consensus sites for N-glycosylation, at Asn-160, in a large polar region, and Asn-578 near the C-terminal tail (Pajor & Sun, 1996a). However, based upon mutagenesis experiments, Asn-578 is the site which is glycosylated in rbNaDC1. Thus, this study places the C-terminus of rbNaDC1 on the outside of the cell. This glycosylation site is a conserved motif within NaDC1 across all species as well as NaS1. In rbNaDC1, N-glycosylation appears to be required for protein sorting or targeting as reflected in decreased protein expression in mutants lacking the N-glycosylation site at position 578 (Pajor & Sun, 1996a). In hNaS1, the mutation of N-glycosylation site at position Asn-591 affected transport function by changing V_{max} without affecting the K_m for sulfate, but protein expression was increased (Li & Pajor, 2003).

A positive immunofluorescent signal with anti-NaDC1 antibodies in COS-7 cells expressing rbNaDC1 and Flag-tagged NaDC1 at the amino acid terminus was observed only after permeabilization of the plasma membrane (Zhang & Pajor, 2001). This data provided evidence that the N-terminus and part of hydrophilic loop 4 Ser-164 to Ser-233 is inside the cell. Although hydropathy analysis predicts the secondary structure models of members of the SLC13 family contain between 11 and 14 TMs (Pajor, 2006), evidence showing that the C-terminus and the N-terminus are on opposite sides of the membrane indicates that there are an odd number of TMs, either 11 or 13 (Joshi & Pajor, 2007).

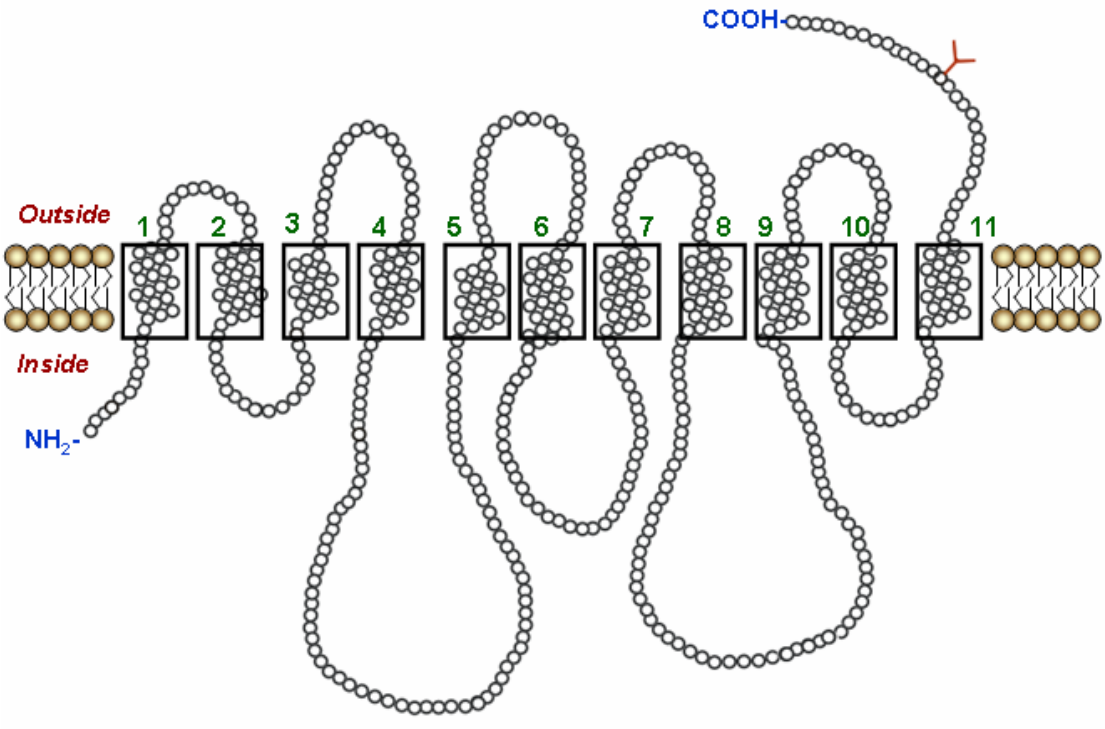

Figure 1.4 Secondary structure model of NaDC1. The current secondary structure of NaDC1 contains 11 transmembrane helices (shown by the numbered rectangles) based on the membrane buried helix parameter (Rao & Argos, 1986). The amino terminus is on the cytoplasmic side of the membrane, and the carboxy terminus is on the outside of the cell. Y designates the N-glycosylation site at Asn-578 (Figure modified from Kahn and Pajor, 1999).

Structure-function studies of NaDC1

Due to the difficulties in the purification and crystallization of membrane transport proteins, the 3D-crystal structures for all members of the SLC13 family are unavailable. The actual membrane topology of NaDC1 remains unknown. Currently, the working secondary structure model of NaDC1 used for the present study contains 11 transmembrane helices (TMs) with an intracellular N-terminus and an extracellular C-terminus (Pajor, 1995; Zhang & Pajor, 2001). So far, the more detailed structure

function studies employ the use of chimeras, site-directed mutagenesis and the substituted-cysteine scanning accessibility method. A summary from earlier studies showing the important residues for substrate recognition and structure was shown in Figure 1.5.

Earlier studies from Pajor's group have shown that the carboxy terminus half of NaDC1 is required for substrate recognition (Pajor *et al.*, 1998b; Kahn & Pajor, 1999). Evidence from a chimera made between rbNaDC1 and rNaS1 showed that substrate recognition domain is found in the carboxy-terminal portion of the protein, past amino acid 141 (Pajor *et al.*, 1998b). The first four transmembrane helices contain residues that affect substrate, cation affinity and anion inhibitors, including furosemide and flufenamate (Pajor *et al.*, 1998b). Furosemide is a loop diuretic acting by inhibiting the Na^+-K^+-$2Cl^-$ symporter in the thick ascending loop of Henle. Flufenamate is a nonsteroidal anti-inflammatory drug and a Cl^- channel inhibitor. The study of chimeras between rbNaDC1 and hNaDC1 revealed that TM 7, 10 and 11 including their connecting loops are involved in determining citrate and cation binding (Kahn & Pajor, 1999). TM 11 is responsible for sensitivity to lithium inhibition in rbNaDC1 (Kahn & Pajor, 1999).

The most recent chimera study between rbNaDC1 and mNaDC1, which share 74% sequence identity, but have differences in handling long-side chain dicarboxylates, glutarate and adipate, indicated that different multiple transmembrane helices (TMs) are involved in NaDC1 substrate recognition (Oshiro *et al.*, 2006). The differences in glutarate transport are determined by residues found throughout the protein, including TM3, 4, 7, 8 and 10. However the greatest contribution is derived from TM3 and 4 and their associated loops. There is a functional interaction in the

transition state between amino acids in TM3 and TM4. The TM8-10 region is important for adipate transport. The main determinants of adipate transport are found in the C-terminus half of protein, particularly TM10, not in TM3-4. Ala-504 is the single amino acid difference between mouse and rabbit NaDC1 in TM10. Mutation from mouse to rabbit sequence at this position (A504S) increases the $K_{0.5}$ for adipate, thus Ala-504 appears to be a determinant of adipate transport (Oshiro & Pajor, 2006).

Site-directed mutagenesis studies in NaDC1 revealed that charge neutralization of two conserved cationic amino acid residues, Lys-84 in TM3 and Arg-349 in TM9, result in a decrease in transport activity and a change in succinate K_m. Thus, Lys-84 and Arg-349, have been identified as key amino acids for succinate binding (Pajor *et al.*, 2000). Moreover, acidic amino acid residues Arg-349 at the top of TM7, Asp-373 and Glu-475 in TM8 and 9, respectively, are important for substrate or cation binding (Griffith & Pajor, 1999).

Cysteine scanning studies in NaDC1 disclosed that certain substituted cysteine mutants at the extracellular ends of TM7, 8, 9 and the connecting extracellular loop between 9 and 10 are sensitive to chemical modification by membrane-permeant and -impermeant methanethiosulfonate (MTS) reagents (Pajor, 2001; Yao & Pajor, 2002; Pajor & Randolph, 2005). (2-amino-ethyl)methanethiosulfonate (MTSEA) is a somewhat membrane-permeant MTS reagent. [2-(trimethylammonium)ethly]-methanethiosulfonate (MTSET) and (2-sulfonatoethyl)methane thiosulfonate (MTSES) are membrane-impermeant MTS reagents that selectively and rapidly bind to cysteine sulfhydryl groups accessible from the outside which provides information on the extracellular accessibility of a cysteine residue. The cysteine scanning studies in NaDC1 showed that the R349C mutant lost activity but the function can be

restored by chemical labeling with MTSEA, which as a group similar in size and charge density to an arginine. Thus, this result suggested that Arg-349 is important to transport function (Yao & Pajor, 2002). The mutant D373C in TM8 is very sensitive to inhibition by MTSET or MTSEA, both of which add a positive charge, but it is not inhibited by MTSES, which adds a negative charge. This study suggested that charge reversal at position 373 by chemical modification with MTSET or MTSEA produces inhibition of transport. In the absence of sodium (choline buffer), the transporter is most likely to be in the unloaded state with binding sites exposed either to the inside or outside of the cell. It was found that the D373C mutant is sensitive to inhibition by MTSET in both sodium and choline, thereby implying that Asp-373 is accessible from the extracellular medium in several conformational states. The pre-exposure of the D373C mutant to substrate prevents chemical modification by MTSET, suggesting that the substrate-induced conformational change occludes the residue.

The substituted cysteine mutants at Ser-478, Ala-480, Ala-481 and Thr-482, located at the top of TM9, are sensitive to MTSET and show substrate protection from MTSET labeling. These four cysteine mutants can be accessible to the outside medium in the presence of sodium, which parallels the exposure of the substrate binding site, so TM9 appears to form part of substrate permeation pathway (Pajor, 2001). Continued study of TM10 and the connecting extracellular loop (residues 483-528), six substituted cysteine mutants at Thr-483, Thr-484, Thr-485, Leu-487, Ile-489 and Met-493 in the extracellular loop are inhibited by MTSET (Pajor & Randolph, 2005). The accessibility to extracellular medium is highest in the presence of sodium. These residues exhibit substrate protection with underlying mechanism of steric hindrance rather than a large scale conformational change. Taken together, the

studies indicated that TM9 and connecting loop to TM10 are involved in the conformation changes during transport cycle and appear to form part of the substrate permeation pathway through the transporter (Pajor, 2001; Pajor & Randolph, 2005).

In addition, some residues were involved in stability or trafficking to the membrane. Mutagenesis of the 11 histidine residues, one at a time, in rbNaDC1 revealed that the mutation at position His-106 in TM3 shows decreased uptake of succinate without changing the K_m, but a decrease in V_{max}. A decrease in succinate transport is correlated with the decreased abundance of cell surface expression, suggesting that His-106 appears to be involved in protein expression rather than transport function (Pajor *et al.*, 1998c).

A mutagenesis study of conserved prolines in TM7 and 10 showed that the prolines in TM7 (P327 and P351) result in completely abolished protein expression and activity when changed to alanine or glycine (Joshi & Pajor, 2006). Pro-327 is a critical residue because the substitution of proline with glycine results in no protein expression, and is unable to be rescued by chemical chaperones, such as glycerol or dimethylsulfoxide (DMSO), or insertion of a proline at a second site. The P351A mutant can be rescued by chemical chaperones and the addition of a protein at position 347 to the inactive P351A mutant results in restoration of transport activity. Hence, Pro-351 appears to be essential for cell surface expression and regulation of protein trafficking to the plasma membrane. Since mutations of prolines in TM10 (P523 and P524) with alanine or glycine produce little change in the transport activity, Pro-523 and -524 do not appear to have functional roles. Replacement of Pro-524 with alanine results in a lower protein expression than the replacement with glycine, thus suggesting that a preference for flexibility or kink in TM10. Therefore,

the prolines in TM10, at position 523 and 524, do not appear to have functional effects, but are likely to be necessary to maintain structure.

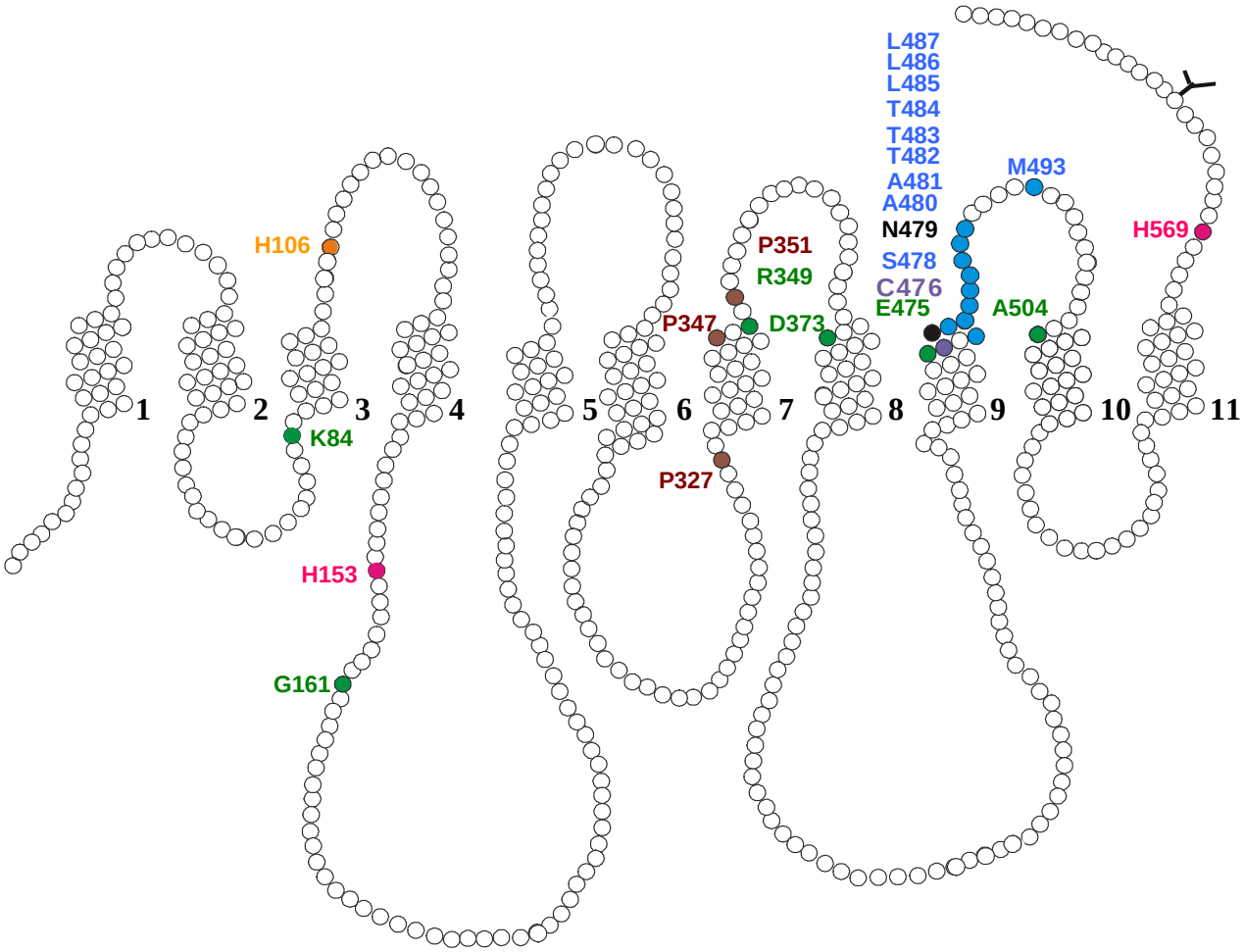

Figure 1.5 Summary of site-directed mutagenesis, chimeric and cysteine scanning mutagenesis results. The secondary structured model of NaDC1 predicts 11 transmembrane helices, numbered. Y designates the N-glycosylation site at Asn-578. Histidine-106 is involved in protein stability or trafficking; histidines at position 153 and 569 react with diethylpyrocarbonate (DEPC) which inhibited succinate transport. Residues in *green*: Lys-84 and Gly-161 in TM3; Asp-373 in TM7, Arg-349 in TM8; Glu-475 in TM9; Ala-504 in TM10 are important to substrate binding. Prolines at position 327, 347, 351 in TM7 are important to transport and protein stability. Asn-479 is irreplaceable residue important both transport activity and protein stability. Residue in *purple*: Cys-476 is inhibited by cysteine-selective reagents *p*-chloromercuribenzenesulphonate (pCMBS). Residues in *blue* are amino acids that are accessible from the outside and may be involved in conformational changes in NaDC1 during transport cycle.

Physiological role of NaDC1 and relevance to human health

The main functional relevance of NaDC1 to human health has been shown in kidney and intestine. In the gastrointestinal tract, the function of NaDC1 is to absorb dicarboxylates from digested diet and from gastrointestinal secretions, such as pancreatic juice (Pajor, 1999b). Physiological function of NaDC1 is to reabsorb citric acid cycle intermediates from the renal proximal tubule. As illustrated in Figure 1.6, NaDC1 mediates the first step in the reabsorption of plasma citric acid cycle intermediates which are filtered through the glomerulus (Pajor, 2006). These substrates include succinate, α-ketoglutarate and citrate, important energy sources for the kidney. Citrate, for example, provides 10-15% of the fuel for renal oxidative metabolism (Nieth & Schollmeyer, 1966). Furthermore, NaDC1 plays an important role in regulating the urinary citrate concentrations, which affect the development of kidney stones.

Low concentrations of citrate in the urine are associated with increased risk of kidney stones formation since citrate chelates calcium ions and prevents the precipitation of calcium salts (Pak, 1991). The calcium will form insoluble complex with other anions, such as oxalate and phosphate, if urinary citrate concentrations are very low. Approximately 50% of nephrolithiasis patients have hypocitraturia (Pak, 1991). Moreover, increased expression of NaDC1 has been correlated with a decrease in urinary citrate excretion (Aruga *et al.*, 2000) and thus associating with occurrence of nephrolithiasis. A recent study was carried out *in vivo*, NaDC1-deficient mice showed that there is significant difference in their ability to reabsorb various citric acid cycle intermediates in the kidney among $NaDC1^{+/+}$, $NaDC1^{+/-}$, to $NaDC1^{-/-}$ mice (Ho *et al.*, 2007). NaDC1-deficient mice have a defect in their ability

to reabsorb citric acid cycle intermediates. These substrates are being excreted at a higher level in NaDC1-deficient mice, resulting in an increase in urinary excretion of these metabolites. Thus, NaDC1 appears to be a major determinant of urinary citrate excretion.

Based on the genetic analysis of Japanese patients with recurrent renal calcium stone formation (RSF) and non-renal stone formation (NSF), Aruga *et al*. found a single nucleotide polymorphism (SNP) in exon 12 of hNaDC1, I550V (Okamoto *et al.*, 2007). The association between urinary citrate excretion and SNPs in a gene for renal sodium dicarboxylate cotransporter (hNaDC1) was investigated. The results suggested that I550V polymorphism of hNaDC1 may contribute to hypocitraturia in renal stone patients and that it may also be associated with a reduction in urinary citrate excretion in volunteers with NSF.

As depicted in Figure 1.6, in kidney, NaDCs cooperatively function with dicarboxylate/organic exchangers, including organic anion transporter 1 (OAT1), OAT3, located on the basolateral membrane (Anzai *et al.*, 2006) and OAT4, expressed on the apical membrane (Ekaratanawong *et al.*, 2004; Hagos *et al.*, 2007). NaDCs are involved in the process of secreting organic anions, including drugs and xenobiotics out of the cells (Wright & Dantzler, 2004). Transported dicarboxylates provide a substrate to the organic anion/dicarboxylate exchangers, which are responsible to take up organic anions from the blood circulation to the cells. The organic anions are eliminated from the cells via OAT4, which mediates bidirectional organic anion transport and is proposed to be involved in renal secretion and reabsorption of endogenous substances as well as many drugs and xenobiotics (Ekaratanawong *et al.*, 2004; Hagos *et al.*, 2007), and MRP members (MRP2,

MRP4), which function as the extrusion pump for OA^- from the apical membrane (see review (Anzai *et al.*, 2006; Sekine *et al.*, 2006)).

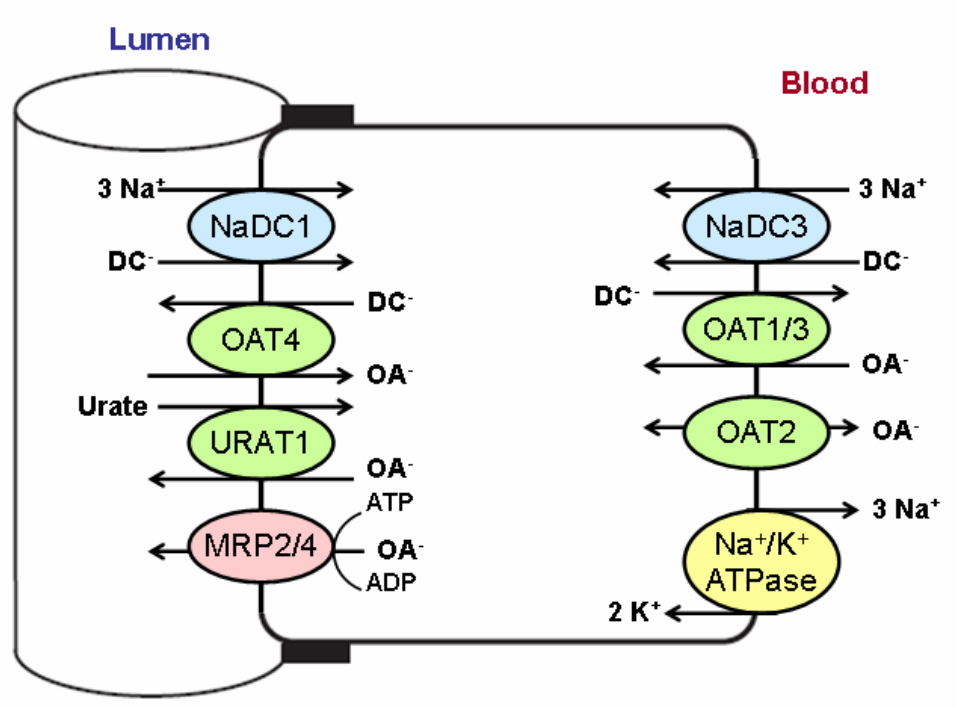

Figure 1.6 Proposed schematic representation of dicarboxylate transport in renal proximal tubules. The low-affinity Na^+/dicarboxylate cotransporter, NaDC1, is expressed on the apical membrane of renal epithelial cells. The high-affinity Na^+/dicarboxylate cotransporter, NaDC3, is expressed on the basolateral membrane of renal epithelial cells. The Na^+/K^+-ATPase located on the basolateral membrane generates electrochemical gradient of sodium, which is a driving force of NaDCs. Using electrochemical gradient of sodium, NaDCs transport one divalent dicarboxylate (DC^{2-}) inside the cell coupled with three sodium ions. The intracellular dicarboxylates are mostly utilized for metabolism, and also involved in uptake of organic anions (OA^-) from the blood circulation or the lumen which is mediated by the dicarboxylate/organic anion exchangers (OAT) on the apical or basolateral membrane. The intracellular OA- are then secreted into urine by an organic anion exchanger URAT1, and MRP members (MRP2, MRP4) in proximal tubular cells, which function as extrusion pump for OA^- from the apical membrane (Figure modified from Anzai *et al*., 2006).

A recent study also showed that succinate and α-ketoglutarate serve as natural ligands for orphan G-protein-coupled receptors in the proximal and distal tubules (He *et al.*, 2004). He *et al*. showed that succinate can increase blood pressure in mice. The effect of succinate-induced hypertension involves the renin-angiotensin system. This study suggested that dicarboxylate concentration surrounding proximal tubular cells seems to be an important factor that regulates renovascular hypertension. Thus, the NaDC transporter may affect such processes as blood pressure regulation via G-protein-coupled receptors for succinate and α-ketoglutarate in the proximal tubule.

A potential role of NaDCs in metabolism has come from the discovery of a Na^+/dicarboxylate cotransporter homolog from *Drosophila*, called *Indy* (I'm not dead yet) (Rogina *et al.*, 2000). *Indy* codes for a Na^+-independent succinate transporter. It is expressed in the midgut, which is analogous to the small intestine, fat body and oenocyte important for metabolism. Rogina *et al*. showed that the mutation in one copy of *Indy* gene leads to the decrease transport activity and elongation of life span of the mutant flies. This suggested that low activity of *Indy* affects the metabolism of *Drosophila*, thereby leading to increased lifespan. In 2003, NaDC1 homologs from *Caenorhabditis elegans* (*C. elegans*) was isolated and named ceNaDC1, ceNaDC2, and ceNaDC3. The ceNaDC1 is designated as a low-affinity Na^+/dependent dicarboxylate transporter, and the ceNaDC2, ceNaDC3 are high-affinity Na^+/dependent dicarboxylate transporters. These transporters are expressed in the intestinal tract. Knockdown of the function of ceNaDC2 significantly increases the lifespan of the worm compared with the wild-type worm by 15% (Fei *et al.*, 2003). Caloric restriction or suppression of metabolic energy production within the mitochondria in *C. elegans* is associated with a significant increase in life span

(Lakowski & Hekimi, 1998). In mammals, caloric restriction is the only known physiological intervention that increases longevity (Masoro, 2000). Therefore, it suggested a potential role for NaDC1 in regulation of aging and metabolic disorders, such as obesity. It seems there may be a direct link between NaDC transport activity and metabolism, and NaDC1 in the intestine may mediate the effect of caloric restriction. However, a study was carried out *in vivo*, NaDC1-deficient mice are normal in appearance and in body weight. There is no significant difference in metabolic or physiological changes associated with caloric restriction between $NaDC1^{+/+}$, $NaDC1^{+/-}$, and $NaDC1^{-/-}$ mice (Ho *et al.*, 2007), suggesting that NaDC1 may not mediate the effect of caloric restriction.

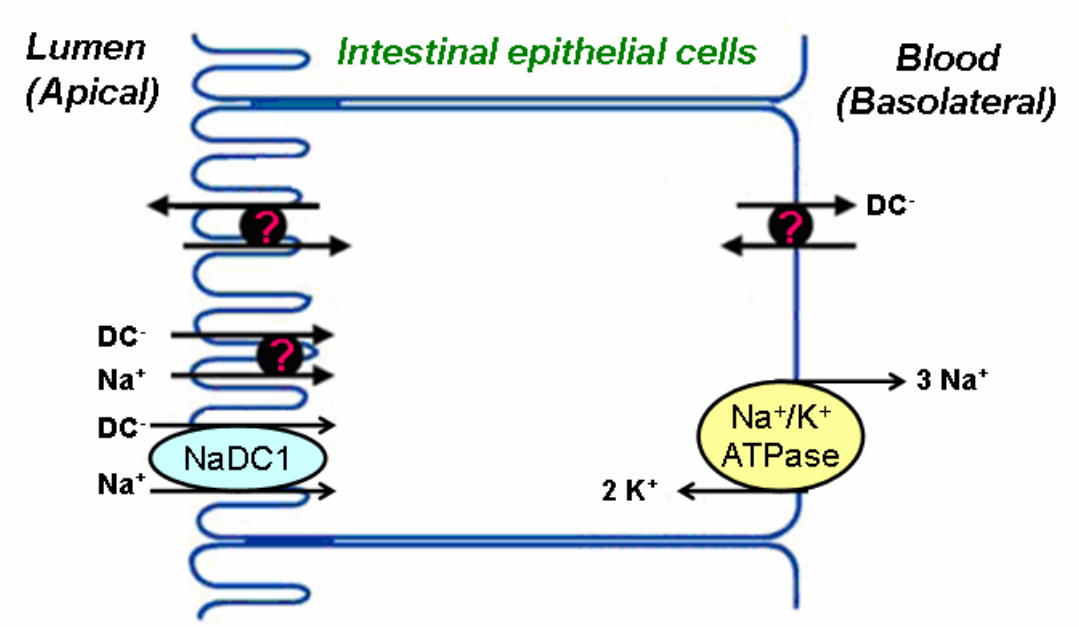

Figure 1.7 Overview of dicarboxylate transport in intestinal epithelium.

Currently, there is very little known about dicarboxylate transport in the small intestine (Figure 1.7). Previous studies only revealed that citric acid cycle intermediates can be transported across intestinal brush border membrane vesicles by a Na^+-dependent mechanism (Wolffram *et al.*, 1990; Wolffram *et al.*, 1992; Wolffram *et al.*, 1993; Wolffram *et al.*, 1994). There is evidence that di- and tricarboxylates can be transported across the intestinal epithelium (Browne *et al.*, 1978; Sakhaee *et al.*, 1992). Pajor *et al*. demonstrated that NaDC1 is expressed on the apical membrane of intestinal epithelium (Pajor, 1995).

Regulation of NaDC1

Little information is available about the regulation of NaDC1. NaDC1 shows adaptive changes in response to chronic treatments such as metabolic acidosis (Aruga *et al.*, 2000), potassium deficiency, which causes extracellular alkalosis and intracellular acidosis (Levi *et al.*, 1991), and starvation (Sheridan *et al.*, 1983; Windus *et al.*, 1986). Aruga and coworkers demonstrated that rats given NH_4Cl in their drinking water for 7 to 14 days show increased NaDC1 protein abundance. This study suggested that chronic metabolic acidosis leads to an increase in renal cortical NaDC1 mRNA abundance and apical membrane NaDC1 protein abundance (Aruga *et al.*, 2000). The studies from fasting rats using isolated renal brush border membrane and perfused proximal tubules showed increased transport of α-ketoglutarate and citrate (Sheridan *et al.*, 1983; Windus *et al.*, 1986). The citrate and α-ketoglutarate transport is increased in response to these treatments, mediated by an increased in V_{max} with no change in K_m.

There is evidence of acute regulation of NaDC1 by protein kinase C (Pajor & Sun, 1999). The activity of rbNaDC1 expressed in *Xenopus* oocytes was sensitive to inhibition by two activators of protein kinase C (PKC), phorbol 12-myristate 13-acetate (PMA) and *sn*-1,2-dioctanoylglycerol (DOG), but not by activators of protein kinase A. The inhibition of NaDC1 by PKC activation was independent of consensus sites for protein kinase C phosphorylation in NaDC1, Thr-186 and Ser-366. However, the inhibition effects of PMA were partially prevented by cytochalasin D, which disrupts microfilaments and endocytosis. The activation of PKC was associated with a decrease in the amount of NaDC1 protein expressed on the plasma membrane, thus suggesting that NaDC1 is likely to be regulated through changes in the endocytosis pathway.

Based on earlier studies, citrate excretion is tightly regulated by acid-base balance. NaDC1 in kidney is regulated in parallel to the Na^+/H^+ exchanger and the Na^+/HCO_3^- cotransporter (Boehmer *et al.*, 2004). The targeting and trafficking of Na^+/H^+ exchanger and the Na^+/HCO_3^- cotransporter are regulated by the NHE regulating factor NHERF-1 and NHERF-2. The NHERF-2 is also modified by the glucocorticoid inducible kinase SGK1. The signaling mechanisms mediating the effect of acidosis to the trafficking of NaDC1 into the cell membrane was investigated by Boehmer *et al.* (Boehmer *et al.*, 2004). The results demonstrated that the NHE regulating factors NHERF-2 increases substrate-induced currents in NaDC1. The glucocorticoid inducible kinase SGK1 and SGK1 homologues, SGK3, as well as PKB, a ubiquitous serine/threonine kinase B known to govern the trafficking of glucose transporter, also stimulate NaDC1 mediated currents. This activation occurs by an increased of V_{max} with no change of substrate affinity, thus suggesting that

NHERF-2 and the kinases are involved in regulation of NaDC1 by increasing abundance of the protein in the plasma membrane.

THE HIGH-AFFINITY Na^+/DICARBOXYLATE COTRANSPORTER, NaDC3

NaDC3 has been cloned from different animal species including rat, flounder, human, mouse, and *Xenopus* (Kekuda *et al.*, 1999; Steffgen *et al.*, 1999; Wang *et al.*, 2000; Pajor *et al.*, 2001; Oshiro & Pajor, 2005). NaDC3 is classified as a high affinity transporter and has K_m for succinate of approximately 20 μM in human. The human NaDC3 is 43% identical in amino acid sequence to hNaDC1 (Wang *et al.*, 2000). The gene for human ortholog has been mapped to chromosome 20 (*q*12-*q*13.1).

NaDC3 has broad substrate selectivity among the dicarboxylates and the divalent form of tricarboxylates. Although there are similarities in substrate selectivity, NaDC3 exhibits an array of preferred substrates different from NaDC1. NaDC3 has a higher affinity for dicarboxylates of five- and six-carbon long chain, such as α-ketoglutarate, glutarate and adipate, and also accepts bulky dicarboxylates, including 2,3-dimethylsuccinate (2,3-DMS), and meso-2,3-dimercaptosuccinic acid (DMSA), which is used as oral chelator agent for the treatment of heavy metal poisoning (Burckhardt *et al.*, 2002). This implies that longer and bulkier dicarboxylates are favored by NaDC3 but not by NaDC1. NaDC3 appears to interact with some monovalent organic anions such as benzylpenicillin (Burckhardt *et al.*, 2004).

Like NaDC1, the transport of NaDC3 is sodium-dependent involving three sodium ions with one divalent substrate, and transport is electrogenic as characterized by the two-electrode voltage clamp (Chen *et al.*, 1999; Burckhardt *et al.*, 2000; Wang *et al.*, 2000). The cation specificity of NaDC3 orthologs is similar to that of NaDC1. In mNaDC3, lithium can bind its cation binding sites and substitute for sodium; however, the transport rate is much lower than observed in sodium (Pajor *et al.*, 2001). In the presence of sodium, lithium acts as an inhibitor. There are species differences in potency of lithium inhibition, mNaDC3 is insensitive to lithium (Pajor *et al.*, 2001) but rat, flounder, and human NaDC3 transporters are more sensitive to lithium inhibition (Kekuda *et al.*, 1999; Steffgen *et al.*, 1999; Wang *et al.*, 2000). The differences between mNaDC3 and other NaDC3 orthologs in their sensitivity to inhibition by lithium, suggesting that mNaDC3 may contain cation binding sites different from other orthologs.

The tissue distribution of NaDC3 as determined by Northern blot analysis using rat and mouse cDNA NaDC3 as a probe showed positive signals in kidney, liver and brain (Chen *et al.*, 1999; Kekuda *et al.*, 1999; Pajor *et al.*, 2001). By RT-PCR analysis to detect NaDC3 mRNA transcripts, positive reactives were seen in choroid plexus and placenta (Kekuda *et al.*, 1999; Pajor *et al.*, 2001). By *in situ* hybridization, the expression of rNaDC3 mRNA was seen in kidney, liver and brain (Chen *et al.*, 1999). The membrane localization of NaDC3 was identified in winter flounder using anti-fNaDC3 antibody to stain kidney section. Immunohistochemistry of fNaDC3 revealed positive staining of the basolateral membrane of the secretory part of the flounder proximal tubule; therefore, localization of fNaDC3 in the

secretory part suggested that the organic anion secretion depends on the activity of NaDC3.

The importance of NaDC3 has been described in renal, hepatocyte, and neuron cells. In kidney, NaDC3 is responsible for transport of citric acid cycle intermediates from peritubular capillaries. NaDC3 mediates the cellular entry of dicarboxylates from the circulation for subsequent use in cellular metabolism. NaDC3 also participates in organic anion secretion process by providing intracellular dicarboxylates for anion/dicarboxylate exchanger in all cells (Pritchard & Miller, 1993; Wright & Dantzler, 2004). This exchange secretory process is of clinical relevance to the elimination and detoxification of anion substances such as non-steroidal anti-inflammatory drug (NSAID) (Burckhardt *et al.*, 2004), nephrotoxic drug, and renal heavy metal (Burckhardt *et al.*, 2002). In hepatocytes, uptake of α-ketoglutarate mediated by NaDC3 provides a substrate for glutamine synthetase, thus NaDC3 plays an important role in regulating glutamate synthesis (Stoll *et al.*, 1991; Zimmerli *et al.*, 1992). In brain, the uptake of α-ketoglutarate, a neurotransmitter precursor, released by astrocytes to replenish intracellular pools of neurotransmitters occurs via NaDC3 (Shank & Bennett, 1993). Moreover, NaDC3 plays an essential role in organic anion secretion from cerebrospinal fluid (CSF) by generating intracellular dicarboxylates for exchange with organic anion transporter in choroid plexus (Pritchard *et al.*, 1999).

THE Na^+-COUPLED CITRATE TRANSPORTER, NaCT

In 2002, the first cDNA for mammalian NaCT transporter was isolated from rat brain and functional expression was analyzed by expression in a mammalian cell

line (Inoue *et al.*, 2002b). NaCT is a plasma membrane transporter that functions predominantly in the cellular uptake of citrate. Sequence alignments revealed that human NaCT (hNaCT) shares approximately 54% and 47% amino acid identity with hNaDC1 and hNaDC3, respectively (Inoue *et al.*, 2002a). The gene for human NaCT has been mapped to chromosome 12 (*p*12-*p*13). hNaCT is structurally and functionally related to NaDC1 and NaDC3, but there are differences in terms of substrate specificity, substrate affinity and tissue expression pattern. NaCT transports the trivalent form of citrate rather than the divalent form. Inoue *et al*. showed that hNaCT can transport succinate but with lower affinity (K_m ~ 1.9 mM) compared to citrate (K_m ~ 600 μM). NaCT is expressed predominantly in the liver which is a different tissue distribution pattern than NaDC1 and NaDC3. (Inoue *et al.*, 2002a).

There are species differences in substrate affinity among the NaCT orthologs. The rat NaCT (rNaCT) mediates the transport of citrate with high affinity (K_m ~20 μM). In the case of hNaCT, the K_m value for citrate is 600 μM (Inoue *et al.*, 2002a), suggesting that the affinity of human NaCT for citrate is about 30-fold less than that of rat NaCT. In mouse NaCT, the K_m values for citrate and succinate are the same, around 38 μM and 37 μM, respectively (Inoue *et al.*, 2004). Therefore, mNaCT mediates the Na^+-coupled transport of citrate and succinate.

The lithium effect on NaCT is species-specific (Inoue *et al.*, 2003). With millimolar concentration of lithium and in the presence of sodium, lithium has stimulation effect on hNaCT (Inoue *et al.*, 2003), whereas other species, for example rat, mouse, are either unaffected or inhibited by lithium (Inoue *et al.*, 2002b; Inoue *et al.*, 2004). The stimulation effect of lithium on hNaCT is mediated by a combination of an increased V_{max} and decreased K_m for citrate (Inoue *et al.*, 2003).

Northern blot analysis demonstrated that NaCT mRNA is expressed in a restricted manner in rat and human tissues. The NaCT mRNA is expressed most predominantly in the liver, with moderate expression detectable in the brain and testis (Inoue *et al.*, 2002b; Inoue *et al.*, 2002a). By *in situ* hybridization analysis the expression of rNaCT mRNA is abundant in neuron regions such as the hippocampal formation, cerebellum, cerebral cortex and olfactory bulb (Inoue *et al.*, 2002b). The physiologic and therapeutic importance of NaCT has not been shown yet. Because citrate serves as a key precursor in cellular metabolism, NaCT is believed to be involved in fatty acid synthesis and cholesterol synthesis in the liver (Inoue *et al.*, 2002b; Inoue *et al.*, 2003).

PROGRESS IN STRUCTURAL BIOLOGY OF MEMBRANE PROTEINS

Membrane proteins are of medical importance. Specific defects in membrane transport process can cause many diseases such as cystic fibrosis (Welsh & Smith, 1993), diabetes mellitus (Garvey *et al.*, 1998), renal tubular acidosis (Kittanakom *et al.*, 2004), congestive heart failure (Nielsen *et al.*, 1997), and cholestasis (Trauner *et al.*, 1998). Membrane proteins are the targets of a large number of pharmacologically and toxicologically active substances and are responsible, in part, for their uptake, metabolism, and clearance (Sadee *et al.*, 1995). In order to identify the useful targets, it is important to understand their structure or how they operate at the molecular level. Membrane protein structure studies are notoriously difficult due to insufficient quantities of pure protein, and because they are flexible proteins, not easily crystallized proteins. However, in the recent past, with an effort and advances in

methods for crystallization and analysis of proteins by x-ray and electron diffraction as well as improvement in nuclear magnetic resonance (NMR) methods have led to overcome the limitation of membrane proteins.

There are some high-resolution structures available for prokaryotic transport proteins, although the number is small. Transport proteins with known 3D-structure currently reported include cytochrome C oxidase (Iwata *et al.*, 1995), bacteriorhodopsin (Luecke *et al.*, 1998), KcsA potassium channel (Doyle *et al.*, 1998), G-protein-coupled receptor (Rhodopsin) (Palczewski *et al.*, 2000), calcium ATPase (Toyoshima *et al.*, 2000), H^+/Cl^-exchange transporters (Dutzler *et al.*, 2002), multi-drug efflux transporters (Murakami *et al.*, 2002), *Lac*Y lactose permease (Abramson *et al.*, 2003), AQPO aquaporin water channel (Harries *et al.*, 2004), glutamate transporter homologue (Glt_{Ph}) (Yernool *et al.*, 2004), NhaA Na^+/H^+ antiporter (Hunte *et al.*, 2005), $LeuT_{Aa}$ leucine transporter (Yamashita *et al.*, 2005). Each bacterial structure has made a major contribution in our knowledge of the structure of mammalian membrane proteins. For example, as seen in the case of serotonin transporter (SERT), the high-resolution structure from bacterial homologs, LeuT from *Aquifex aeolicus* (Yamashita *et al.*, 2005) provides a framework to understand the molecular motion within the structure of serotonin transporter (see review (Rudnick, 2006)).

At present none of these proteins belongs to the SLC13 family. Some high-resolution structures, such as *lac* permease (Abramson *et al.*, 2003), the glutamate transporter (Yernool *et al.*, 2004) and the Na^+-coupled leucine transporter, $LeuT_{Aa}$ (Yamashita *et al.*, 2005) which their mechanism of transport is similar in some ways to NaDC1, could explain some parts of mutagenesis experiments conducted in

NaDC1. Since membrane proteins are dynamic molecules, they must be highly flexible to allow conformational changes and translocation of substrates. The images of *lac* permease, the glutamate transporter, and the Na^+-coupled leucine transporter show the static structure, so they cannot provide information how NaDC1 works. Therefore, some information of NaDC1 movement during the transport cycle is still lacking.

AIMS OF STUDIES IN THIS DISSERTATION

This dissertation is divided into two main parts: the first part is the identification of di-and tricarboxylate transport pathway in the small intestine using Caco-2 cells as a model. The second part is the investigation the permeation pathway in NaDC1, focused on TM3, and identification of amino acid residues responsible for determining the differences in citrate and sodium affinity between human and rabbit NaDC1 transporters, particularly in TM10.

Aim 1: To identify the succinate and citrate transport pathways in Caco-2 cells

It was found that after oral citrate administration, citrate was found in the blood. Further studies found that citric acid cycle intermediates could be transported across intestinal epithelia by Na^+ driven transport mechanism. NaDC1 protein was also found on the small intestinal epithelial cells. However, we currently do not know and understand dicarboxylate transport pathway in small intestine. Thus, the aim of this study was to elucidate the pathways for succinate and citrate transport in the human colonic adenocarcinoma cell line (Caco-2) as a model of enterocytes.

Aim 2: To investigate whether TM3 forms part of the permeation pathway in NaDC1 and contributes to the substrate binding sites

The amino acid sequence of transmembrane helix (TM) 3 is highly conserved among the members of SLC13 family. A previous study indicated that the mutation of Lys-84 to Ala led to an increased in *Km* for succinate, suggesting that Lys-84 might have a role in succinate binding. Recently, chimera study between mouse and rabbit NaDC1 showed that glutarate transport mediated by NaDC1 was shown to be an interaction of multiple amino acids found in TM3 and TM4. Therefore, the objective of this study was to investigate the extracellular accessibility and substrate binding sites of TM3 in NaDC1 using the substituted-cysteine scanning accessibility method and the experimental system was transiently transfected HRPE cells.

Aim 3: To identify amino acid residues that determine differences in citrate K_m between human and rabbit NaDC1

The human and rabbit NaDC1 are 78% identical in amino acid sequence. Previous study showed that human and rbNaDC1 exhibited similar affinities to succinate. However, there were differences in some functional properties between human and rbNaDC1, including the *Km* for citrate in human is greater than in rbNaDC1; rbNaDC1 had a greater affinity for sodium than hNaDC1; hNaDC1 was insentitive to lithium, whereas rbNaDC1 was inhibited by lithium. Based on previous chimera study between human and rabbit NaDC1, rbNaDC1 had citrate *Km* 0.9 and hNaDC1 was 7.2. Single chimera R7, R10 and R11 had intermediate citrate *Km*, whereas triple chimera R7/10/11 had citrate *Km* similar to rbNaDC1. Therefore, chimera R7/10/11 contains the amino acids that are important in determining the differences of citrate affinity between rbNaDC1 and hNaDC1. Therefore, the

objective of this study was to identify the residues which determine differences in substrate and cation affinity in human and rabbit NaDC1 using the site-directed mutagenesis method. The experimental system was transiently transfected COS-7 cells because I subsequently found that the expression of NaDC1 in COS-7 cells is higher than HRPE cells.

These studies provide fundamental information on the physiologically important SLC13 family and contribute to a better understanding of ion-coupled transport mechanism of NaDC1. Knowledge of the structure of NaDC1 may lead to the development of valuable agonist, antagonists, or inhibitors. It may also pave the way for further development therapeutic agent for treatment or prevention of kidney disease or other disorders mediated by NaDC1.

CHAPTER 2: IDENTIFICATION OF TRANSPORT PATHWAYS FOR CITRIC ACID CYCLE INTERMEDIATES IN THE HUMAN CARCINOMA CELL LINE, Caco-2

INTRODUCTION

The function of NaDC1 has been studied mostly in the kidney, where it reabsorbs filtered citric acid cycle intermediates; however, it is also important in the intestine. The normal function of the intestinal NaDC1 is to absorb dicarboxylates from the diet and from gastrointestinal secretions (Pajor, 1999b). In recent years, a new role for NaDC1 in metabolism and aging has been suggested since mutations in NaDC1 homolog in *Drosophila (Indy* protein*)* and *Caenorhabditis elegans* produce lifespan extension (Rogina *et al.*, 2000; Fei *et al.*, 2003). Both *Indy* and the *C. elegans* protein are found in the midgut, analogous to small intestine, suggesting that the mechanism of lifespan extension may be similar to that produced by caloric restriction (Masoro, 2000).

There is very little information about intestinal transport of citric acid cycle intermediates in mammals. There is evidence for intestinal transepithelial transport of citrate in humans (Sakhaee *et al.*, 1992) and of citrate, succinate and α-ketoglutarate in hamsters (Browne *et al.*, 1978). Studies with isolated brush border membrane vesicles suggest that transport across the apical membrane is entirely sodium-dependent, with properties very similar to those of NaDC1 (Wolffram *et al.*, 1990; Wolffram *et al.*, 1992; Wolffram *et al.*, 1993; Wolffram *et al.*, 1994). The intestinal basolateral membrane appears to contain sodium-independent pathways for transport of citrate and tricarballylate, a non-metabolizable tricarboxylate. The basolateral

transporter may be an anion exchanger, since it is *trans*-stimulated by other di- or tricarboxylates (Wolffram *et al.*, 1994). Nevertheless, detailed information is lacking on the transport systems for citric acid cycle intermediates in the small intestine and there are no model systems currently available for the study of regulation of these transporters. The human colon adenocarcinoma cell line, Caco-2, has extensively been used as a model of enterocytes, because Caco-2 cells differentiate into polarized cells with many of the functional properties of enterocytes. Enterocyte-like differentiated Caco-2 cells are very similar to normal the small intestine in regards to morphology and the presence of microvillous membrane enzymes-associated enzymes. The time course of differention process mimics the situation found in the small intestine, with the differentiation taking place during the crypt to villus migration. Caco-2 cells form polarized monolayers with well-formed tight junctions, their brush border membrane is well developed and ion transport charcteristics (Hillgren *et al.*, 1995; Sambuy *et al.*, 2005). Since Caco-2 cells are the closet analogy to the small intestine among other intestinal cell line, including HT-29 and T84 cells, Caco-2 cells are chosen as a potential model system for investigation of intestinal di- and tricarboxylate transport pathways.

The results of this study show that the apical membrane of differentiated Caco-2 cells contains at least three transport systems for di- and tricarboxylates. The Na^+-dependent transport of succinate and citrate in Caco-2 cells is mediated by a combination of NaDC1 and the Na^+/citrate transporter, NaCT, although NaDC1 is the predominant transport pathway. NaCT is not normally expressed in small intestine (Inoue *et al.*, 2002a). The Na^+-independent transport of citrate in Caco2 cells is likely mediated by one or more organic anion transporters, possibly OAT2 and/or OAT4.

There is also transepithelial transport of methylsuccinate across Caco-2 cell monolayers, indicating the presence of an additional Na^+-independent transporter on the basolateral membrane. RT-PCR experiments show that Caco-2 cells express different dicarboxylate and organic anion transporters than human small intestine. The current studies establish that di- and tricarboxylate uptake by Caco-2 cells occur via multiple transport pathways, predominantly by NaDC1 as well as by NaCT and organic anion transporters that are not found in normal small intestine. It is concluded that the Caco-2 cell line is probably useful for studying regulation of NaDC1, but is not a good model of the transport pathways for citric acid cycle intermediates in small intestine.

MATERIALS AND METHODS

Caco-2 cell culture

The human colon adenocarcinoma cell line, Caco-2, was obtained from the American Type Culture Collection and cultured in DMEM with 4.5 g/l glucose (GIBCO-Invitrogen) supplemented with 10% heat-inactivated fetal calf serum (Hyclone), 100 units/ml penicillin G, 100 μg/ml of streptomycin, 1% (v/v) sodium pyruvate, and 1% (v/v) nonessential amino acids (Sigma). Cells were maintained at 37°C in an atmosphere of 5% CO_2 and cultures were passaged at about 90% confluence. For transport experiments with cells attached to plastic, cells were plated at a density of 2×10^5 cells/well onto 24 well plates coated with 5 μg/cm^2 rat-tail collagen I (BD Bioscience-Clontech). For transepithelial transport measurements, cells were seeded at high density (1×10^6 cells/24 mm insert or 2×10^5 cells/6.5 mm insert) on Transwell™ polycarbonate filter tissue culture inserts (Costar). Cell

monolayers were maintained with daily medium changes for 20 or 21 days after seeding. Cells were incubated with serum-free medium for 24 hours prior to transport assays to exclude possible complications from hormones, growth factors or serum, although preliminary experiments showed that there was no effect of serum starvation. The differentiated phenotype of the cells was observed by microscopy. The integrity of cell monolayers grown on Transwells was evaluated by measuring the transepithelial electrical resistance (TEER) with an epithelial voltmeter (EVOM; World Precision Instrument) and the magnitude of paracellular flux of [^{3}H] or [^{14}C]-labeled mannitol.

Transport studies in attached cell monolayers

The transport of [^{14}C]succinate (40 mCi/mmol, Moravek), [^{14}C]citrate (55 mCi/mmol, American Radiolabeled Chemical Inc.), or [^{3}H]methylsuccinate, a gift from Dr. Chari Smith (GlaxoSmithKline), in attached cells was conducted using a modification of a previous protocol (Pajor & Randolph, 2005). Briefly, cells were washed twice with 1 ml choline buffer (120 mM choline chloride, 5 mM KCl, 1.2 mM $CaCl_2$, 1.2 mM $MgSO_4$, 5 mM D-glucose, 25 mM HEPES, adjusted to pH 7.4 with 1M Tris) to remove medium. The uptake experiments were performed at 37^{o}C on a platform rotator. The transport of succinate and citrate was measured in sodium buffer (same as choline buffer, except that choline is replaced by NaCl) or choline buffer. The transport buffer also contained [^{3}H] or [^{14}C]-labeled extracellular marker to determine the residual extracellular volume. After the incubation period, the uptakes were stopped with four washes of ice-cold choline buffer (1 ml each) and the buffer was removed. The cells were then solubilized in 0.25 ml of 1% sodium

dodecyl sulfate (SDS). The radioactivity was determined using dual-label liquid scintillation counting. Uptake values were normalized for the residual extracellular volume determined from the extracellular marker counts, and expressed in fmol/well-min.

Transepithelial transport and intracellular accumulation

Cells plated on Transwell inserts were used for studies of transepithelial transport. Transport studies were conducted 21-23 days after seeding when TEER values exceeded 600 $\Omega \cdot cm^2$ (after correction for resistance values of inserts alone). Prior to initiating the transport studies, culture inserts were washed twice by dipping in 250 ml of choline buffer, and placed in fresh 6 or 24 well plates. Cell monolayers were preincubated from the apical and basolateral sides with 1.5 ml and 2.6 ml of pre-warmed choline buffer per well, respectively (in 6 wells), or with 0.1 ml and 0.6 ml per well, respectively (in 24 wells) and allowed to equilibrate for 30 min at 37^oC. Transport was initiated by adding sodium or choline buffer containing [^3H] methylsuccinate at a final concentration of 100 μM. [^{14}C]mannitol was also added to determine the magnitude of paracellular fluxes across the epithelium and confirm maintenance of monolayer integrity during the flux measurements. Data were used only if paracellular fluxes of [^{14}C]mannitol were less than 0.2%. Epithelial layers were incubated for 60 min at 37^oC. To measure transepithelial transport, 500 μl samples were taken from the non-radioactive or receiver side, either the apical or basolateral chamber. Fluxes in the absorptive (apical to basolateral) and secretory (basolateral to apical) direction were measured and expressed as fmol/hr-cm^2. To determine the intracellular accumulation, at the end of the incubation period, the

intact epithelial monolayer on the tissue culture insert was sequentially transferred through 4 beakers each containing 500 ml of cold choline buffer, then the membrane containing the cell monolayer was carefully excised from the insert. Cell-associated radioactivity was determined by dual-label liquid scintillation counting.

Construction of human NaCT expression plasmids

The full length coding sequence of human NaCT (GenBank AY151833) was amplified from human liver cDNA (Clontech) using the following primers: sense, 5′-TTG AAT TCC CGC CAT GGC CTC GGC GC-3′ and antisense, 5′-CCC GCT CGA GCT AAG TCT CAA TAT GTG TC-3′, including *EcoRI* and *XhoI* restriction sites (underlined) to facilitate subcloning. The PCR product was subcloned into pCR 2.1 vector using the TopoTA cloning kit (Invitrogen), followed by subcloning into the mammalian expression plasmid, pcDNA3.1 (Invitrogen). The sequence was verified by the Protein Chemistry Laboratory of the University of Texas Medical Branch, using an Applied Biosystems Model 3100 automated DNA sequencing unit.

Functional expression in HRPE cells

Human retinal pigment epithelial (HRPE) cells (Coriell Institute) were maintained in Modified Eagle's medium (MEM) supplemented with 10% heat-inactivated fetal bovine serum, 100 units/ml penicillin G, 100 μg/ml of streptomycin at 37^{o}C with 5% CO_2. For transient transfections, cells were seeded onto 24 well culture plates at a density of 1.2×10^5 cells/well. Transient transfections with plasmids containing hNaDC1 (Pajor & Randolph, 2005) or hNaCT with FuGENE 6

(Roche) were conducted 24 hours later according to the manufacturer's instructions. Each well was transfected with 1.8 μg FuGENE 6 and 0.6 μg DNA. Transport assays were performed 48 hours after transfection as described for Caco-2 cells except that the extracellular marker correction was not done. Instead, uptake by HRPE cells was corrected for background counts in control cells transfected with the pcDNA3.1 vector plasmid.

Cell surface biotinylation of Caco-2 cells

The cell surface expression of NaDC1 was performed using Sulfo-NHS-LC-Biotin (Pierce) followed by streptavidin precipitation and immunoblotting, as previously described (Pajor & Randolph, 2005). Caco-2 cells grown to 21 days in six-well plates were washed three times with PBS-CM (PBS buffer pH 9.0 containing 1 mM Ca^{2+} and Mg^{2+}). Cell surface proteins were biotinylated with 1.5 mg/ml Sulfo-NHS-LC-Biotin (Pierce) in PBS-CM for 30 minutes at room temperature. The biotinylation reagent was removed with two washes of 1 ml cold Quench buffer (PBS-CM containing 100 mM glycine). The plates were incubated on ice 20 min with 3 ml/well cold Quench buffer. Cells were then dissolved in lysis buffer (containing 20 mM Tris-base, 150 mM NaCl, 5 mM EDTA, 1% Triton X-100, 10 μg/ml pepstatin A, 10 μg/ml leupeptin, 0.5 mM PMSF, pH 7.5) on ice with gentle rocking for 30 min. Three wells of solubilized cells were combined for each group and centrifuged at 14,000 × g for 15 min. The supernatants were transferred to new tubes. Biotinylated proteins were then incubated with 50 μl ImmunoPure Immobilized Streptavidin beads (Pierce) with end-over-end rotation at 4^{o}C overnight. The biotin-streptavidin-agarose bead complexes were washed with lysis buffer.

Biotinylated proteins were eluted from beads with sample buffer for SDS-PAGE and analyzed by Western blotting.

Western blotting

The Western blot procedure was performed as previously described (Pajor *et al.*, 1998c). The human small intestine (duodenum) brush border membrane vesicle samples, a gift from Dr. Chari Smith (GlaxoSmithKline), were separated by SDS-polyacrylamide gel electrophoresis (SDS-PAGE) using a 7.5 % Tricine gel and then electrophoretically transferred to nitrocellulose membranes (0.45 μM; Schleicher & Schuell). The blots were blocked, washed, and incubated overnight at 4^{o}C with anti-rabbit NaDC1 antiserum (diluted 1:1,000 in PBS-TM; phosphate buffered saline containing 0.5% non-fat dried milk and 0.05% TWEEN 20), followed by 1 hour incubation with 2^{o} antibody (horseradish peroxidase-coupled donkey anti-rabbit IgG diluted 1:5,000; Amersham Biosciences) at room temperature. Immunoreactive proteins were detected using the Supersignal West Pico chemiluminescent substrate kit (Pierce) and visualized by Image Station 440CF (Eastman Kodak). The molecular mass was estimated by comparison with chemiluminescent protein size standards (MagicMark Western XP; Invitrogen).

RT-PCR

Total RNA was extracted from Caco-2 cells 21 days after confluence using RNeasy mini kits (Qiagen) according to manufacturer's instructions. First-strand cDNA was synthesized from 5 μg of RNA using the SuperScript II RNaseH-Reverse Transcriptase kit (Invitrogen) with random hexamer primers. Human small intestine

cDNA was purchased from Origene. The quality of cDNA was assessed by amplification of β-actin using primers from Clontech. The PCR reaction mixture (50 μl) contained 20 pmol each primer, 0.2 mM dNTP, 1.5 mM $MgCl_2$, 5 μl cDNA, and 2.5 units of Taq DNA polymerase in the buffer provided (Roche). The sequence-specific primers used for PCR amplification are shown in Table 2.1. The PCR cycle was 94°C for 3 min, followed by 28 cycles of 94°C for 45 sec, 60°C for 45 sec, 72°C for 1 min, and 72°C for 15 min final elongation. PCR products were visualized on agarose gel stained with ethidium bromide. The identity of PCR products obtained from Caco-2 cells was verified by sequencing after subcloning into the pCR2.1 plasmid (TA cloning kit).

Statistical analysis

Statistical analysis was performed using Student's *t*-test to compare two groups or a One-way Analysis of Variance (ANOVA) and the *post-hoc* Dunnett's multiple comparison method for multiple groups (SigmaStat program, Jandel Scientific). Statistically significant difference was considered to be $p < 0.05$.

Table 2.1 Oligonucleotide primers used for PCR amplification of human Na^+/dicarboxylate cotransporters (NaDC and NaCT), and organic anion transporters (OAT).

Protein (Genbank No.)	Primer sequences (5′ to 3′)	Predicted size (bp)
hNaDC1	CCCTTAATCCTGTTCCCTATGA	581
(U26209)	TGGGGGAAGAGCGAGTTGA	
hNaDC3	CACCGCCTCCACTGCCATGAT	749
(AF154121)	GACGGGAAGAAGAACAAGATGG	
hNaCT	GGAGCTGCCAGGGAGTCAAGTG	647
(AY151833)	GGAGGGGGATAAAATGGAGTTTTC	
hOAT1	GGTTCTTCATTGAGTCGGCCC	690
(AF124373)	GCCACAGGCAAAGCACCGTA	
hOAT2	CCAGGAGGCTGTGAGCAAAGTG	612
(AF210455)	CTGTGCCTGCCTCGTCTCTG	
hOAT3	CACCGCAAGTGACCTGTTCC	540
(NM_004254)	CAGGAAGAGGGCAGCACTG	
hOAT4	ATGCTGGACAATGGCTCTGC	778
(NM_018484)	GTCAGGTTCTTGGCCTCCTTG	

RESULTS

Extracellular volume measurement in Caco-2 cells

The extracellular marker, mannitol, is often used for estimating the extracellular volume of attached cell monolayers, including Caco-2 (Kimelberg *et al.*, 1992). However, it was found that the extracellular volume measured with both [^{3}H] and [^{14}C]mannitol appeared to increase over time (Figure 2.1), suggesting that

mannitol is not a good measure of extracellular volume in Caco-2 cells grown on plastic.

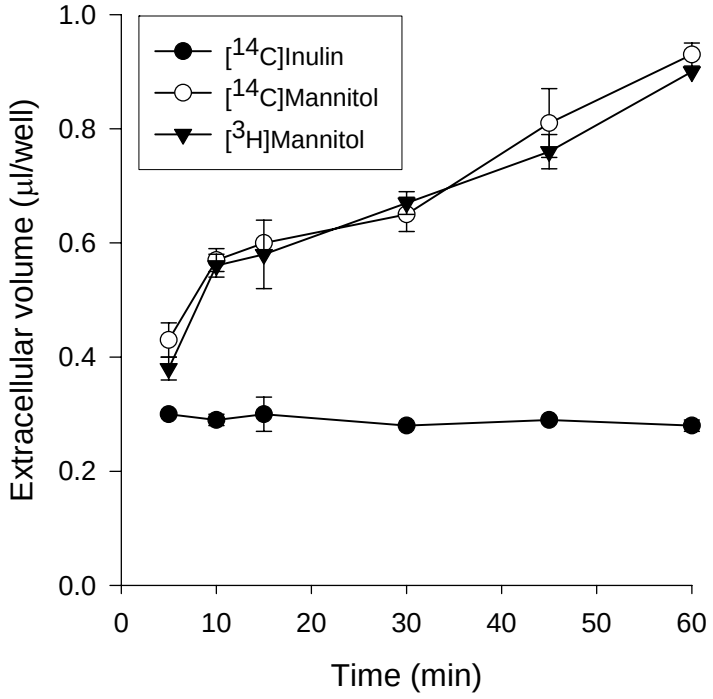

Figure 2.1 The apparent extracellular volume of Caco-2 cell monolayers was determined using [^{3}H] and [^{14}C]mannitol and [^{14}C]inulin in a time course up to 1 hour. Caco-2 cells plated at a density of 2×10^{5} cells/well and grown onto 24 well plates were incubated in sodium buffer containing [^{3}H]-and [^{14}C]mannitol or [^{14}C]inulin for the time indicated. After the incubation period, the uptake was stopped with four washes of choline buffer and then the buffer was aspirated. Cells were then solubilized in 1% SDS. The radioactivity accumulated in each cells was determined by using liquid scintillation counting. Each data point represents the mean ± range, n = 2 wells, from a single experiment.

In a previous study using isolated sympathetic ganglia, mannitol was found to be metabolized, with different metabolites depending on the isotope (^{3}H or ^{14}C), which produced differences in apparent extracellular volume (Garthwaite, 1979). Another possible explanation could be that the radiolabeled mannitol is accumulating through paracellular pathways in aqueous domes under the monolayer (Ramond *et*

al., 1985). [^{14}C]inulin was tested as an alternative extracellular marker and there was no change in apparent volume over time. Therefore, [^{14}C]inulin counts were used to estimate the extracellular volume of the Caco-2 monolayers, approximately 0.35 µl per well, which was then used in correcting uptake calculations.

Succinate and citrate transport in Caco-2 cells grown on plastic

The time course of succinate and citrate uptake in Caco-2 cells was measured in the presence and absence of sodium over a 60-minute time course (Figure 2.2). Transport of succinate was essentially linear over 60 minutes (Figure 2.2A). The sodium-independent component of succinate transport was not evident until after 45 minutes. In order to maximize the signal above the counts associated with the extracellular fluid, 60-minute uptake was used for the experimental time points. For example, in the experiment shown in Figure 2.2A, the [^{14}C]succinate counts associated with extracellular fluid were approximately 4.5 pmol/well, approximately one third of the intracellular accumulation. The citrate time course is very different from that of succinate (Figure 2.2B). The sodium-dependent component of citrate transport was not evident until after 30 minutes, and there was a substantial sodium-independent component. A possible explanation of why the choline data follow the sodium data for 15 minutes before the sodium-dependent component of the citrate transport was seen may be due to the electrochemical/concentration gradients that drive the citrate transport. The sodium-independent component dropped or reached a plateau after 15 minutes. This could be due to the intracellular citrate concentrations. In the early of the sodium-dependent time course there may be a leak of citrate through the sodium-independent component, but later the sodium-dependent

component is visible because the electrochemical gradient for sodium is continually generated by the Na^+-K^+-APTase. Again, for accurate measurement above the extracellular [^{14}C]citrate counts, 60 minute time point was used.

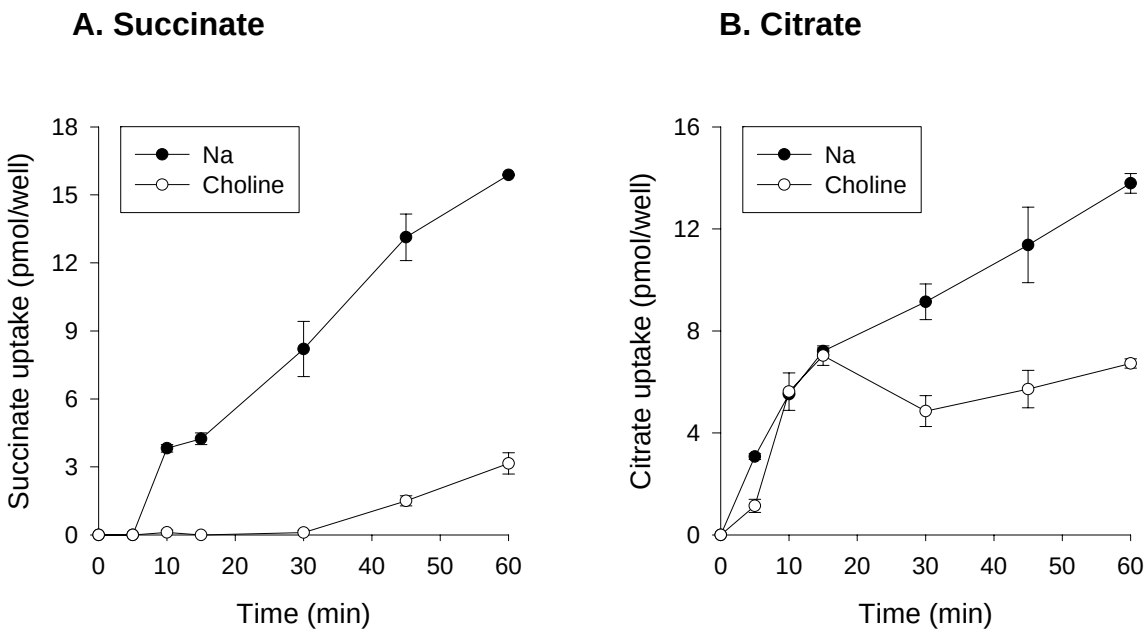

Figure 2.2 Time course of uptake of succinate and citrate by Caco-2 cells. Monolayers plated at a density of 2×10^5 cells/well and grown onto 24 well plates were incubated with 10 μM [^{14}C]succinate (A) or [^{14}C]citrate (B) in sodium or choline buffer for time points up to 1 hour. After the incubation period, the uptake was stopped with four washes of choline buffer and then the buffer was aspirated. Cells were then solubilized in 1% SDS. The radioactivity accumulated in each cells was determined by using liquid scintillation counting. Each data point represents the mean ± S.E.M, n = 4 wells, from a single experiment.

The sodium-dependent and -independent succinate and citrate transport activity in Caco-2 cells is shown in Figure 2.3. Most of the succinate transport was sodium-dependent, whereas approximately half the citrate transport was sodium-dependent. The proportion of sodium-independent citrate transport varied

considerably between experiments, and in some experiments there was no sodium-independent transport of citrate, suggesting variability in expression of the sodium-independent citrate transporters. At present there is no explanation for this variability. The sodium-independent citrate transport pathway was not influenced by cell passage number, differentiation state, glutamine supplementation or by lot or source of serum.

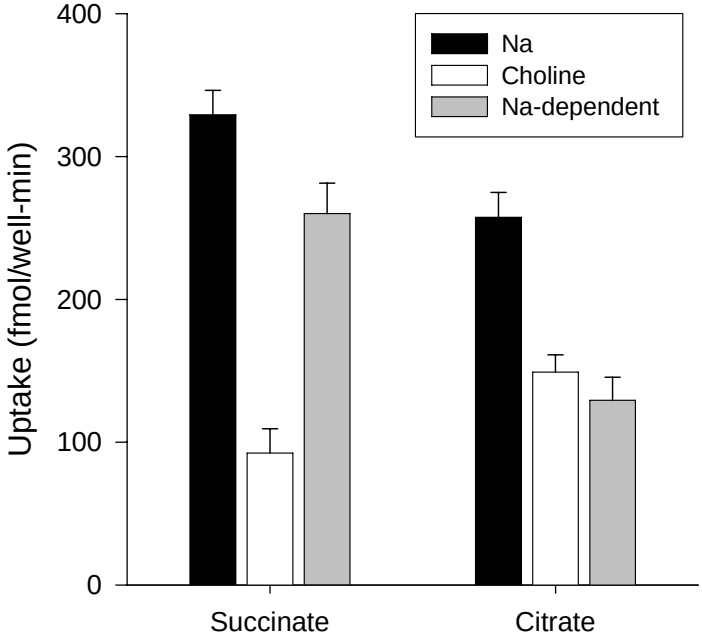

Figure 2.3 Transport of succinate and citrate in Caco-2 cells. Caco-2 cells were plated at a density of 2×10^5 cells/well and grown onto 24 well plates. Transport of 10 μM [^{14}C]succinate or [^{14}C]citrate in Caco-2 cells after 60 minutes was measured in sodium- or choline-containing transport buffer as described in Materials and Methods. Na^+-dependent transport was calculated from the difference between uptake in sodium and choline. Data shown are means ± S.E.M. of 9-24 independent experiments.

RT-PCR analysis of Na^+-dependent dicarboxylate transporters

On the basis of previous observation (Figure 2.3), the transport of succinate and citrate was sodium-dependent in Caco-2 cells. Therefore, one hypothesis to

explain the observation is that Na^+-dependent succinate and citrate transport is mediated by Na^+/di-tricarboxylate cotransporters belonging to the SLC13 family. There are three known Na^+-coupled succinate and citrate transporters in humans: NaDC1, NaDC3 and NaCT (Pajor, 2006). Therefore, RT-PCR was used to examine whether message for these transporters is found in Caco-2 cells and in normal human intestine. Normal human intestine contained mRNA for NaDC1 but not NaCT (Figure 2.4), consistent with the tissue distribution pattern of NaDCs (Pajor, 1996) and NaCT (Inoue *et al.*, 2002a).

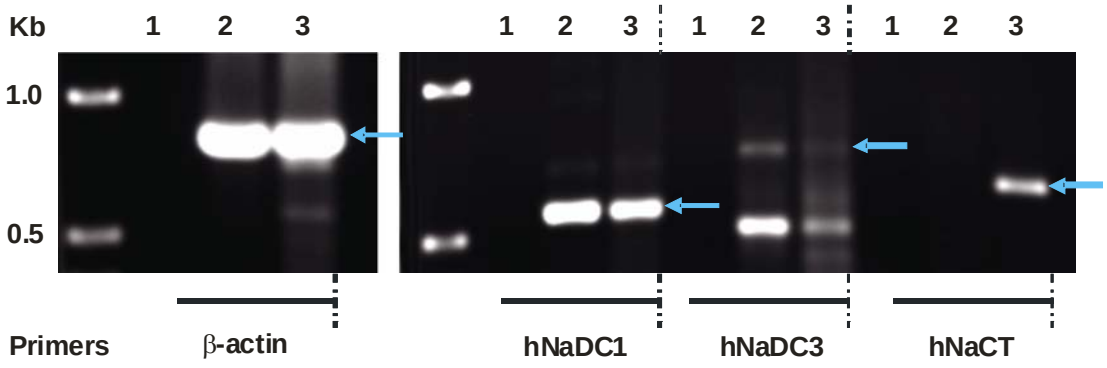

Figure 2.4 RT-PCR analysis of Na^+/dicarboxylate cotransporter mRNA in human intestine (lane 2) and Caco-2 cells (lane 3), water controls (lane 1) using specific primers for hNaDC1, hNaDC3 and hNaCT. Amplification with β-actin primers to test the quality and relative quantity of cDNA was performed in parallel. Size standards were shown in leftmost lane. Arrows showed the expected size of products. Both hNaDC1 and hNaCT bands were confirmed and verified by sequencing.

There was a faint signal in the NaDC3 RT-PCR reaction, indicating that NaDC3 may be present in human intestine. Northern blots of rat intestinal mRNA do not contain NaDC3 message (Kekuda *et al.*, 1999), but the sensitivity of RT-PCR is greater than Northern blotting and there may be species differences. Caco-2 cells resembled normal intestine since they expressed NaDC1 (Figure 2.4). However, the RT-PCR reaction with NaCT primers was also positive in Caco-2 cells, unlike normal

human intestine. There was a very faint signal with NaDC3 primers at the correct size but it was not possible to verify the identity by sequencing. Therefore, potential candidates for Na^+-dependent transport of succinate and citrate in Caco-2 cells are NaDC1 and NaCT.

Succinate kinetics in Caco-2 cells

The succinate kinetic transport of Caco-2 was further examined. The K_m for succinate was 691 μM (Figure 2.5), and in a second experiment, 766 μM, or a mean of 730 μM. The K_m value in Caco-2 cells is similar to K_m values of about 600 – 800 μM in hNaDC1 (Pajor & Sun, 1996b). This saturation of uptake at high substrate concentration confirms the carrier-mediated transport process.

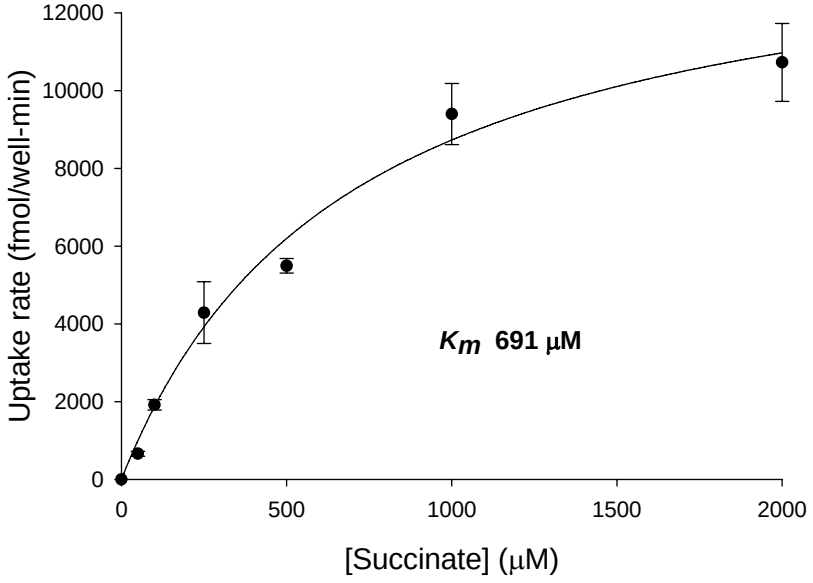

Figure 2.5 Succinate kinetics in Caco-2 cells. The kinetics of succinate transport were determined in Caco-2 cells. Caco-2 cells were plated at a density of 2×10^5 cells/well and grown onto 24 well plates. The transport activity of [^{14}C]succinate was measured for 30 min in either sodium or choline buffer as described in Materials and Methods. Na^+-dependent transport was calculated from the difference between uptakes in sodium and choline. Each data point shows the mean ± range (n=2), from a single experiment.

Expression of NaDC1 protein in Caco-2 cells and small intestine

Previous studies have shown that NaDC1 mRNA is expressed in the small intestine and kidney of rabbit and human (Pajor, 1996; Pajor & Sun, 1996a). To confirm whether NaDC1 protein is expressed on the plasma membrane in Caco-2 cells, cell-surface protein expression was examined using a membrane impermeant reagent, Sulfo-NHS-LC-biotin. As shown in Figure 2.6, both human small intestinal brush border membranes and cell-surface biotinylated Caco-2 cells expressed an immunoreactive protein with an approximate mass of 72 kDa. Therefore, NaDC1 protein in addition to mRNA is found in both human small intestine and Caco-2 cells. There are no antibodies available yet against NaCT.

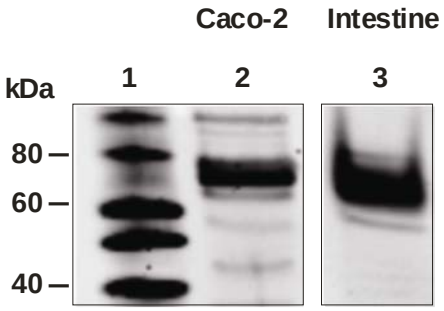

Figure 2.6 Expression of Na^+/dicarboxylate cotransporter (NaDC1) protein in Caco-2 cells and human small intestinal brush border membrane vesicles. Cell-surface biotinylated Caco-2 cells treated with Sulfo-NHS-LC-biotin (lane 2) and human jejunum brush border membrane vesicles (BBMV) (lane 3) were separated on 7.5% tricine-SDS gel and transferred to nitrocellulose. Blots were probed with anti-NaDC1 antibodies (1:1000 dilution) followed by horseradish peroxidase-linked anti-rabbit IgG (1:5000 dilution). Chemiluminescent size standard (MagicMark XP) is shown in lane 1. Note that the two samples are from two separate blots.

Succinate and citrate transport by HRPE cells transfected with hNaDC1 or hNaCT

The Na^+-dependent transport of 10 μM succinate and citrate was tested in HRPE cells transiently transfected with hNaDC1 or hNaCT. For both NaDC1 and NaCT, there was no sodium-independent transport of succinate or citrate. As shown in Figure 2.7A, HRPE cells transiently transfected with hNaDC1 had about 10-fold higher rate of succinate transport compared with citrate. The HRPE cells transiently transfected with hNaCT cDNA (Figure 2.7B) had lower transport of both succinate and citrate compared with hNaDC1-expressing cells, and the rate of succinate transport was about half the citrate transport. This result is consistent with previous findings that NaDC1 prefers succinate; whereas, NaCT transports citrate most efficiently (Pajor, 2006; Inoue *et al.*, 2002a; Inoue *et al.*, 2002b). By comparison, the rate of Na^+-dependent citrate transport relative to succinate transport in Caco-2 cells is greater than would be expected if Caco-2 cells expressed only NaDC1. This result supported the hypothesis that NaDC1 and NaCT are involved in succinate and citrate transport in Caco-2 cells.

Human NaDC1 and NaCT exhibit very different responses to the addition of lithium to the transport solution. Succinate transport by human NaDC1 is insensitive to Li^+ in the millimolar range, but citrate transport has not been tested (Pajor & Sun, 1996b). In contrast, citrate transport by hNaCT is stimulated by Li^+, but succinate transport has not been tested (Inoue *et al.*, 2003). To determine the contribution of those transporters to sodium-dependent succinate and citrate transport in Caco-2 cells, the effects of 2.5 mM Li^+ on both succinate and citrate transport were tested in HRPE cells transiently transfected with hNaDC1 and hNaCT cDNA and in Caco-2 cells (Figure 2.8).

Succinate and citrate transport mediated by hNaDC1 expressed in HRPE cells was unaffected by Li^+ (Figure 2.8A). In contrast, succinate and citrate transport by HRPE cells transfected with hNaCT was stimulated approximately 3-fold by Li^+ (Figure 2.8B), consistent with previous findings (Inoue *et al.*, 2003). In Caco-2 cells, the addition of Li^+ did not significantly affect succinate or citrate transport (Figure 2.8C). Therefore, based on the relative transport of succinate and citrate, and lithium effect, Na^+-dependent transport of succinate and citrate in Caco-2 cells appears to be mediated predominantly by NaDC1, with some contribution by NaCT or another sodium-dependent transporter.

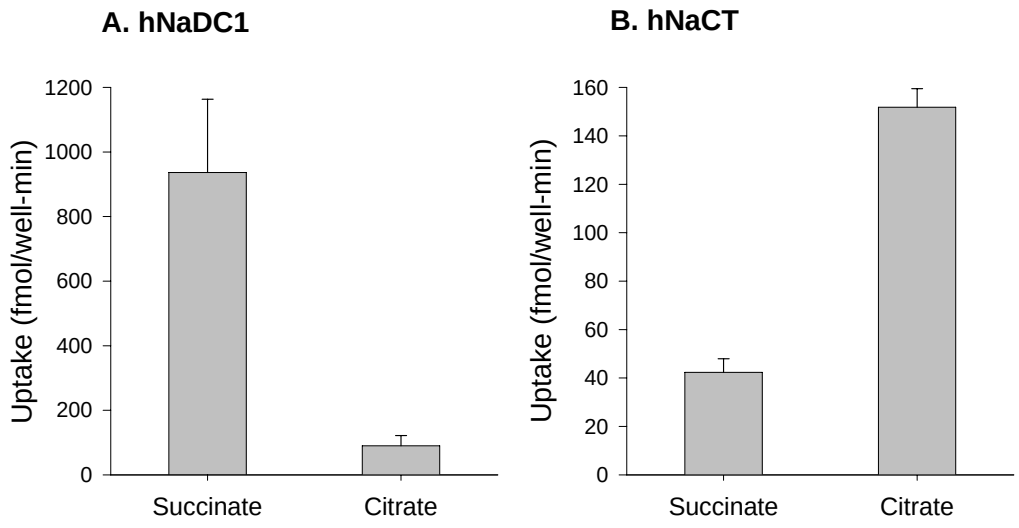

Figure 2.7 Transport of succinate and citrate by transfected HRPE cells with hNaDC1 or hNaCT in pcDNA3.1 vector and ratio of citrate to succinate transport in transfected HRPE cells and Caco-2 cells. Uptakes of 10 μM [^{14}C]succinate or [^{14}C]citrate in HRPE cells expressing hNaDC1 (A), or hNaCT (B) were measured in sodium- or choline-containing transport buffer as described in Material and Methods. Na^+-dependent transport was calculated from the difference between uptakes in sodium and choline. Data shown are the means ± range or S.E.M. (n= 2-8 separate transfection experiments).

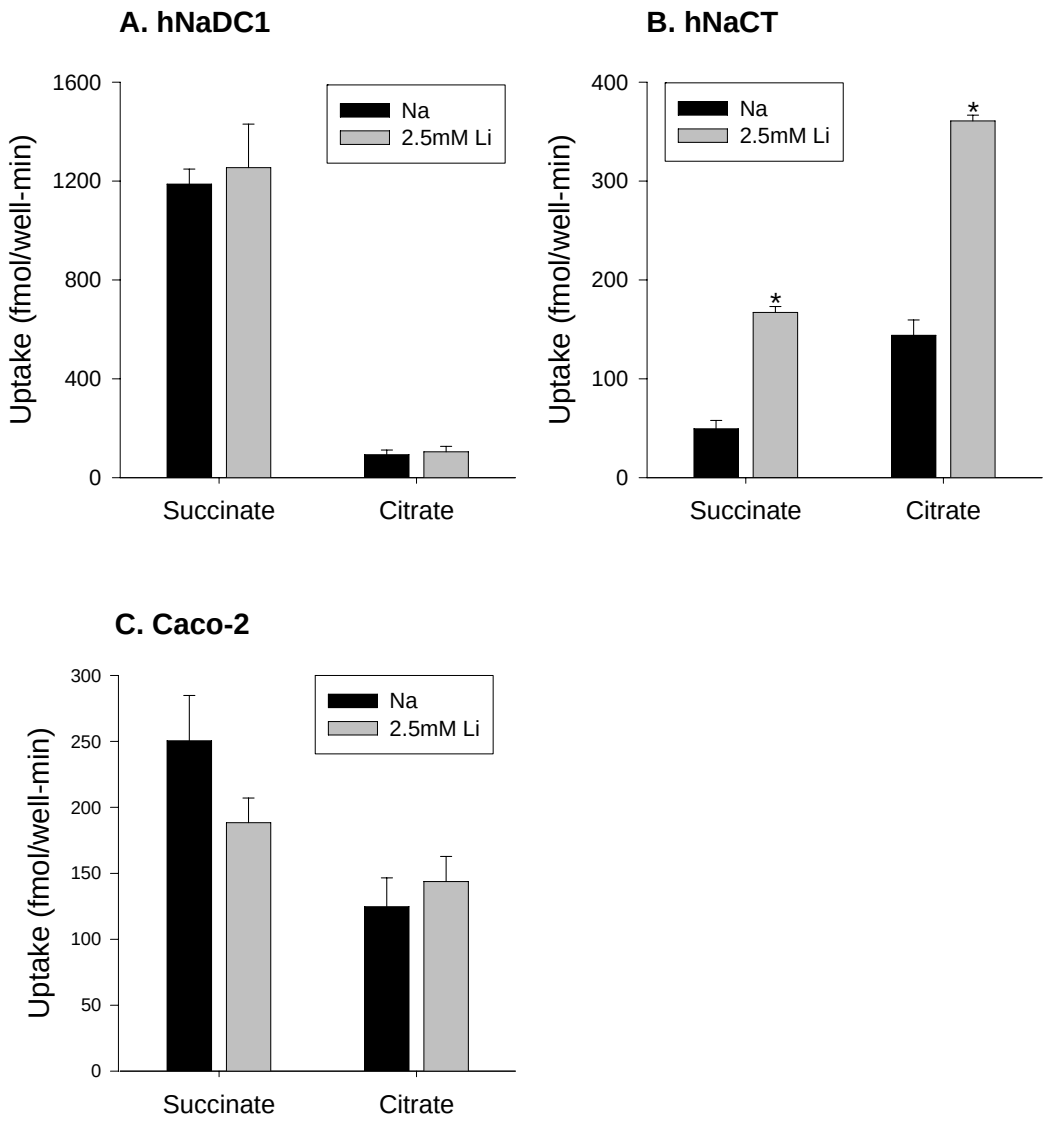

Figure 2.8 Effect of 2.5 mM Li^+ on succinate and citrate transport in transfected with hNaDC1 or hNaCT and Caco-2 cells. Uptakes of 10 μM [^{14}C]succinate or [^{14}C]citrate were measured in the presence and absence of 2.5 mM Li^+ containing sodium or choline transport buffer in HRPE cells transfected with hNaDC1 (A), hNaCT (B) cDNA or Caco-2 cells (C). hNaDC1 and hNaCT-mediated transport were corrected for background uptakes in cells transfected with vector only (pcDNA3.1). The data shown are the means ± range or S.E.M. of 2-8 separate experiments. * $p< 0.05$, significantly different from the uptakes in control group.

Na^+-independent citrate transport in Caco-2 cells

There have been no reports in the literature of sodium-independent transporters for citrate. Since other dicarboxylates, such as α-ketoglutarate and glutarate, are carried by the organic anion transporters or OATs (Koepsell & Endou, 2004; Wright & Dantzler, 2004), the substrate specificity of the sodium-independent citrate transport pathway was examined by using test inhibitors, particularly inhibitors of the OAT family. Na^+-independent citrate transport in Caco-2 cells was inhibited by other di- or tricarboxylates including citrate, methylsuccinate and glutarate, but not by succinate (Figure 2.9). Citrate transport was also inhibited by probenecid, bumetanide and *p*-amino-hippurate (PAH) which are substrates of the known OATs (Hasannejad *et al.*, 2004; Hosoyamada *et al.*, 1999; Kobayashi *et al.*, 2005; Sweet *et al.*, 2003). Moreover, citrate transport was inhibited by substrates of OAT4 including taurine, and estrone sulfate (Cha *et al.*, 2000; Ekaratanawong *et al.*, 2004; Benyajati & Pritchard, 2005). However, citrate transport was not inhibited by rifampicin, which rules out other organic anion transporters, including OATPs, as potential transporters (Hagenbuch & Meier, 2004). Furthermore, citrate transport was insensitive to phosphate, aspartate, or sulfate. These results are consistent with the functional characteristics of OAT transporters, possibly OAT2 and OAT4, mediating sodium-independent transport of citrate in Caco-2 cells.

RT-PCR analysis of organic anion transporters

Since the inhibitor experiment suggested that the Na^+-independent transport of citrate might be mediated by OAT2 and OAT4, a further experiment was performed to test whether these transporters are expressed in Caco-2 cells using RT-PCR with

sequence-specific primers. Previous studies indicate that OAT transporters are not expressed in human and rat small intestine (Cha *et al.*, 2000; Cha *et al.*, 2001; Hosoyamada *et al.*, 1999; Sekine *et al.*, 1998b), and these findings were verified here (Figure 2.10). In contrast, RT-PCR reactions with Caco-2 cells produced positive signals with OAT2 and OAT4 primers, consistent with the mRNA expression profile of OATs in Caco-2 cells (Seithel *et al.*, 2006). There were multiple products with the OAT3 primers, which may or may not represent a positive signal. Therefore, OAT2 and OAT4 may be the transporters responsible for Na^+-independent transport of citrate in Caco-2 cells.

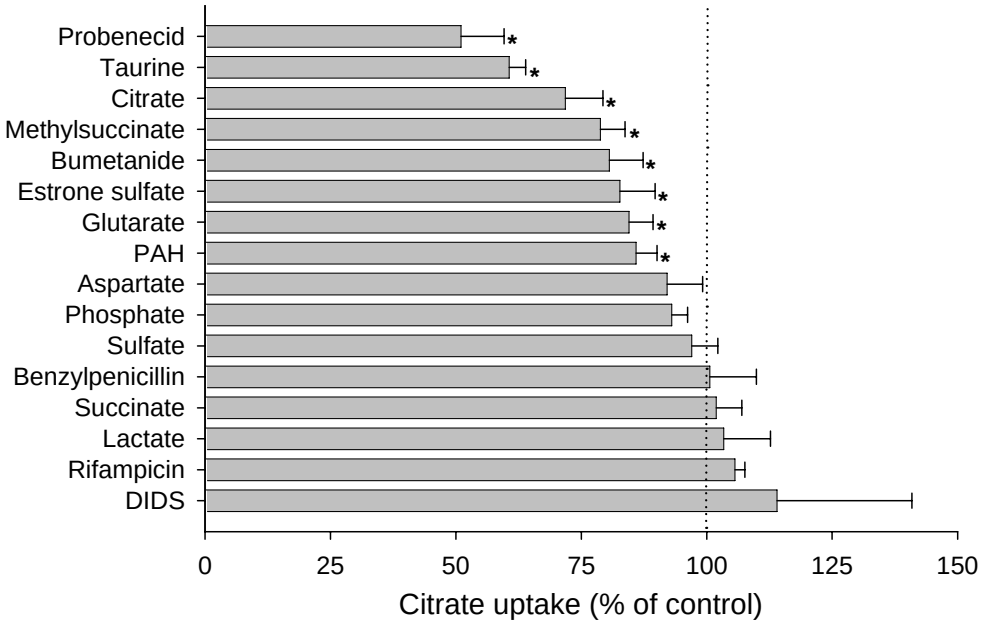

Figure 2.9 Substrate specificity of Na^+-independent citrate transport in Caco-2 cells. Caco-2 cells were plated at a density of 2×10^5 cells/well and grown onto 24 well plates. Uptakes of 10 μM [^{14}C]citrate transport in Caco-2 cells were measured in choline buffer in the absence (control) or presence of the indicated test inhibitors or substrates. Inhibitor concentrations were 1 mM, except for 4,4′-diisothiocyanostilbene-2,2′-disulfonic acid (DIDS, 0.1 mM) and p-aminohippuric acid, (PAH, 5mM). The data are expressed as a percentage of control in the absence of test inhibitor. Data shown are means ± range or S.E.M. of 2-8 experiments. * $p<$ 0.05, significantly different from the uptakes in control group without test inhibitors.

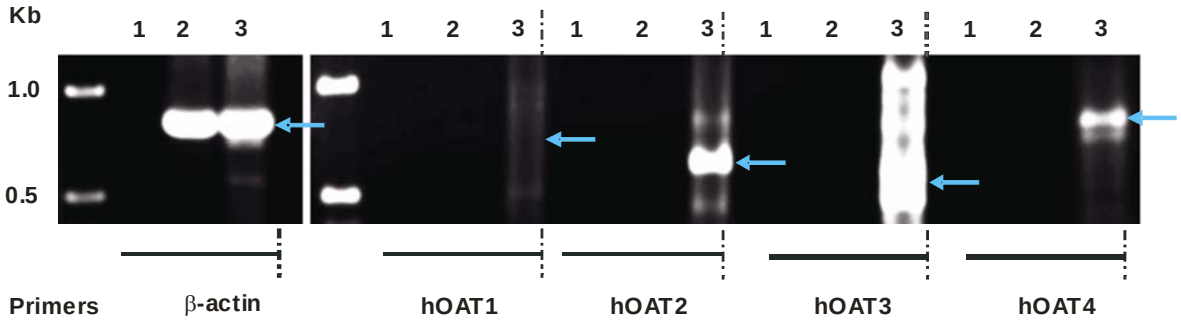

Figure 2.10 RT-PCR analysis of human organic anion transporters (hOATs) in human intestine (lane 2) and Caco-2 cells (lane 3). Controls containing water in place of primers are in lane 1. Control amplification with β-actin primers was performed in parallel. Size standards are shown in leftmost lane. Arrows show the expected size of PCR products. Bothe OAT2 and OAT4 were confirmed and verified by sequencing.

Transepithelial transport and intracellular accumulation of methylsuccinate by Caco-2 cells

In initial experiments, the transepithelial fluxes of succinate and citrate were too low to measure accurately. Therefore, the transport of the non-metabolizable substrate, methylsuccinate, in Caco-2 cells grown on permeable supports was tested. Methylsuccinate is a known substrate of NaDC1 (Yao & Pajor, 2000) and OAT4 (Benyajati & Pritchard, 2005). In the apical to basolateral direction, methylsuccinate accumulation in the cell across the apical membrane exhibited both sodium-dependent and -independent components, whereas transepithelial methylsuccinate fluxes across the epithelium were only sodium-independent (Figure 2.11A).

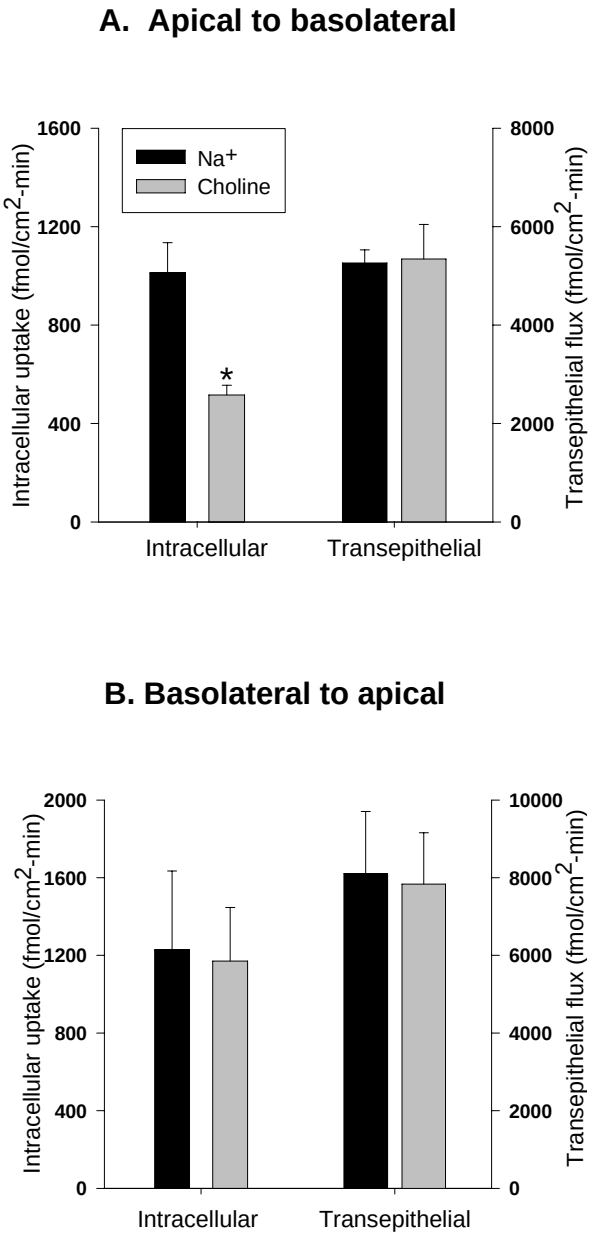

Figure 2.11 Transepithelial transport of [^{3}H]methylsuccinate by Caco-2 cells grown on permeable supports (at a density of 2×10^5 cells/6.5 mm insert). Intracellular accumulation and transepithelial transport of [^{3}H]methylsuccinate (100 μM) were determined in the apical to basolateral (A) or basolateral to apical direction (B). Uptake was measured in sodium and choline buffers as described in Material and Methods. Mannitol fluxes in each direction were similar. Data are the means ± S.E.M, n = 3 independent experiments. * $p < 0.05$, significantly different from the uptakes in sodium group.

In the basolateral to apical direction, both the intracellular accumulation and transepithelial flux were only sodium-independent (Figure 2.11B). The rate of transepithelial transport from the basolateral to apical side of the membrane was approximately double that in the apical to basolateral direction. In a single experiment, cellular accumulation of methylsuccinate across the basolateral membrane was not affected by the organic anion transport inhibitors, DIDS (0.1 mM) or bumetanide (1 mM) (Figure 2.12).

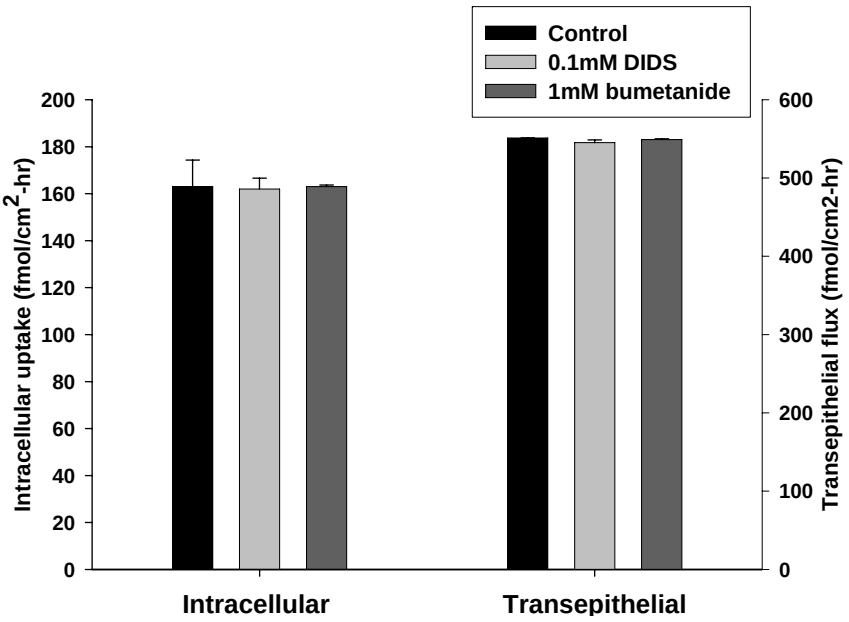

Figure 2.12 Effect of organic anion inhibitor on transepithelial methylsuccinate fluxes and cellular accumulation across basolateral membrane by organic anion inhibitors by Caco-2 cells grown on permeable supports (at a density of 2×10^5 cells/6.5 mm insert). Transwell uptake was measured in choline buffer in the presence of 100 μM [^{3}H] methylsuccinate from basolateral to apical direction with or without organic anion transport inhibitors, DIDS (0.1 mM) and bumetanide (1 mM). Each data point represents mean ± S.E.M. of three transwells, from a single experiment.

DISCUSSION

In the current study, the transport pathways for di- and tricarboxylates in the Caco-2 cell line, originally derived from human colon carcinoma, have been examined. Succinate transport in Caco-2 cells appears to be almost entirely sodium-dependent with properties consistent with the low affinity Na^+/dicarboxylate cotransporter, NaDC1. Although NaCT is present in the cells, it probably does not contribute much to succinate transport. Citrate transport is mediated by a combination of sodium dependent and sodium-independent pathways, including NaDC1, NaCT and possibly OAT2 and OAT4. Transepithelial transport across Caco-2 monolayers was studied using the non-metabolizable dicarboxylate, methylsuccinate. Methylsuccinate is a substrate of NaDC1, but it is also carried by several sodium-independent transporters found on the apical and basolateral membranes.

The Na^+-dependent transport of succinate and citrate, and probably also methylsuccinate, across the apical membrane of Caco-2 cells was determined to be mediated by a combination of the Na^+/dicarboxylate cotransporter, NaDC1, and the Na^+/citrate cotransporter, NaCT. NaDC1 transports both succinate and citrate, with K_m values of 0.8 mM (succinate) and 7 mM (citrate) and similar V_{max} values in human (Pajor & Sun, 1996b). NaCT transports both succinate and citrate with similar K_m values of about 0.6 mM each in human and 38 μM each in mouse, but the V_{max} is approximately twofold higher for citrate than for succinate (Inoue *et al.*, 2002a; Inoue *et al.*, 2004). It was found that Caco-2 cells and human intestine contain NaDC1 protein and mRNA. Unlike normal human intestine, NaCT message is also present in Caco-2 cells. Functional assays indicate that both NaDC1 and NaCT are active in

Caco-2 cells. Na^+-dependent succinate transport in Caco-2 cells is approximately double that of citrate transport. In NaDC1 expressed in HRPE cells, succinate transport is about 8-fold higher than citrate, whereas in NaCT, succinate transport is less than half of citrate transport. Therefore, NaDC1 appears to be the predominant Na^+-dependent transporter in Caco-2 cells, with some contribution by NaCT, particularly to citrate transport.

In addition to the Na^+-dependent transport systems, the apical membrane of Caco-2 cells contains one or more Na^+-independent citrate transport pathways. Previous studies have shown that organic anion transporters, OAT, transport dicarboxylates such as α-ketoglutarate, glutarate and methylsuccinate in a Na^+-independent manner (Ekaratanawong *et al.*, 2004; Kobayashi *et al.*, 2005; Benyajati & Pritchard, 2005). RT-PCR analysis showed that mRNA for both OAT2 and OAT4 are found in Caco-2 cells, unlike normal human intestine which does not express OAT1-4 (Cha *et al.*, 2000; Cha *et al.*, 2001; Hosoyamada *et al.*, 1999; Sekine *et al.*, 1998b). Functional assays indicate that OAT4 is a possible candidate for the citrate transporter on the apical membrane of differentiated Caco-2 cells since citrate transport was inhibited by bumetanide, taurine and estrone sulfate, all of which are OAT4 substrates (Ekaratanawong *et al.*, 2004; Hasannejad *et al.*, 2004; Benyajati & Pritchard, 2005). OAT4 is located on the apical membrane in renal proximal tubule and is thought to contribute to the first step in reabsorption of organic anion substances (Ekaratanawong *et al.*, 2004). OAT2 is also a likely candidate to transport citrate since it was inhibited by PAH (Kobayashi *et al.*, 2005; Sun *et al.*, 2001). I did not find inhibition of sodium-independent citrate transport by succinate although a previous study reported that succinate is transported by hOAT4 (Anzai *et al.*, 2005a).

The lack of inhibition could be explained by differences in affinity, but the definitive experiment will be to test whether OAT4 transports citrate. Verification of protein expression of OAT2 and OAT4 was attempted by Western blotting. However, commercially available OAT2 and OAT4 antibodies (Alpha Diagnostics) failed to recognize the native proteins in human kidney homogenate even at higher antibody concentrations.

Although there is experimental evidence for transepithelial transport of succinate and citrate in the small intestine, it was not possible to measure transepithelial fluxes of succinate and citrate across Caco-2 cells. The substrates could be metabolized within the cells or the transport rates are too low to measure accurately. The non-metabolizable dicarboxylate, methylsuccinate, was used to evaluate transepithelial transport. Transport of methylsuccinate across the apical membrane into the cell was both Na^+-dependent and -independent, possibly mediated by NaDC1 and OAT4, since both are known to transport methylsuccinate (Yao & Pajor, 2000; Benyajati & Pritchard, 2005). It is not known whether NaCT or other OATs transport methylsuccinate. Transport of methylsuccinate across the basolateral membrane of Caco-2 cells grown on permeable supports is completely sodium-independent and not sensitive to inhibitors such as bumetanide or DIDS, ruling out an OAT transporter and indicating the presence of another sodium-independent transporter. Methylsuccinate is likely to exhibit net secretion, since the transepithelial flux from the basolateral to apical side is greater than from the apical to basolateral.

A model of the possible transport pathways for succinate, citrate and methylsuccinate in Caco-2 cells was shown in Figure 2.13. The sodium-dependent uptake of di-and tricarboxylates across the brush border membrane into the cells

occurs primarily by the activity of NaDC1, with some contribution from NaCT. The energy for the sodium-dependent transport comes from the inwardly-directed electrochemical gradient for sodium, maintained by the Na^+/K^+-ATPase at the basolateral membrane. One or more sodium-independent transporters for citrate and methylsuccinate, possibly OAT2 and/or OAT4, are also located on the apical membrane. Bidirectional transport of methylsuccinate across the basolateral membrane occurs on an unknown transporter that is not likely to be a member of the OAT family.

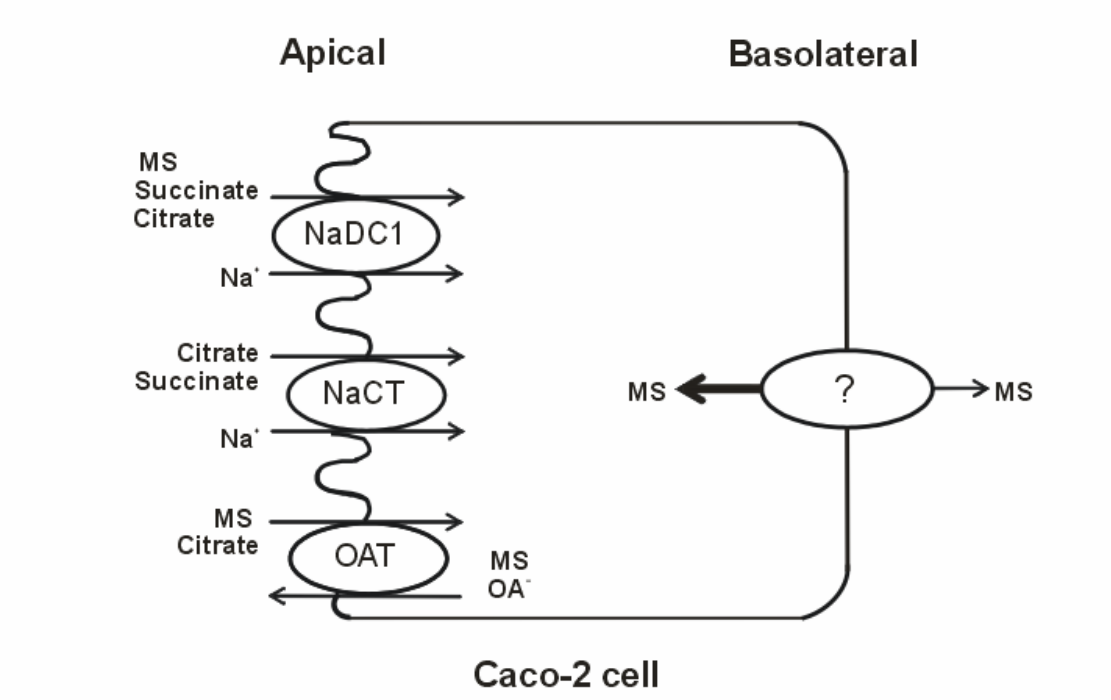

Figure 2.13 Model for transport of di- and tricarboxylates by Caco-2 cells. The Na^+/dicarboxylate cotransporter (NaDC1) on the apical membrane transports succinate, methylsuccinate (MS) and divalent citrate. The Na^+-coupled citrate transporter (NaCT) transports succinate and trivalent citrate. An organic anion transporter, probably OAT4, transports citrate and methylsuccinate in exchange for organic anions (OA^-). The basolateral membrane contains an unknown sodium-independent transporter for methylsuccinate.

In conclusion, this study demonstrates that multiple transport pathways are involved in transport of citric acid cycle intermediates in differentiated Caco-2 cells. The apical membrane of Caco-2 cells contains at least three transport systems, both Na^+-dependent and -independent, for di- and tricarboxylates. The Na^+-dependent pathways include NaDC1 and NaCT, and the Na^+-independent transporters are possibly the OAT2 or OAT4 organic anion transporters. There is also a Na^+-independent transporter on the basolateral membrane. RT-PCR experiments show that Caco-2 cells express different dicarboxylate and organic anion transporters than human small intestine. Although the Caco-2 cells may be useful for studying succinate transport by NaDC1 *in vitro*, their suitability as a model for studying citrate and methylsuccinate transport is limited since these cells express transporters that are not found in native intestine. The difference between Caco-2 cells and normal intestine could reflect the transformed state of the Caco-2 cells, resulting in altered metabolism, gene expression and phenotypes (Anderle *et al.*, 2003). In normal human intestine expression of a number of genes is markedly different from that in Caco-2 cells (Anderle *et al.*, 2003). For example, a high-affinity isoform of the glucose transporter (GLUT3) is more highly expressed in Caco-2 cells than in normal human intestine tissue. In addition, it was suggested that the decrease of GLUT3 mRNA expression upon differentiation, is compatible with a phenotype change from colon-carcinoma-like into a non-tumor like epithelial cell (Anderle *et al.*, 2003).

CHAPTER 3: SODIUM-DEPENDENT EXTRACELLULAR ACCESSIBILITY OF LYS-84 IN THE SODIUM/ DICARBOXYLATE COTRANSPORTER

(Studies in this chapter have been reproduced from: Weerachayaphorn J. and Pajor A. M (2007). Sodium-dependent extracellular accessibility of Lys-84 in the sodium/dicarboxylate cotransporter. *J Biol Chem* 282 (28): 20213-20220)

INTRODUCTION

The current secondary structure model of NaDC1 contains 11 transmembrane helices (TM) with an extracellular carboxy terminus containing a site for N-linked glycosylation, and the amino terminus facing the cytoplasmic side of the membrane (Zhang & Pajor, 2001). Many of the functionally important residues for substrate and cation recognition are located in the carboxy-terminal half of protein (Pajor *et al.*, 1998b; Kahn & Pajor, 1999). In addition, Pajor and colleagues have identified amino acids in TM9 and the connecting loop whose accessibility to extracellular reagents changes during the transport cycle (Pajor, 2001; Pajor & Randolph, 2005). The amino-terminal half of the protein, in particular TM3, appears to be important in determining substrate specificity and affinity. For example, glutarate transport is determined primarily by residues found in TM3 -TM4 (Oshiro *et al.*, 2006). The sequence of TM3 and the connecting loops is highly conserved in the SLC13 family (Fig.1). Lys-84, predicted to be in an intracellular loop at the base of TM3, was found to be important for succinate transport since replacement of Lys-84 with Ala produced a large decrease in succinate affinity (Pajor *et al.*, 2000). His-106, at the extracellular part of TM3, is required for proper targeting of NaDC1 to the membrane (Pajor *et al.*, 1998c).

In the present study the amino acids in the extracellular half of TM3 from Ile-98 to Arg-112, as well as Lys-84, were investigated using the substituted-cysteine accessibility method used to study structure-function relationships in ion channels and transporters (Javitch, 1998; Karlin & Akabas, 1998). A total of sixteen residues in NaDC1 were mutated one at a time to cysteine and the sensitivity of the substituted cysteines to the membrane-impermeant cysteine-specific reagents, (2-sulfonatoethyl)methanethiosulfonate (MTSES) and [2-(trimethylammonium)ethyl]-methane-thiosulfonate (MTSET), was then determined. TM3 in NaDC1 contains several residues involved in substrate recognition, K84, E101, W103, H106 and L111, since their mutation to cysteine resulted in a change in Transport Specificity Ratio (TSR). Of all the mutants, only K84C was sensitive to inhibition by MTSES, with differences in accessibility that parallel the exposure of the substrate binding site in NaDC1. The substrate protection of MTSES inhibition of K84C appears to occur early in the transport cycle, before the large-scale conformational change associated with translocation of substrate. The results indicate a new location for Lys-84, either in the transmembrane helix facing a water-filled pore in or in a reentrant loop accessible to the outside.

MATERIALS AND METHODS

Construction of TM3 Cysteine Mutants

The cysteine mutants were made using the PCR-based QuikChange site-directed mutagenesis kit (Stratagene) according to the manufacturer's instructions. The C476S mutant of rbNaDC1 in pcDNA3.1 vector was used as a template for mutagenesis. The rbNaDC1 contains an endogenous cysteine at position 476 that is

sensitive to labeling by some cysteine-specific reagents such as *p*-chloromercuribenzesulfonate (pCMBS) (Pajor *et al.*, 1999), although it is insensitive to hydrophilic methanethiosulfonate reagents such as [2-(tri-methylammonium) ethyl] methane-thiosulfonate (MTSET) (Pajor, 2001). The cell surface expression of NaDC1 is related to the number of cysteines (Pajor *et al.*, 1999) and the C476S mutant (containing 10 of the 11 endogenous cysteines) was used to allow increased protein expression of the cysteine-substituted mutants, since the mutations can sometimes result in decreased activity. Previous study showed that cysteine mutants made in the C476S background had the same results as constructs containing only 3 endogenous cysteines, but the protein expression and transport activity were higher in the C476S background (Pajor, 2001; Pajor & Randolph, 2005). The cDNA sequences of mutants were verified by sequencing at the Protein Chemistry Laboratory at the University of Texas Medical Branch, using an Applied Biosystems Model 3100 automated DNA sequencing unit.

Expression of TM3 Mutants in HRPE Cells

Human retinal pigment epithelial (HRPE) cells transformed with SV40 (AG 06096; Coriell Institute), were cultured in Modified Eagle's Medium (MEM) containing Glutamax and 25 mM HEPES (Invitrogen) supplemented with 10% heat-inactivated fetal calf serum, 100 units/ml penicillin and 100 µg/ml streptomycin. Cells were incubated at 37 °C in 5% CO_2. Since HRPE cells have no endogenous Na^+/dicarboxylate cotransporters and provide a low background of radioactivity, HRPE cells were used in this study. HRPE cells were plated in 24-well plates for transport assays, at a density of 1.2×10^5 cells/well, or 6-well plates for biotinylation

reactions, at a density of 1.5×10^5 cells/well. Twenty-four hours after seeding, cells were transiently transfected with 1.8 μl of FuGENE6 (Roche Applied Science) and 0.6 μg of plasmid DNA (9:3 ratio) for 24-well plates, or with 3 μl of FuGENE6 and 1 μg of plasmid (3:1 ratio) for 6-well plates (Pajor & Randolph, 2005).

Transport Assays

Succinate and citrate transport assays were carried out 48 hours after transfections, as described previously (Pajor & Randolph, 2005). For the standard assay, each well was washed twice with 1 ml of sodium buffer containing 120 mM NaCl, 5 mM KCl, 1.2 mM $MgSO_4$, 1.2 mM $CaCl_2$, 5 mM D-glucose, 25 mM HEPES, pH adjusted to 7.4 with 1 M Tris. Transport was measured by incubating the cells with 250 μl of sodium buffer containing 100 μM succinate (combination of [^{3}H]succinate (ViTrax) and non-radioactive succinate). For citrate kinetic measurements, a combination of [^{14}C]citrate (Amersham GE Healthcare) and non-radioactive citrate were used. The surface radioactivity was removed with five washes of 1 ml sodium buffer and lysed in 250 μl of 1% SDS for 60 min, then transferred to scintillation vials for liquid scintillation counting. The uptake rates were corrected for background counts in control cells transfected with pcDNA3.1 vector alone. Kinetic constants were calculated by nonlinear regression to the Michaelis-Menten equation using SigmaPlot 2000 software (Jandel Scientific).

Dual-label Competitive Transport Experiments

For dual-label transport assays sodium buffer containing both 10 μM [^{3}H]succinate and 20 μM [^{14}C]citrate was added to the cells in 24 well plates and

competitive transport of these substrates was measured, as described previously (Joshi & Pajor, 2006). The transport specificity ratio (TSR) was calculated using: $TSR = (\nu_{succinate} / \nu_{citrate}) \times ([citrate] / [succinate])$ where $\nu_{succinate}$ and $\nu_{citrate}$ are the rates of transport of [^{3}H]succinate and [^{14}C]citrate, [citrate] and [succinate] are the concentrations of citrate and succinate (King, 2004).

Chemical Labeling with MTSES

The NaDC1 mutants in HRPE cells were preincubated with 250 µl of 1 mM (2-sulfonatoethyl)methanethiosulfonate (MTSES; Toronto Research Chemicals) in sodium buffer. For experiments with 1 mM MTSES, the reagent was weighed out fresh for each experiment, kept on ice, and diluted in buffer just before using. For experiments with 10 µM MTSES, a stock solution of 5 mM MTSES in water was kept dark and on ice, and diluted in buffer just before using. Control groups were preincubated in sodium buffer without MTSES. After 20 min of incubation at room temperature (or ice, for temperature dependence experiment), the cell monolayers were washed three times with sodium buffer, then assayed for succinate transport activity as described above. For cation replacement experiments, choline buffer was substituted for sodium buffer and for substrate protection experiments; the incubation with MTSES was done in the presence or absence of 10 mM succinate.

Cell Surface Biotinylation and Total Protein Expression

Cell surface protein expression of NaDC1 was determined using a membrane impermeant biotin reagent, Sulfo-NHS-LC-biotin (Pierce), and the biotinylated

proteins were precipitated using ImmuoPure-immobilized streptavidin beads (Pierce), as described previously (Pajor *et al.*, 1998c) and shown in Figure 3.1. To determine intracellular protein abundance, the supernatants after centrifugation to separate the biotin-streptavidin-agarose bead complexes were transferred to new tubes. These samples were subjected to immunoblotting in parallel with the cell surface protein samples; the remaining procedures were identical to those in the cell surface biotinylation protocol, as described in Chapter 2.

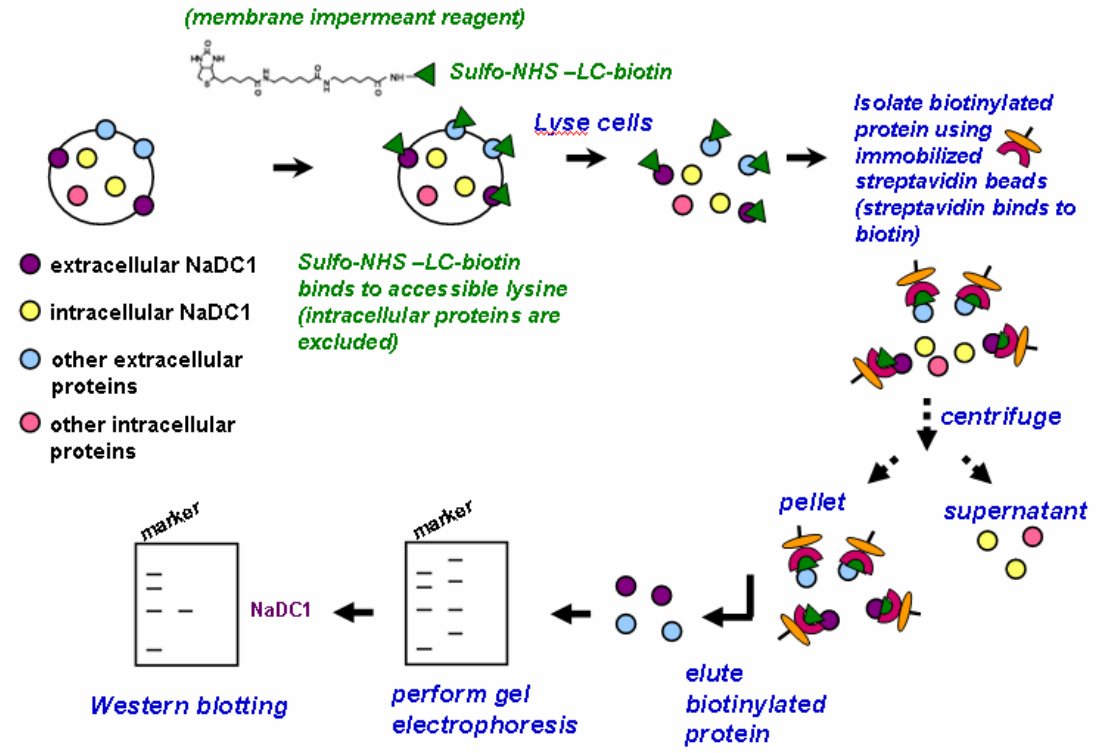

Figure 3.1 The flow diagram of cell surface and total protein expression of NaDC1. Sulfo-NHS-LC-biotin labels all proteins with extracellularly accessible lysine residues. After cells are lysed, biotinylated proteins were isolated using immobilized streptavidin beads, which bind to biotin. After centrifugation, biotinylated proteins (pellet), were eluted and separated by gel electrophoresis, followed by Western blotting to detect cell surface expression of NaDC1. The intracellular protein expression was determined from Western blot of non-biotinylated proteins (supernatant).

MTSEA-Biotinylation

HRPE cells expressing NaDC1 mutants were pretreated with sodium buffer with or without 1 mM MTSES for 20 min at room temperature. The MTSES was removed with 3 washes of 3 ml PBS/CM, pH 7.5 (phosphate buffered saline pH 7.5 with 1 mM Ca^{2+} and Mg^{2+}). For each experiment, a 200 mM stock solution of N-biotinaminoethyl methanethiosulfonate (MTSEA-biotin; Toronto Research Chemicals) was prepared in DMSO and kept cold and dark. The MTSEA-biotin was diluted to 2 mM with PBS/CM, pH 7.5 just before use and added to the cells for 30 min at room temperature with gentle rocking. The cells were rinsed with cold PBS/CM pH 7.5. The remaining procedures were identical to those in the cell surface biotinylation protocol, as described above.

Statistical analysis

Statistical analysis was performed using Student's *t*-test to compare two groups or a One-way Analysis of Variance (ANOVA) and the *post-hoc* Dunnett's multiple comparison method for multiple groups (SigmaStat program, Jandel Scientific). Statistically significant difference was considered to be $p < 0.05$.

RESULTS

Cysteine Scanning Mutagenesis of Conserved Residues in TM3

The sequence alignment of amino acids in NaDC1 with other members of the SLC13 family shows the highly conserved region predicted to form TM3 and the connecting loops (Figure 3.2). Fifteen amino acid residues from Ile-98 to Arg-112 as

well as Lys-84, previously reported to affect substrate binding (Pajor *et al.*, 2000), were selected for cysteine scanning mutagenesis in which the amino acids were replaced with cysteine one at a time.

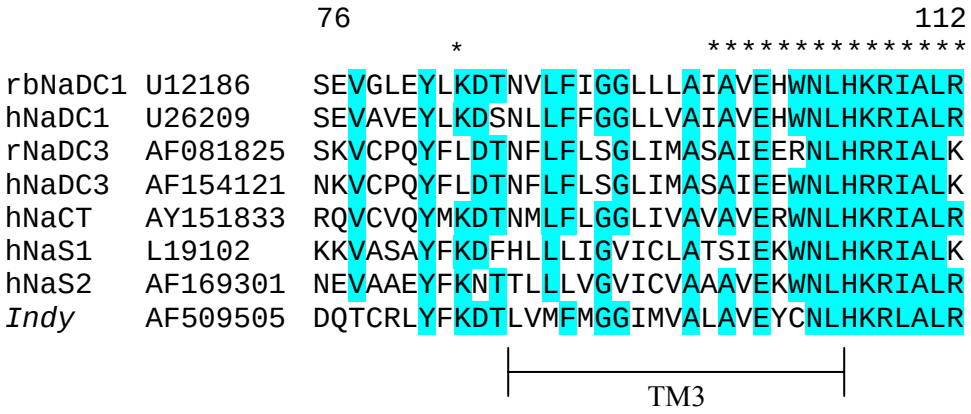

Figure 3.2 Multiple sequence alignment of TM3 and connecting loops in members of the SLC13 family. The amino acid numbering (76-112) is based on the rbNaDC1 sequence. The sequence alignment was performed using the ClustalW program (default parameters, Gonnet matrix). Other members of the SLC13 family include the high affinity Na^+/dicarboxylate cotransporters (NaDC3), Na^+/citrate cotransporter (NaCT), Na^+/sulfate cotransporters (NaS) and the *Drosophila* dicarboxylate exchanger (*Indy*). The Genbank™ accession numbers for nucleotide sequences are next to the names. Positions of conserved amino acid residues in the proteins are highlighted in grey. Amino acids in rbNaDC1 mutated in this study are indicated by * above the sequence. The amino acids before the predicted TM3 sequence are part of the intracellular loop connecting TM2 and 3.

Protein Expression and Transport Activity of Cysteine-Substituted Mutants

The cell surface expression of the mutants was monitored by biotinylation with the membrane impermeant reagent, Sulfo-NHS-LC-biotin, followed by Western blotting. Total intracellular expression of the mutant proteins was also determined. Figure 3.3 shows single representative blots of cell surface and total intracellular protein expression for each cysteine mutant compared with the parental transporter,

the C476S mutant of rbNaDC1. The two bands on the Western blots represent differently glycosylated forms of the transporter (Pajor *et al.*, 1998c). The blots were scanned to quantitate the protein expression, and each mutant was expressed as a percentage of the parental C476S protein abundance.

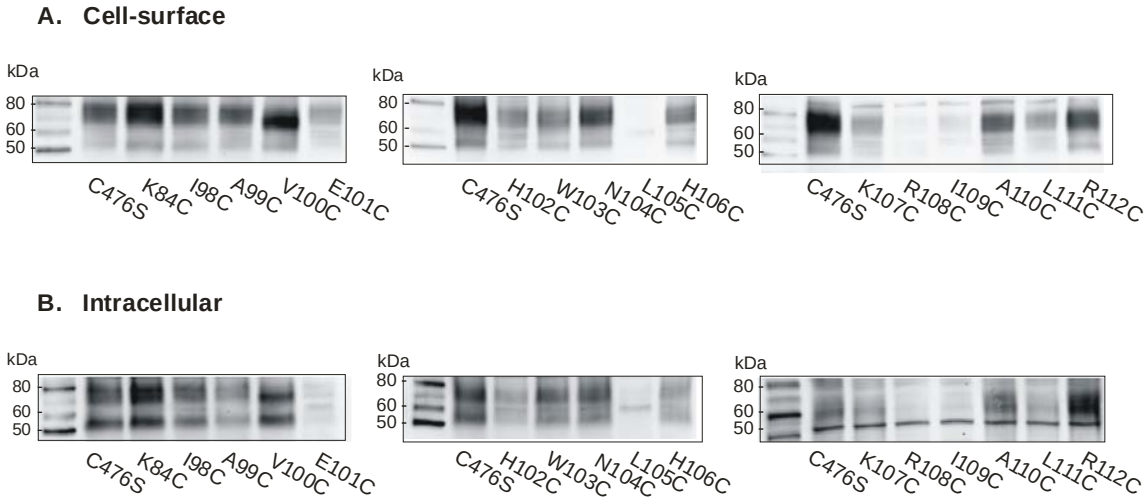

Figure 3.3 Western blots of (A) cell-surface and (B) total protein expression. HRPE cells expressing cysteine mutants were treated with Sulfo-NHS-LC biotin as described in "Materials and Methods". The upper panel shows the cell surface protein expression, and the lower panel shows the intracellular protein expression. Western blots were probed with anti-NaDC1 antibodies (1:1000 dilution). Each blot includes an internal control of the parental transporter, C476S. The positions of the molecular mass standard (MagicMark XP) are indicated on the left. Two immunoreactive bands at approximately 70 and 55 kDa represent differently glycosylated forms of rbNaDC1 (Pajor *et al.*, 1998c).

The succinate transport activity and protein expression of the mutants are summarized in Figure 3.4. Most of the cysteine substitutions were tolerated, as reflected in some measurable succinate transport activity in most of the cysteine mutants, approximately 30-75% activity compared with the parental C476S. The

majority of the mutants were expressed at the plasma membrane. Four of the mutants (V100C, L105C, R108C and A110C) were either entirely inactive or had activity that was less than 5% of the parental transporter activity. L105C was absent from the plasma membrane and there was little intracellular protein. R108C, was found to be absent from the plasma membrane although total intracellular expression was high, suggesting impairments in protein trafficking or stability. The other two mutants, V100C and A110C, were completely inactive despite a high level of cell surface expression, implying that these two residues have functionally important roles in succinate transport in NaDC1.

Transport Specificity Ratio (TSR) Analysis of Cysteine Mutants

Transport specificity ratio (TSR) analysis was used to detect substrate-selective perturbations in catalytic specificity in the cysteine mutants. TSR is a method to compare the effects of site-directed mutagenesis on function by monitoring relative changes in catalytic efficiency (k_{cat}/K_m) of two substrates (King, 2004). One great advantage to TSR analysis is that it is independent of protein expression, so that mutants with low expression can be analyzed even when the expression is too low for kinetic analysis. TSR is also valid over a wide range of substrate concentrations (King, 2004). To investigate whether substrate specificity determinants exist within TM3, cells expressing cysteine mutants with measurable transport activity were assessed by measuring competitive uptakes of [^{3}H]succinate and [^{14}C]citrate (Figure 3.5A). The succinate:citrate transport specificity ratios (TSR) of most cysteine mutants and the C476S parental transporter were approximately 3 (Figure 3.5B) similar to wild type rbNaDC1 (Joshi & Pajor, 2006). Five mutants showed

significant increases in TSR: K84C, E101C, W103C, H106C and L111C (Figure 3.5B). Consequently, these 5 residues might play an important role in distinguishing succinate from citrate in NaDC1.

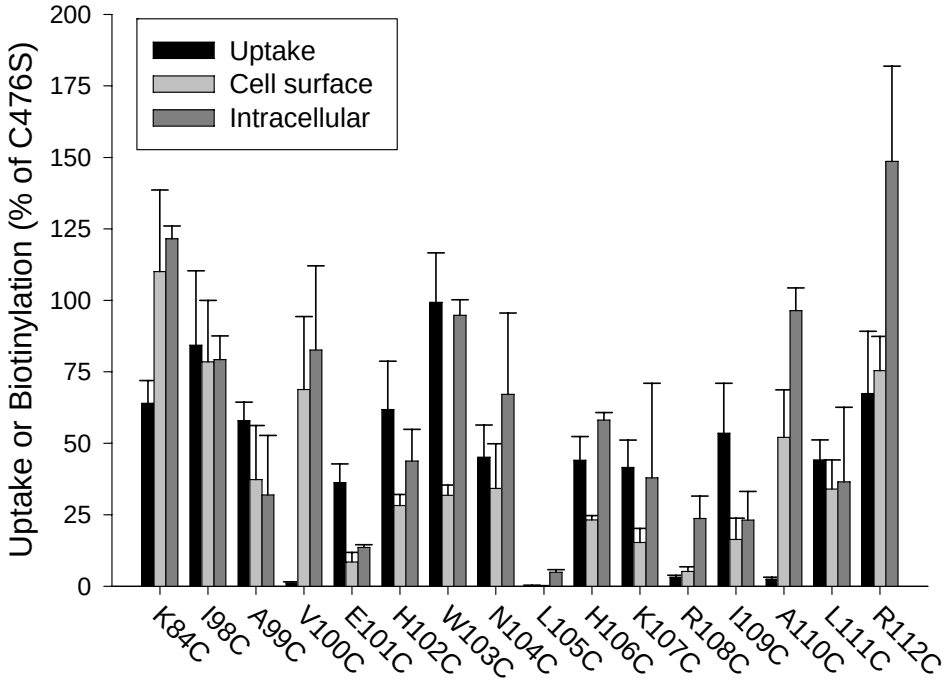

Figure 3.4 Transport activity and protein expression of cysteine-substituted mutants. The data were shown as a percentage of the C476S control from the same blot or uptake experiment. Transport of 100 μM [^{3}H]succinate was measured with 30 min incubation in sodium containing buffer. Transport results shown are mean ± S.E.M. (n = 3-11). Protein abundance was determined by quantitating the intensities of NaDC1 protein bands from Western blots, such as those shown in Fig. 2. The bars represent mean ± range or S.E.M. (n = 2-4 blots, separate transfections).

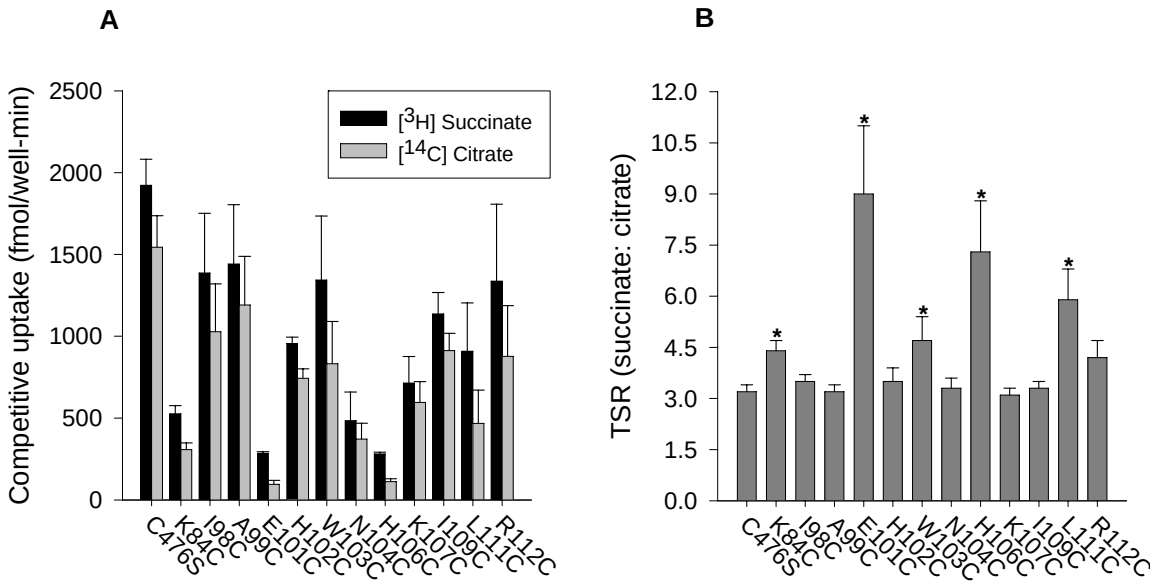

Figure 3.5 Dual-label competitive transport of cysteine-substituted NaDC1 mutants. (A) Competitive uptake of [^{3}H]succinate (10 μM) and [^{14}C]citrate (20 μM) by cysteine-substituted mutants. HRPE cells were plated on 24-well plates at a density of 1.2×10^5 cells/ well, and were then transfected with plasmid DNA of cysteine mutants. The transport assay was performed for 20 min. (B) Transport specificity ratios (TSR succinate: citrate) of NaDC1 mutants, calculated from data shown in (A). Bars are mean ± S.E.M. (n = 4). * $p <$ 0.05, significantly different from C476S control group.

Functional Characteristics of Cysteine Mutants

The kinetics of succinate and citrate transport were measured in the cysteine mutants showing differences in TSR (K84C, E101C, W103C, H106C and L111C). The time courses of uptake were measured between 1-10 min (Figure 3.6). 6 min uptakes were chosen for subsequent kinetic study.

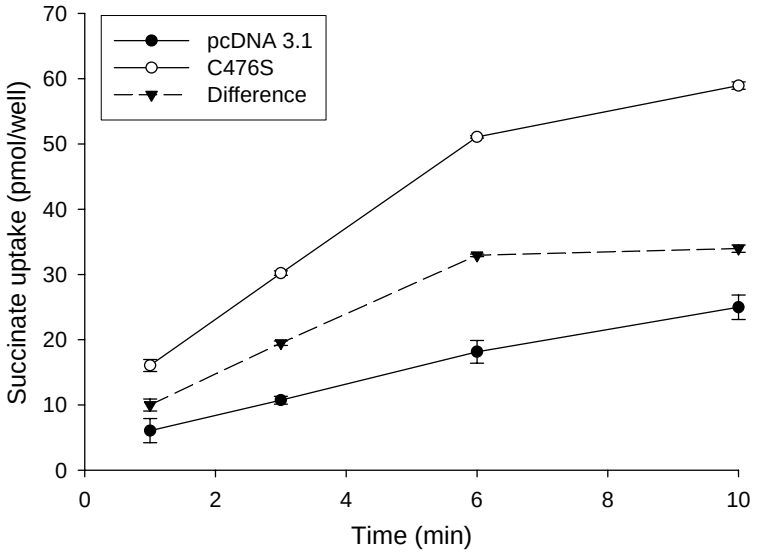

Figure 3.6 Time dependence of uptake of succinate by HRPE cell expressing the C476S mutant. Monolayers were incubated with 1mM [^{3}H]succinate in sodium buffer at variable incubation times. Each value represents the mean ± range of two determinations.

As shown in Table 3.1, the mean apparent K_m for succinate in K84C, W103C, H106C, and L111C was similar to that of the parental C476S transporter (the single experiments are shown in Figure 3.7). The K_m in E101C was significantly greater than the parental, by approximately 2-fold. There were no significant differences between succinate V_{max} values in any of the mutants compared with the parental C476S transporter. However, the decreased cell-surface protein abundance in E101C, W103C, H106C and L111C (Figure 3.4) indicates that the succinate k_{cat} values of these mutants are likely to be increased relative to C476S.

There were differences in citrate kinetics between the substituted-cysteine mutants and the C476S parental transporter (Table 3.1, the single experiments are shown in Figure 3.8). All of the mutants had increased citrate K_m values compared with C476S. Two of the mutants, E101C and H106C, also had much lower V_{max}

values, which were comparable to the abundance of these transporter proteins on the plasma membrane (Figure 3.4). The increased TSR in the K84C, E101C, W103C, H106C and L111C mutants indicates an increase in relative catalytic efficiency (k_{cat}/K_m) of succinate compared with citrate. Therefore, for many of the mutants, the TSR value reflects a combination of an increased catalytic efficiency for succinate and a decreased catalytic efficiency for citrate.

It should be noted that the succinate K_m value in C476S in the present study is about 10-fold lower than Pajor and colleages have previously reported. The succinate K_m in wild-type rbNaDC1 is similar to that of C476S when expressed in HRPE cells, and the succinate:citrate TSR values are also similar. Under two-electrode voltage clamp conditions, the K_m for wild-type rbNaDC1 expressed in *Xenopus* oocytes is around 180 μM at -50 mV (Pajor *et al.*, 1998a). In radiotracer uptake assays with *Xenopus* oocytes, not under voltage-clamp, the K_m for wild-type rbNaDC1 or the C476S mutant is between 0.2-0.5 mM (Griffith & Pajor, 1999; Pajor, 2001). Pajor and colleages have previously measured a K_m of 0.5 mM for wild-type NaDC1 expressed in HRPE cells (Joshi & Pajor, 2006). At present it is unknown why the K_m values in this study are lower than in our previous studies. The cDNA has been resequenced to make sure there are no mutations, both authors of this paper have done kinetic measurements of C476S and obtained similar results, and the effects of transport conditions (time points, preincubations) and cell passage number have tested. The effect may be specific to the rbNaDC1 ortholog since the succinate K_m for hNaDC1 expressed in HRPE cells is similar to that in oocytes, around 0.7 mM. All of the experiments reported in this study have compared mutant values with C476S in the same transfection experiment.

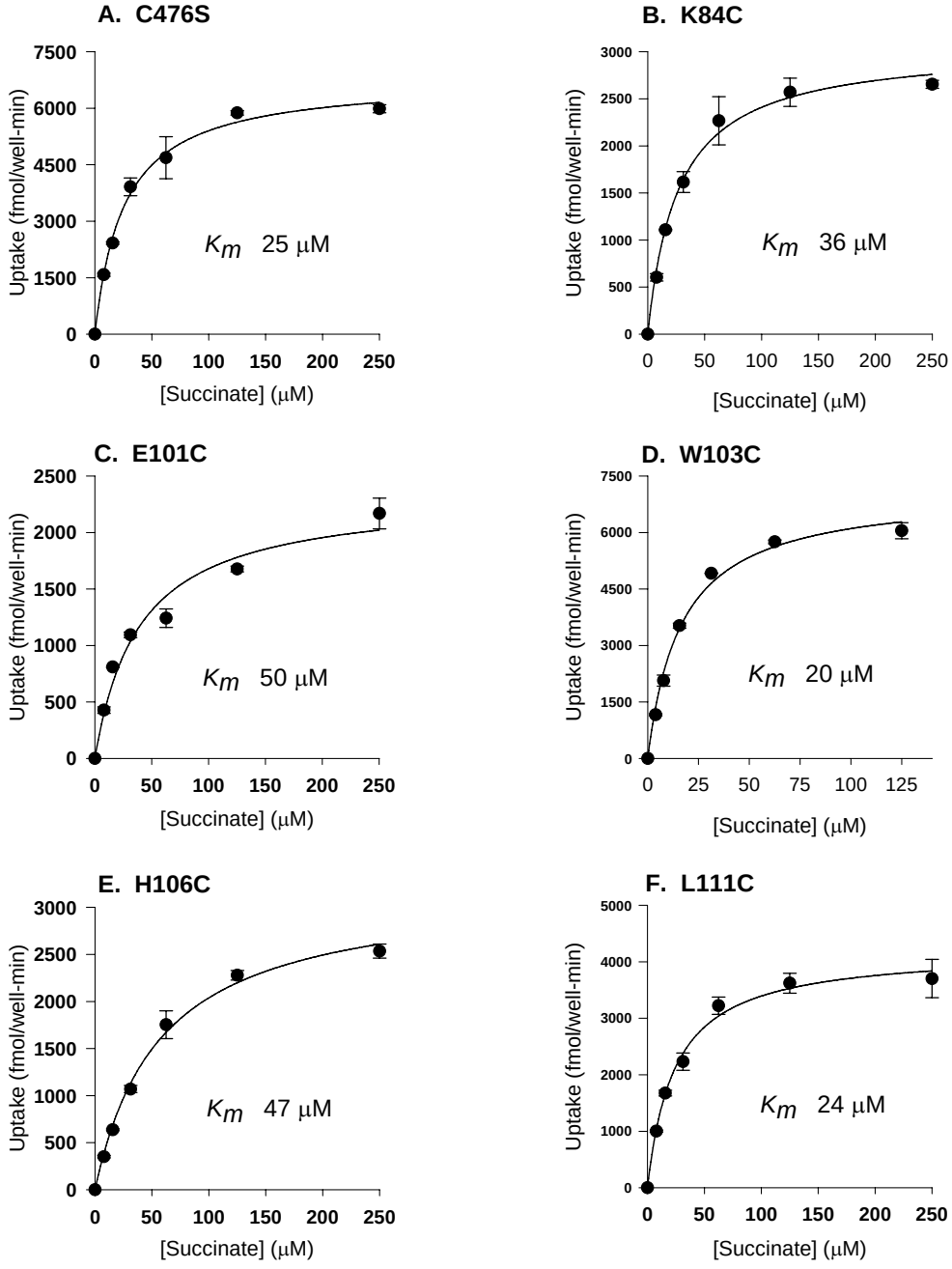

Figure 3.7 Succinate kinetics were determined in HRPE cells expressing cysteine substituted mutants showing change in TSR. Each data point shows the mean ± range of two determinations from a single experiment. The results of 3-5 separate experiments are shown in Table 3.1.

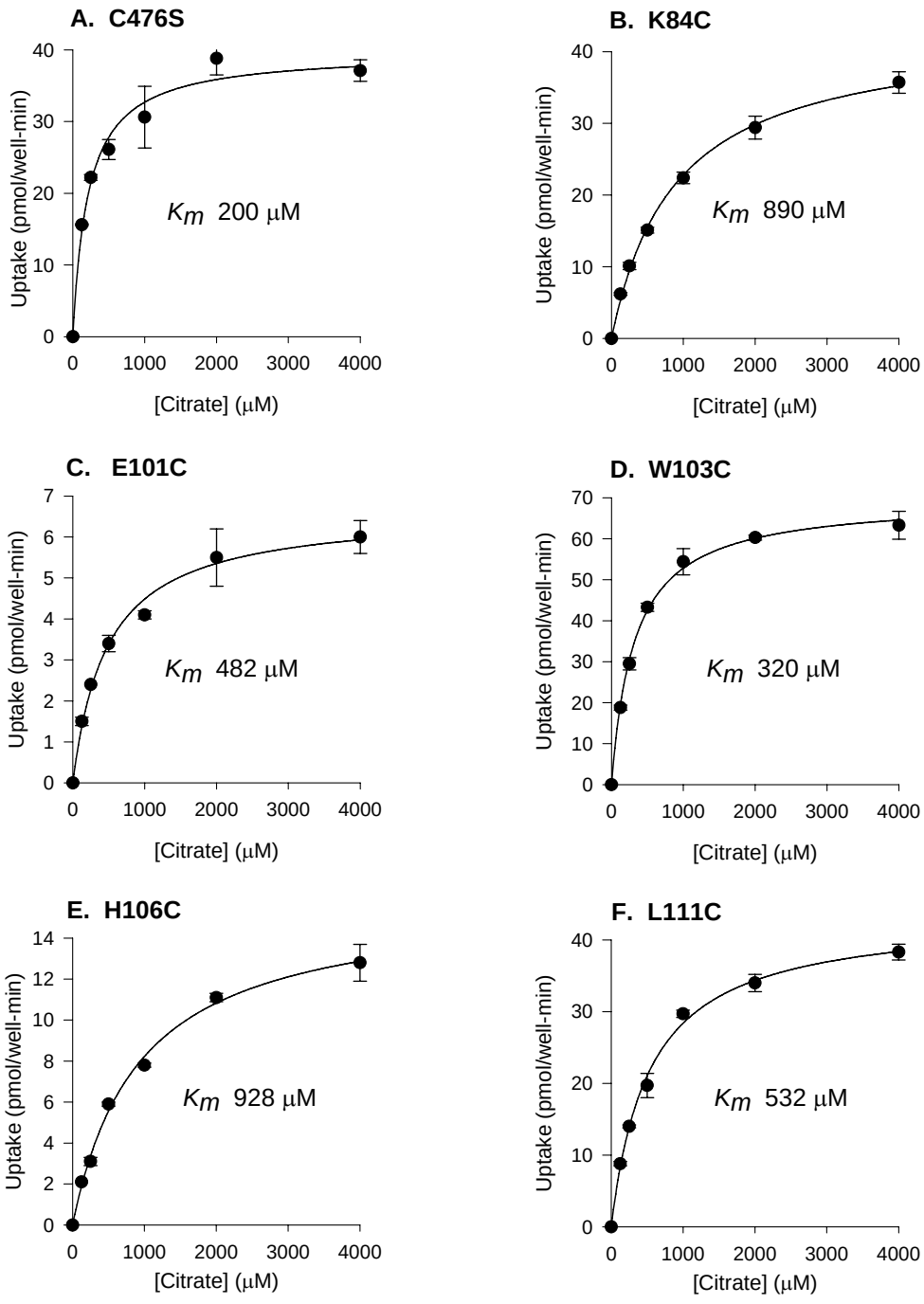

Figure 3.8 Citrate kinetics were determined in HRPE cells expressing cysteine substituted mutants showing change in TSR. Each data point shows the mean ± range of two determinations from a single experiment. The results of three separate experiments are shown in Table 3.1.

Table 3.1 Succinate and citrate kinetics in cysteine substituted mutants. The kinetics of succinate and citrate transport were determined in HRPE cells expressing the parental transporter, C476S, or the cysteine mutants exhibiting changes in TSR. Six minutes uptakes were measured. The kinetic values shown are the mean ± S.E.M., N is sample size. The * denotes significant difference compared with the parental C476S ($p< 0.05$) using ANOVA followed by Dunnett's test. Because of differences in transporter expression between the succinate and citrate kinetics experiments, the V_{max} values are shown relative to internal controls. The C476S V_{max} values are 7.9 (succinate) and 49.1 pmol/well-min (citrate).

NaDC1 mutant	Succinate kinetics			Citrate kinetics		
	K_m (μM)	V_{max} (% of C476S)	N	K_m (μM)	V_{max} (% of C476S)	N
C476S	25 ± 2	100 ± 40	5	203 ± 6	100 ± 12	3
K84C	36 ± 8	63 ± 33	3	617 ± 151*	78 ± 5	3
E101C	50 ± 4*	83 ± 31	4	672 ± 126*	16 ± 1*	3
W103C	20 ± 3	102 ± 44	3	372 ± 52*	111 ± 34	3
H106C	47 ± 8	42 ± 16	3	1075 ± 91*	36 ± 2*	3
L111C	24 ± 0.3	50 ± 6	3	487 ± 40*	74 ± 8	3

MTSES Sensitivity of Cysteine Mutants

The twelve cysteine mutants with measurable transport activity were screened for their sensitivity to the membrane impermeant thiol-reactive reagent, MTSES. The mutant T482C, which is highly sensitive to MTSET, MTSEA and MTSES (Pajor, 2001), was used as a positive control in each experiment. Out of all the TM3

mutants, only K84C showed a decrease in transport activity after chemical labeling with MTSES (Figure 3.9).

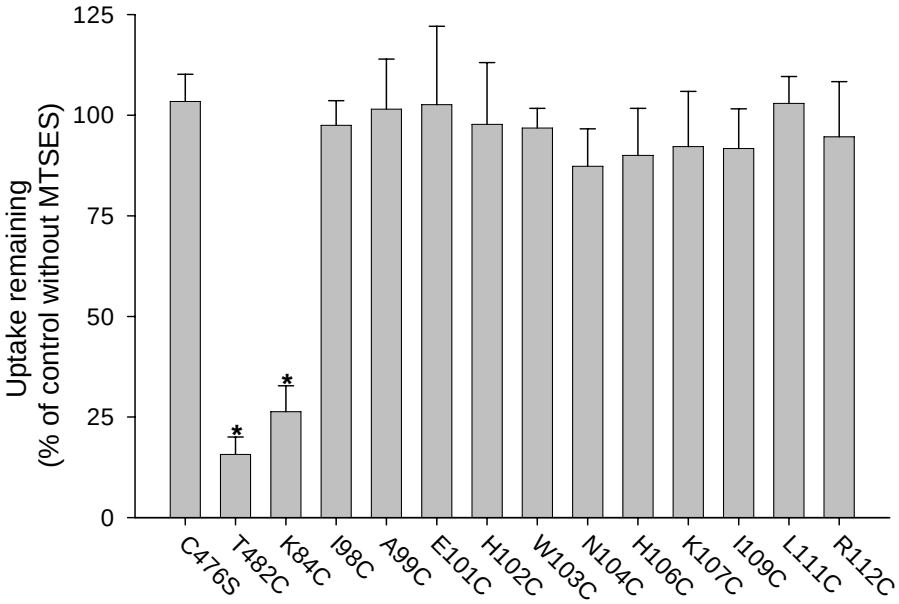

Figure 3.9 Effect of MTSES on succinate transport by cysteine-substituted NaDC1 mutants. HRPE cells expressing mutants were preincubated with 1 mM MTSES in sodium buffer or with sodium buffer alone (control) for 20 min. The [^{3}H]succinate uptake activity remaining after the preincubation was then measured. Uptake activities in cells pretreated with MTSES are expressed as a percentage of the uptakes in cells preincubated with sodium buffer alone. Data shown are means ± S.E.M, n = 3 experiments. * $p < 0.05$, significantly different from control group for that mutant. Each value represents the mean ± S.E.M.

None of the cysteine mutants between positions 98 and 112 was sensitive to inhibition by MTSES (1 mM (Figure 3.9) or 10 mM (Figure 3.10)). The cysteine mutants were also tested with MTSET (1 mM), which adds a positive charge, but it had no effect on any of the cysteine mutants including K84C (Figure 3.11). However, the MTSET does react with K84C, since pretreatment of cells expressing K84C with 1 mM MTSET prevented subsequent inhibition by MTSES (Figure 3.12).

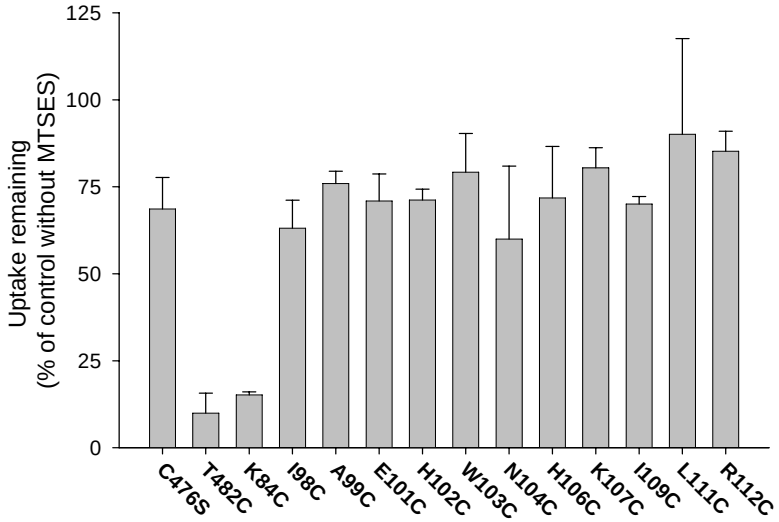

Figure 3.10 Effect of MTSES on succinate transport by cysteine-substituted NaDC1 mutants. HRPE cells expressing mutants were preincubated with 10 mM MTSES in sodium buffer or with sodium buffer alone (control) for 20 min. The [^{3}H]succinate uptake activity remaining after the preincubation was then measured. Uptake activities in cells pretreated with MTSES are expressed as a percentage of the uptakes in cells preincubated with sodium buffer alone. Data shown are means ± S.E.M. of two determinations.

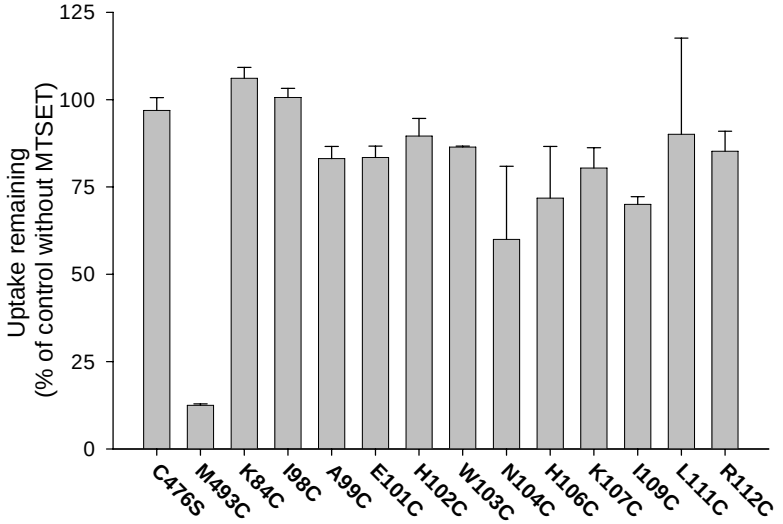

Figure 3.11 Effect of MTSET on succinate transport by cysteine-substituted NaDC1 mutants. HRPE cells expressing mutants were preincubated with 1 mM MTSET in sodium buffer or with sodium buffer alone (control) for 20 min. The [^{3}H]succinate uptake activity remaining after the preincubation was then measured. Uptake activities in cells pretreated with MTSET are expressed as a percentage of the uptakes in cells preincubated with sodium buffer alone. M493C was used as a positive control. Data shown are means ± S.E.M. of two determinations.

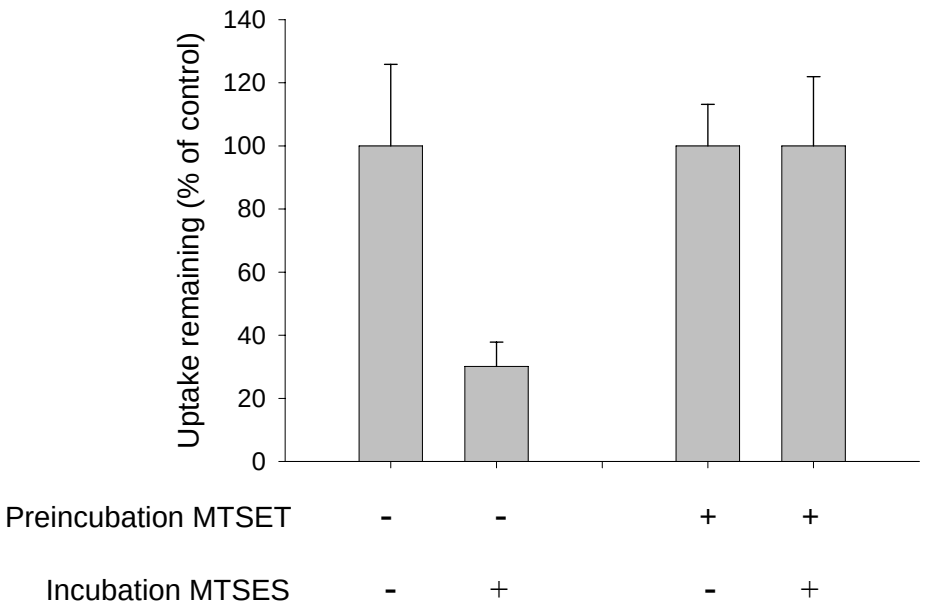

Figure 3.12 MTSET prevents MTSES inhibition in the K84C mutant. HRPE cells expressing K84C mutant were preincubated with 1 mM MTSET in sodium buffer or with sodium buffer alone (control) for 20 min followed by MTSES. The [^{3}H]succinate uptake activity remaining after two preincubations was then measured. Uptake activities in cells pretreated with MTSET and/or MTSES are expressed as a percentage of the uptakes in cells preincubated with sodium buffer alone. Data shown are means ± range (n = 2).

Concentration Dependence of MTSES Inhibition

The concentration dependence of MTSES inhibition of K84C transport activity was next examined. It was found that the maximal inhibition by MTSES reached a plateau at about 80%. One possible explanation to account for incomplete inhibition by MTSES is that the K84C proteins might be in different conformational states, including outward-, inward-facing and intermediate conformations. Since MTSES binds to extracellularly accessible cysteine residues, it is possible that some of the K84C mutant proteins could be present in a conformational state that MTSES

could bind to (MTSES-sensitive component) and others could be a conformational state that MTSES could not reach (MTSES-insensitive component). As shown in Figure 3.13, K84C was very sensitive to inhibition by MTSES, with an IC_{50} value of approximately 6 μM. Therefore, a concentration of 10 μM MTSES was used in subsequent experiments.

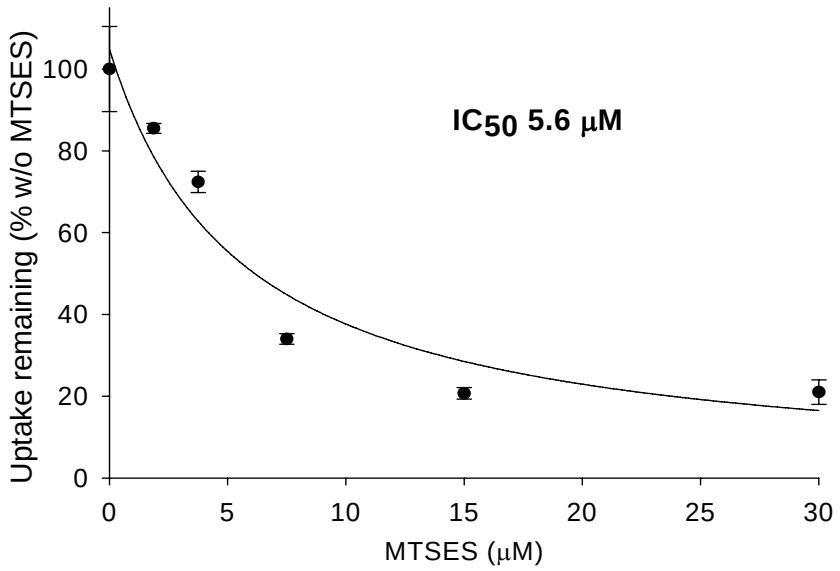

Figure 3.13 Concentration dependence of MTSES inhibition of succinate transport by the K84C mutant. HRPE cells were preincubated with increasing concentration of MTSES in sodium buffer. The succinate transport activity was measured and expressed as a percentage of the transport activity in the control group treated with sodium buffer alone. Each point represents the mean ± range (n = 2) from a single experiment**.**

Effect of Substrate and Cations on the Accessibility of K84C Mutant

The transport process of NaDC1 follows an ordered binding mechanism in which three sodium ions bind first, followed by substrate (Wright *et al.*, 1983; Yao & Pajor, 2000). To determine whether K84C is accessible to MTSES in different

conformational states, the preincubation with MTSES was conducted in either sodium or choline buffer with or without succinate. The inhibition by MTSES in K84C was only seen when the preincubation was done in sodium buffer (Figure 3.14). When the sodium was replaced by choline, or when substrate was present, the effect of MTSES was prevented.

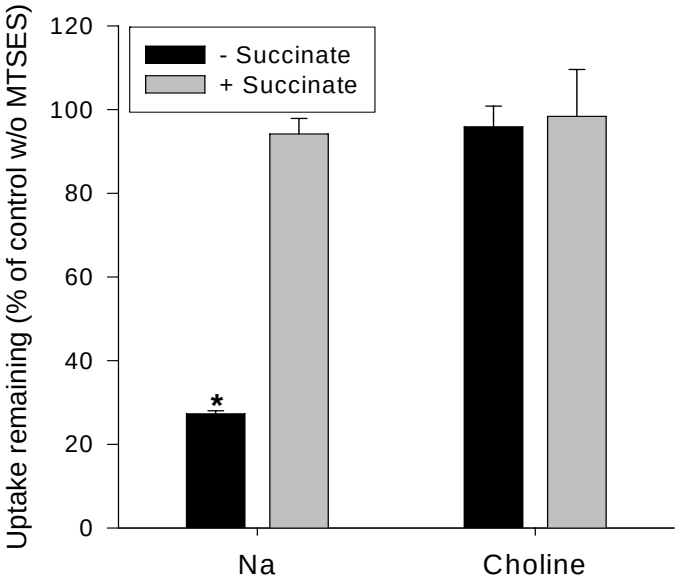

Figure 3.14 Cation and substrate dependence of MTSES labeling. HRPE cells transiently expressing the K84C mutant or the pcDNA3.1 vector were preincubated 20 min at room temperature with or without 10 μM MTSES. The preincubation buffers contained sodium or choline, with or without 10 mM succinate. The preincubation solution was washed away, and the remaining uptake activity with [^{3}H]succinate was then measured, as described previously. Uptake activities of cells pretreated with MTSES are shown as a percentage of the uptake in control cells pretreated with the same buffer without MTSES. Data shown are mean ± S.E.M., n = 3 experiments. * $p < 0.05$, significant difference compared with control group.

Effect of Temperature on MTSES Inhibition

Substrate protection of MTSES labeling could be due to substrate binding preventing the access of MTSES to the cysteine or there could be a conformational

change after substrate binding that occludes the substituted cysteine. At cold temperatures, large-scale conformational changes of transporters are slowed down, but substrate binding is not affected (Parent *et al.*, 1992; Wadiche & Kavanaugh, 1998).

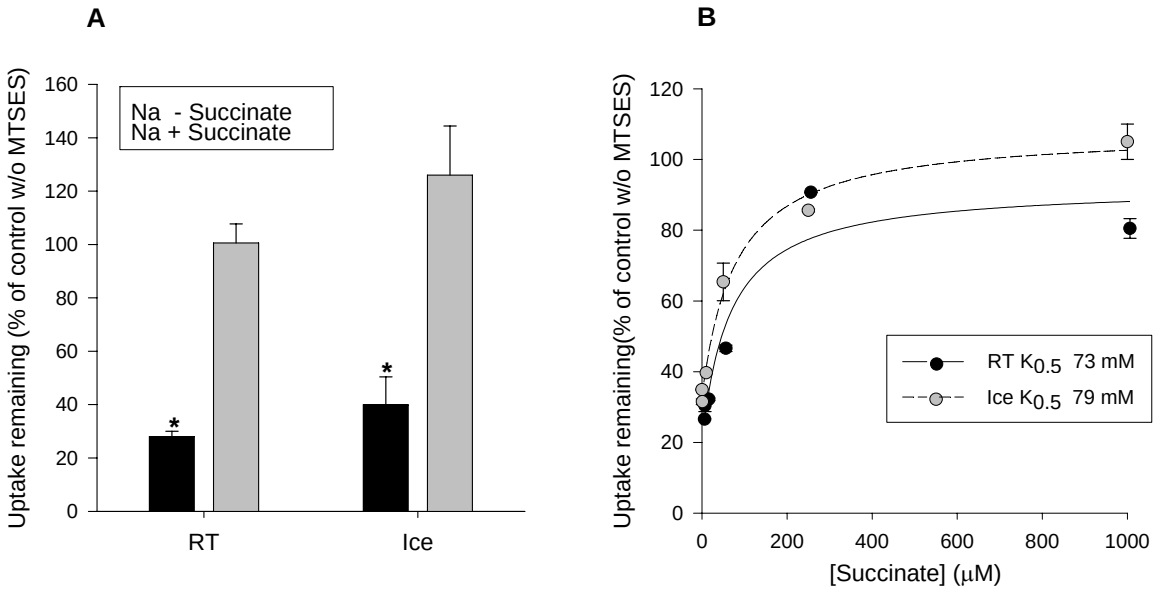

Figure 3.15 Substrate and temperature dependence of MTSES labeling. (A) HRPE cells transiently expressing the K84C mutant or the pcDNA3.1 vector were preincubated at room temperature (RT) or on ice for 20 min with or without 10 μM MTSES. The preincubation buffers contained sodium with or without 10 mM succinate. The preincubation solution was washed away, and the remaining uptake activity with [^{3}H]succinate was then measured, as described previously. Uptake activities of cells pretreated with MTSES are shown as a percentage of the uptake in control cells pretreated with the same buffer without MTSES. Data shown are mean ± S.E.M., n = 3 experiments. * $p< 0.05$, significant difference compared with control group. (B) Effect of temperature on substrate protection. HRPE cells transiently expressing the K84C mutant were preincubated in sodium buffer with increasing concentrations of succinate (0-1000 μM) and with or without 10 μM MTSES. The preincubations were done at room temperature (RT) or on ice for 20 min. After pretreatment, the preincubation solution was washed away and the remaining uptake activity of [^{3}H]succinate was measured at room temperature. Data shown are mean ± range, n = 2. The half-saturation constant was calculated using non-linear regression to $v = (V_{max} * [S])/(K_{0.5} + [S]) + C$, where C represents the transport activity remaining after MTSES treatment in the absence of succinate. C is 26% at room temperature and 35% on ice.

If the major effect of substrate protection is a conformational change due to translocation, then one would predict a reduction in substrate protection of MTSES inhibition at cold temperature. However, there was no change in substrate protection at cold temperatures in the K84C mutant (Figure 3.15A). The $K_{0.5}$ of substrate protection in K84C was about 73 μM at room temperature, compared with 79 μM at 4°C (Figure 3.15B). The $K_{0.5}$ value agrees well with the K_m value for succinate in this mutant (Table 3.1). At both temperatures, there was almost complete protection of transport activity with high concentrations of succinate. This result suggests that the effect of substrate protection in K84C is likely to be steric hindrance of chemical labeling by MTSES.

Labeling of Substituted Cysteines with MTSEA-biotin

Even though most of the TM3 cysteine mutants were insensitive to MTSES, it is possible that some residues might be accessible to MTSES labeling without any functional consequences. It was therefore examined whether some of the substituted cysteines could be labeled directly with MTSEA-biotin. I98C and R112C were chosen because they are at both ends of the cysteine scan and exhibit relatively high protein expression (see Figure 3.3). Pajor and colleagues have found in previous studies that proteins with low expression are difficult to detect after labeling with MTSEA-biotin; the sensitivity appears to be lower than that of Sulfo-NHS-biotin labeling (Pajor & Randolph, 2005). Additionally, the accessibility of the cysteine substitution at position 84 and substrate protection of MTSES inhibition in K84C were verified. The mutant T482C from previous study was used as a positive control (Pajor & Randolph, 2005).

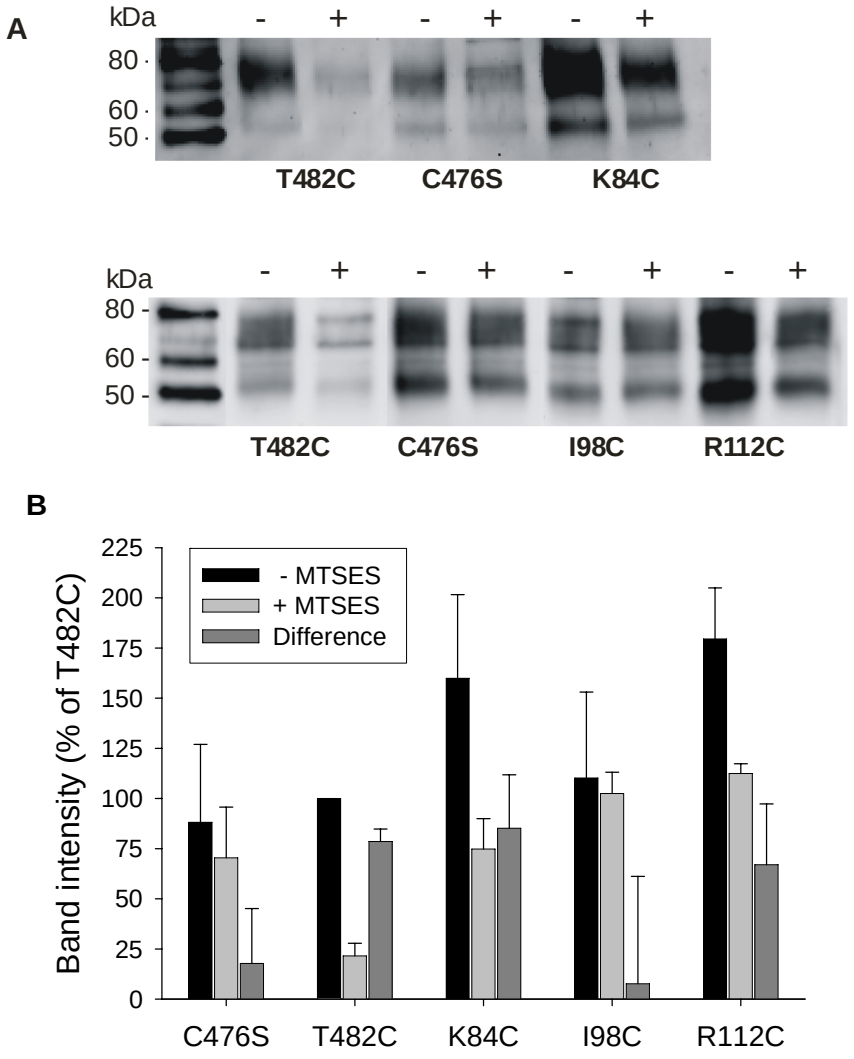

Figure 3.16 Labeling of cysteine-substituted NaDC1 mutants with MTSEA-biotin. (A) HRPE cells expressing K84C, I98C or R112C mutants were initially preincubated in sodium buffer with (+) or without (-) 1 mM MTSES in order to label the accessible cysteines. The preincubation solution was washed away and the cell monolayers were then incubated with MTSEA-biotin and transferred to Western blots. The negative control mutant, C476S, and the positive control, T482C, were included in each biotinylation experiment. The positions of chemiluminescent size standards, MagicMark XP, are shown in the leftmost lane. (B) Comparison of the band intensity analysis of MTSEA-biotinylation. Western blots such as those shown in (A) were quantitated and expressed as a percentage of the T482C intensity from the same blot. The difference between the signal in the presence and absence of MTSES represents specific binding of MTSEA-biotin. The bars represent mean ± range (n = 2 blots, separate transfections).

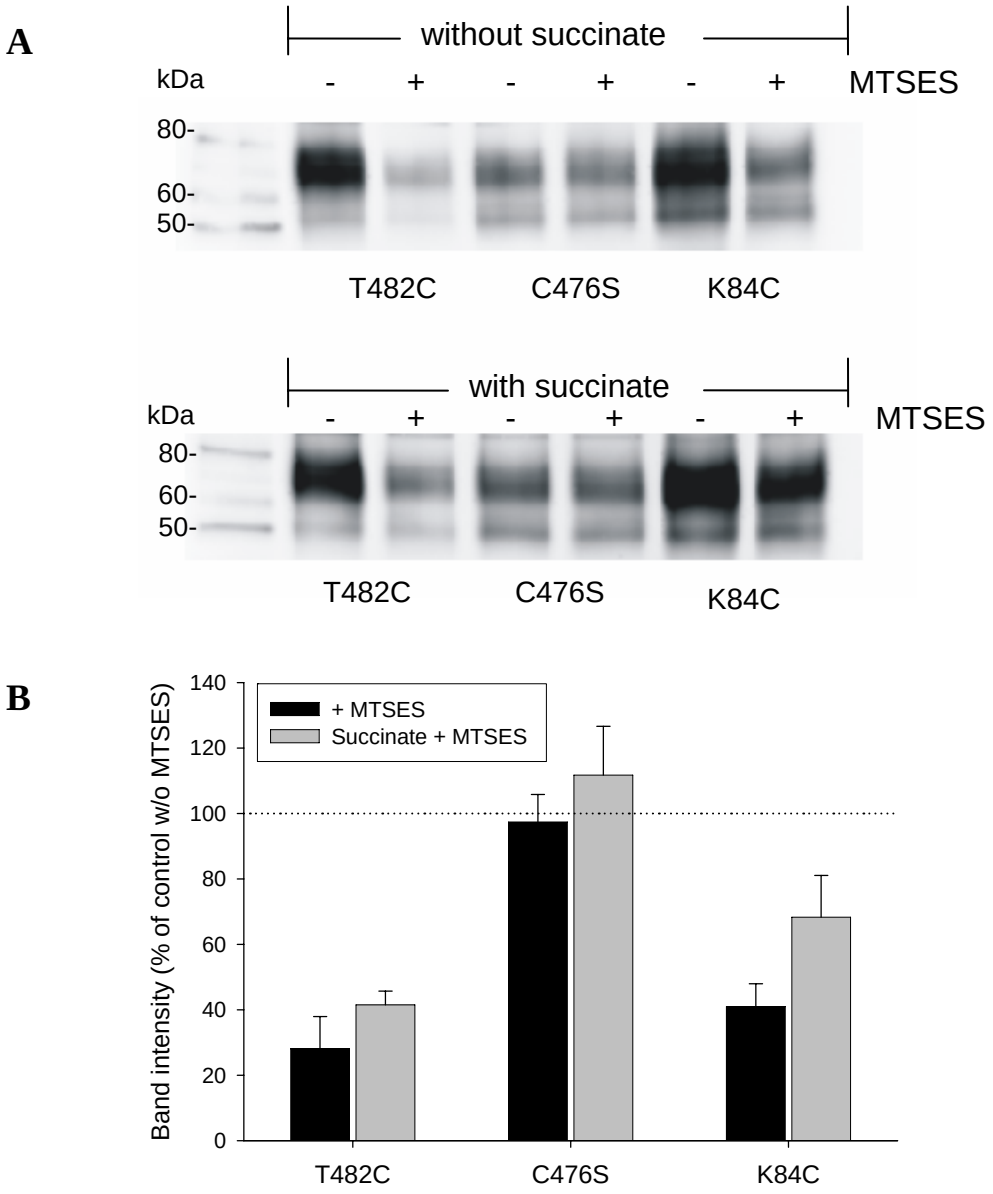

Figure 3.17 Substrate protection of MTSEA-biotin labeling in the K84C mutant. (A) HRPE cells expressing K84C mutant was initially preincubated in sodium buffer with (+) or without (-) 10 μM MTSES. The preincubation buffer contained sodium with or without 10 mM succinate. The preincubation solution was washed away and the cell monolayers were then incubated with MTSEA-biotin and transferred to Western blots. The negative control mutant, C476S, and the positive control, T482C, were included in each biotinylation experiment. The positions of chemiluminescent size standards, MagicMark XP, are shown in the leftmost lane. (B) Comparison of the band intensity analysis of MTSEA-biotinylation. The bars represent mean ± range (n = 2 blots, separate transfections).

There is some background binding of MTSEA-biotin to the C476S control, but this was not decreased by preincubation with MTSES (Figure 3.16). The positive control, T482C, showed a large decrease in the MTSEA-biotin signal after incubation with MTSES (Figure 3.16). There was specific binding of MTSEA-biotin to the K84C and R112C mutants, verifying that they are accessible from the outside of the cell, but there was no specific binding to I98C. After preincubation with succinate, there was increased MTSEA-biotin signal in the K84C mutant compared with preincubation with MTSES alone (Figure 3.17). This result confirms that succinate is protecting the K84C mutant from inhibition by MTSES. It also suggests if the K84 residue is not the actual substrate binding site; it is most likely located near the substrate binding site.

DISCUSSION

Predicted transmembrane helix (TM) 3 of the rabbit Na^+/dicarboxylate cotransporter, NaDC1, is highly conserved with other members of the SLC13 family. Previous studies have shown that individual amino acids from TM3 and connecting loops in NaDC1 have important functions. For example, Ala replacement of Lys-84 decreases affinity for substrate (Pajor *et al.*, 2000). His-106 at the extracellular part of the helix, affects targeting of NaDC1 expressed in *Xenopus* oocytes (Pajor *et al.*, 1998c). Differences in glutarate affinity between the rabbit and mouse NaDC1 are determined by residues in TM3 and 4 (Oshiro *et al.*, 2006). In the present study, it was found that cysteine substitutions at the extracellular portion of TM3 (amino acids 98-112) do not produce transport inhibition by MTS reagents, although several of the amino acids in that region are involved in determining substrate selectivity. Lys-84,

in contrast, was very sensitive to chemical labeling by MTSES, and exhibited its greatest accessibility to the reagent in the presence of sodium. Lys-84 is likely to be located within the substrate binding pocket, and it undergoes conformational changes in accessibility to the outside during the transport cycle. The results indicate a new location for Lys-84 either in a membrane helix facing a water-filled pore or in a reentrant loop.

Transport Specificity Ratio (TSR) analysis is used to identify mutations in transporters that produce changes in relative catalytic efficiency or specificity (k_{cat} / K_m) of one substrate compared with another (King, 2004). The mutations at amino acids Glu-101, Trp-103, His-106 and Leu-111 resulted in increases in succinate:citrate TSR values. These amino acids are highly conserved among the members of the SLC13 family (Figure 3.2). The increased TSR could be, at least in part, determined by an increased k_{cat} for succinate since there was no change in V_{max} but a decrease in cell-surface protein expression. The changes in TSR could also be determined by decreased catalytic efficiency for citrate since all of the mutants with altered TSR had decreased citrate affinity. Since the mutations themselves did not alter succinate K_m and treatment with MTSES or MTSET had no effect on the activity of the mutants, it is possible that the residues determine substrate selectivity indirectly by affecting transporter flexibility or by holding other key residues in position. Mutations far from the active site in proteins can perturb catalytic rate by altering conformational mobility of the entire protein (Wong *et al.*, 2005). Cysteine replacement of two residues in TM3, Val-100 and Ala-110, resulted in inactive proteins although the proteins were present on the plasma membrane, suggesting that these amino acids are critical for transport activity in NaDC1. The positions of these

critical amino acids are adjacent to Glu-101 and Leu-111, both of which are involved in determining substrate selectivity, confirming that this region is important functionally.

Cysteine replacement of Lys-84 had no effect on succinate kinetics, indicating that this residue is not likely to be directly involved in succinate binding, but the citrate K_m was increased about two-fold. The increase in TSR, therefore, reflects changes in citrate transport by this mutant. In previous study, alanine substitution at position 84 had no effect on sodium affinity, but resulted in a large decrease in succinate affinity, with a K_m of 2.2 mM (Pajor *et al.*, 2000). It is not clear why the cysteine substitution at position 84 would have no effect on succinate K_m since it also represents a charge neutralization and replacement with a much smaller side chain. There was also no effect of chemical labeling of K84C with MTSET, which should restore the positive charge. However, charge reversal at position 84 by chemical modification with MTSES, which adds a negative charge, produced inhibition of transport.

The substrate binding sites of all of the known structural models of ion-coupled transport proteins, including the H^+-coupled lactose permease (Abramson *et al.*, 2003), Na^+-dependent leucine transporter, $LeuT_{Aa}$ (Yamashita *et al.*, 2005), and the Na^+-dependent aspartate transporter, Glt_{Ph} (Yernool *et al.*, 2004), are located within aqueous cavities formed by multiple helices. In $LeuT_{Aa}$, the cation and substrate binding sites are located very close together and are formed, in part, by unwound regions of transmembrane helices (Yamashita *et al.*, 2005). Several of the methanethiosulfonate (MTS) derivatives, including MTSES and MTSET, are membrane-impermeant reagents that label cysteine residues in an aqueous

environment (Javitch, 1998;Karlin & Akabas, 1998). The impermeant MTS reagents can be used to map cysteine residues located in extracellular loops or in water-filled pores, such as the substrate access and binding pores of membrane proteins.

The cysteine-scanning approach, particularly when compared with protein crystal structures, is beginning to provide detailed information on conformational changes in ion-coupled transport proteins. The mammalian Na^+/Cl^--serotonin transporter, SERT, exhibits changes in reactivity of substituted cysteines that relate well to the crystal structure of its bacterial homolog, $LeuT_{Aa}$ (Rudnick, 2006). For example, cysteine substitutions of residues in TM5 of SERT, predicted to form part of the cytoplasmic substrate permeation pathway, exhibit decreased accessibility with inhibitor binding, which locks the transporter in an outward-facing conformation. The same substituted cysteines in SERT have increased reactivity with MTS reagents in the presence of ions and substrate, reflecting conformational changes associated with transport (Zhang & Rudnick, 2006). The mammalian glutamate transporters, EAAT1 and GLT-1, also exhibit changes in conformation that can be detected by accessibility of substituted cysteines. For example, the relative positions of the two opposing hairpin loops, thought to form substrate access gates in the crystal structure of the archeal homolog, Glt_{Ph} (Yernool *et al.*, 2004), change during the transport cycle in both EAAT1 and GLT-1 (Leighton *et al.*, 2006; Shlaifer & Kanner, 2007). The lactose permease also exhibits changes in substituted-cysteine accessibility upon substrate binding (Kaback *et al.*, 2007). When superimposed on the crystal structure of the inward-facing conformation of the lactose permease, residues that exhibited increased N-ethylmaleimide labeling in the presence of substrate were found to be located away from the substrate binding site and near the periplasmic surface of the

protein. In contrast, decreased NEM labeling in the presence of substrate (substrate protection) was seen in cysteines located near the inward-facing substrate binding cavity and at the cytoplasmic ends of helices, also an indication of conformational changes that occur with substrate binding.

The transport cycle of NaDC1 involves ordered binding of three sodium ions followed by a divalent anion substrate (Wright *et al.*, 1983; Yao & Pajor, 2000). The accessibility of K84C to MTSES seems to parallel the exposure of the substrate binding site. The inhibition by MTSES was seen in the presence, but not the absence, of sodium, and the addition of substrate produced substrate protection. The succinate $K_{0.5}$ for substrate protection of MTSES inhibition was about 79 μm, similar to the transport K_m of 25 μM. In the absence of sodium the transporter is in a conformational state that prevents accessibility of MTSES to the substituted cysteine at position 84 by placing it in a lipid environment or between two helices that do not have an aqueous pore open to the outside of the cell. Sodium binding triggers a conformational change in NaDC1 in which the helices may tilt or rotate to allow exposure of the substrate-binding site and subsequent increase in substrate affinity. This is also the conformation in which the cysteine at position 84 is most accessible to extracellularly applied MTS reagents. The fully-loaded transporter containing the sodium and substrate undergoes a large conformational change to translocate all substrates to the opposite side of the membrane. Substrate protection could occur either by occlusion of the cysteine at position 84 as a result of the conformational change or by steric hindrance produced by substrate binding. The large scale conformational changes of transporters are inhibited in the cold, although substrate binding is not affected by temperature (Parent *et al.*, 1992; Wadiche & Kavanaugh,

1998). Since cold temperature did not affect substrate protection in K84C, it is likely that substrate binding produces steric hindrance of MTSES binding and this occurs at an early state in the transport cycle prior to translocation. Therefore, the K84 residue is most likely located in the water-filled cavity that contains the substrate binding site.

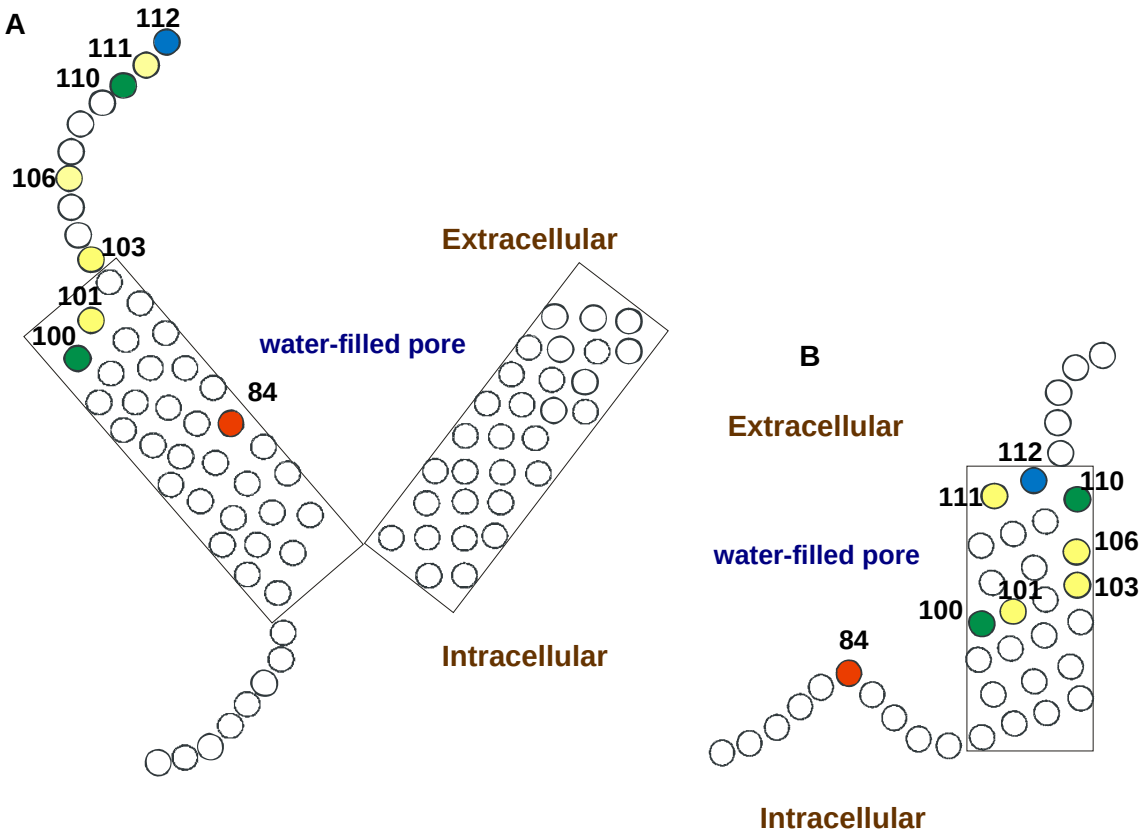

Figure 3.18 Models summarizing results of cysteine-scanning mutagenesis experiments in NaDC1. Two alternative topology models to explain the results are shown in A and B. In model A, Lys-84 is located within the TM3 and in model B, Lys-84 is accessible to the outside of the cell as part of a reentrant loop. K84C is sensitive to inhibition by MTSES, is labeled by MTSEA-biotin and shows substrate protection of labeling. R112C, shown as a blue circle, is labeled by MTSEA-biotin but is insensitive to inhibition by MTSES. Residues that showed changes in transport specificity ratio (TSR) are indicated by yellow circles and the positions of inactive cysteine-substituted mutants are shown by green circles.

The previous model of TM3 was based on hydropathy analysis, and placed Lys-84 in an intracellular loop between TM2 and 3 (Pajor, 1995; Zhang & Pajor, 2001). However, the present study provides experimental evidence that Lys-84 is accessible to the outside of the cell, indicating that it is located either on the extracellular side of the membrane or in an aqueous pore or cavity. It was also found that R112C is located extracellularly, since it can be labeled with MTSEA-biotin, and I98C is located either intracellularly or within the membrane in a transmembrane helix, since it was not labeled by MTSEA-biotin. Two alternative models of the TM3 region of NaDC1 are shown in Figure 3.18. In one model, Lys-84 is located in the transmembrane helix, with part of the helix forming the substrate binding cavity or access pore. If this model is correct, the size of the substrate access pore would be large enough to accommodate MTSEA-biotin, at least as far as Lys-84. In the second model, Lys-84 is located in a reentrant loop which lines an aqueous pore forming the substrate binding pocket. Further experiments will be needed to distinguish between the two models.

In conclusion, this study has shown that the conserved residue at Lys-84 and amino acids at the extracellular half of TM3 are functionally important in NaDC1. Residues in TM3 include Ala-100 and Val-110, which produced inactive proteins when mutated to cysteine, and Glu-101, Trp-103, His-106 and Leu-111, which contain determinants of substrate selectivity although these residues may participate indirectly in substrate binding and translocation. Lys-84 is probably located within the substrate binding cavity of NaDC1. The sensitivity of the K84C mutant to MTSES inhibition was greatest in the presence of sodium, and inhibition could be prevented by addition of substrate or replacement of sodium, indicating that the

accessibility of Lys-84 changes with conformational state. The substrate protection of MTSES inhibition of K84C appears to occur early in the transport cycle, before the large-scale conformational change associated with translocation of substrate. The results indicate a new location for Lys-84 in the substrate access pore formed in part by the transmembrane helix or a reentrant loop.

CHAPTER 4: THREONINE-509 IS A DETERMINANT OF BOTH SUBSTRATE AND CATION AFFINITY IN THE HUMAN Na^+/DICARBOXYLATE COTRANSPORTER

(Studies in this chapter have been submitted for publication in *Biochemistry*. Weerachayaphorn J. and Pajor A. M. Threonine-509 is a determinant of both substrate and cation affinity in the human Na^+/dicarboxylate cotransporter)

INTRODUCTION

The NaDC1 transporters from rabbit (rb) and human (h) are 78% identical in amino acid sequence but they exhibit functional differences (Pajor & Sun, 1996b). For instance, the K_m for citrate and K_{Na} for sodium are larger in hNaDC1 than in rbNaDC1. The transporters also differ in their sensitivity to inhibition by lithium, which competes with sodium at one of the cation binding sites (Pajor *et al.*, 1998a; Wright *et al.*, 1982); the hNaDC1 is insensitive to inhibition by lithium (Pajor & Sun, 1996b). In a previous study, Pajor and colleages found that interactions between transmembrane helices (TM) 7, 10, and 11 contribute to the differences in apparent citrate affinities between human and rabbit NaDC1 (Kahn & Pajor, 1999). The differences in sodium affinities between the human and rabbit Na^+/dicarboxylate cotransporters are determined primarily by residues in TM10 and 11, and the difference in lithium sensitivity is determined by TM11.

The purpose of the present study was to identify individual amino acids in the TM10 region of NaDC1 responsible for differences in substrate and sodium affinity. TM10 and the attached intracellular loop contains four amino acid differences between h and rbNaDC1. Mutant transporters were made containing the amino acid sequence from rbNaDC1 in the hNaDC1 background, and a reverse mutant in the

rbNaDC1 background, rbS512T. The results show that a serine or threonine at position 509 (or 512 in rbNaDC1) in TM10 partially determines differences in K_m for citrate, but is sufficient to confer affinity for succinate and cations, and substrate specificity for four-carbon dicarboxylates. It was further concluded that the substrate and cation binding sites in NaDC1 are located in close proximity to one another.

MATERIALS AND METHODS

Chimeric and mutant transporters

The chimeric transporter R10 is based on hNaDC1 with amino acids 485-539 replaced with the equivalent amino acids (488-541) from rbNaDC1, consisting of TM10 and associated loop (Kahn & Pajor, 1999). The R10 chimera, previously constructed in pSPORT1 plasmid, was subcloned into the pcDNA3.1 (Invitrogen) mammalian expression plasmid, for expression in COS-7 cells. Mutants in this study were generated using the QuikChange^{TM} site-directed mutagenesis kit (Stratagene) according to the manufacturer's instructions. The mutant transporters are named using the single letter amino acid code followed by the number of the position that was mutated. The second letter following the sequence number shows the amino acid substituted at that position. The prefix denotes the parental transporter, either rabbit (rb) or human (h) NaDC1. Mutants were verified by sequencing at the Protein Chemistry Laboratory at the University of Texas Medical Branch, using an Applied Biosystems Model 3100 automated DNA sequencing unit.

COS-7 cell culture

The SV-40 transformed monkey kidney cell line, COS-7, was obtained from the American Type Culture Collection and cultured in DMEM with 4.5 g/l glucose (GIBCO-Invitrogen) supplemented with 10% heat-inactivated fetal calf serum (Hyclone), 100 units/ml penicillin G, and 100 μg/ml streptomycin. Cells were maintained at 37^{o}C in an atmosphere of 5% CO_2. After completing Chapter 3, I found that NaDC1 expression in COS-7 cells is higher than HRPE cells. Therefore, COS-7 cells were used in this study. Cells were plated at a density of 1.2×10^5 cells/well in 24 well plates coated with 5 μg/cm^2 rat-tail collagen I (BD Bioscience-Clontech) for transport assays, or 6-well collagen-coated plates at a density of 3×10^5 cells/well for biotinylation reactions. Cells were transiently transfected with FuGENE 6 twenty-four hours after seeding as same as described in Chapter 3.

Transport Assays

The transport of [^{14}C]succinate (40 mCi/mmol, Moravek) or [^{14}C]citrate (55 mCi/mmol, American Radiolabeled Chemical Inc.) was conducted 48 hours after transfections, same as described in Chapter 3. Except for each well of cells was dissolved in 250 μl OptiPhase Supermix (Wallac/Perkin Elmer) scintillation cocktail for 60 min. The plates were sealed with plastic covers and counted directly in a Microbeta Trilux 1450 plate scintillation counter (Wallac/Perkin Elmer).

In kinetic experiments, 5 min uptakes were measured with increasing concentrations of non-radiolabeled succinate and constant [^{3}H]succinate (50,000 mCi/mmol, ViTrax). [^{3}H]succinate was used instead of [^{14}C]succinate to allow increased specific activity at the higher substrate concentrations. Citrate kinetics

were measured using a combination of [^{14}C]citrate and non-radioactive citrate. Kinetic constants were calculated by nonlinear regression to the Michaelis-Menten equation using SigmaPlot 2000 software (Jandel Scientific). In sodium activation experiments, the rate of [^{14}C]succinate transport was measured in transport buffer containing sodium concentrations between 0 and 120 mM, with NaCl replaced isoosmotically by choline chloride. Kinetic constants were calculated by nonlinear regression to the Hill equation, $v = V_{max} * [Na^+]^{n_H} / (K_{Na}^{n_H} + [Na^+]^{n_H})$, where v is the initial rate uptake, V_{max} is the maximum rate at saturating sodium concentration, $[Na^+]$ is the sodium concentration, K_{Na} is the sodium concentration that produces 1/2 V_{max}, and n_H is the Hill coefficient.

Cell Surface Biotinylation

Cell surface protein expression of NaDC1 and mutants was the same as described in Chapter 3.

Statistical analysis

Statistical analysis was performed using Student's *t*-test to compare two groups or a One-way Analysis of Variance (ANOVA) and the *post-hoc* Dunnett's multiple comparison method for multiple groups (SigmaStat program, Jandel Scientific). Statistically significant difference was considered to be $p < 0.05$.

RESULTS

Mutants in TM10 and loop

Previous study showed that the R10 chimera, hNaDC1 with a substitution of transmembrane helix (TM) 10 and associated loop from rbNaDC1, contains amino acids that are important in determining some of the differences in citrate and sodium affinity (Kahn & Pajor, 1999). This region has only 4 amino acid differences between the human and rabbit NaDC1 (Figure 4.1). To identify the amino acid responsible for functional differences between the rabbit and human orthologs, amino acids in hNaDC1 were replaced one at a time with the corresponding amino acid from rbNaDC1. The four mutants created were: hT509S in the putative transmembrane helix, and hD530G, hK532R and hL534S in the intracellular loop between TM 10 and 11 (the prefix h denotes the hNaDC1 parental transporter).

Figure 4.1 Sequence alignment of amino acids 495-538 of human NaDC1 with amino acids 498-541 of rabbit NaDC1. The four amino acid differences are highlighted in grey and the amino acids that are predicted to form TM10 are underlined. Genbank™ accession numbers of the sequences are in parentheses.

Protein Expression of Mutants

The abundance of mutant proteins on the plasma membrane of transfected COS-7 cells was examined by biotinylation with the membrane impermeant reagent,

Sulfo-NHS-LC-biotin, followed by Western blotting. Figure 4.2A shows single representative blots for human and rabbit mutants compared with the parental transporters, either hNaDC1 or rbNaDC1. The blots were scanned to quantitate the protein expression, and each mutant was expressed as a percentage of the parental protein abundance (Figure 4.2B). The rbNaDC1 expression was 129 ± 11% of that of hNaDC1. All of the mutants were expressed at the plasma membrane, most with more than 60% of the parental transporter abundance, except for hL534S, which was approximately 35%. The rabbit mutant, rbS512T, was more abundant than the parental. Overall, there was no impairment in protein trafficking or stability of the mutants.

Transport Activity of Mutants

The initial rate of uptake was determined by measuring the time courses of citrate and succinate uptake by rb and hNaDC1 transiently transfected in COS-7 cells. The time courses were linear up to 15 min (Figure 4.3). Therefore, an incubation time of 5 min was chosen for subsequent experiments. The transport activity of the mutants was examined by comparing the uptake of 1 mM citrate and 1 mM succinate (Figure 4.4A). As shown in Figure 4.4B, the rate of citrate transport expressed as a percentage of succinate transport was 97% in rbNaDC1 and 19% in hNaDC1, consistent with previous study done with *Xenopus* oocytes (Kahn & Pajor, 1999). The R10 chimera exhibited intermediate citrate:succinate transport activity compared with the two parental transporters. The hT509S mutant also had intermediate citrate:succinate transport activity, but it was significantly lower than the R10

chimera. The hD530G, hK532R and hL534S mutants were not significantly different from the parental hNaDC1.

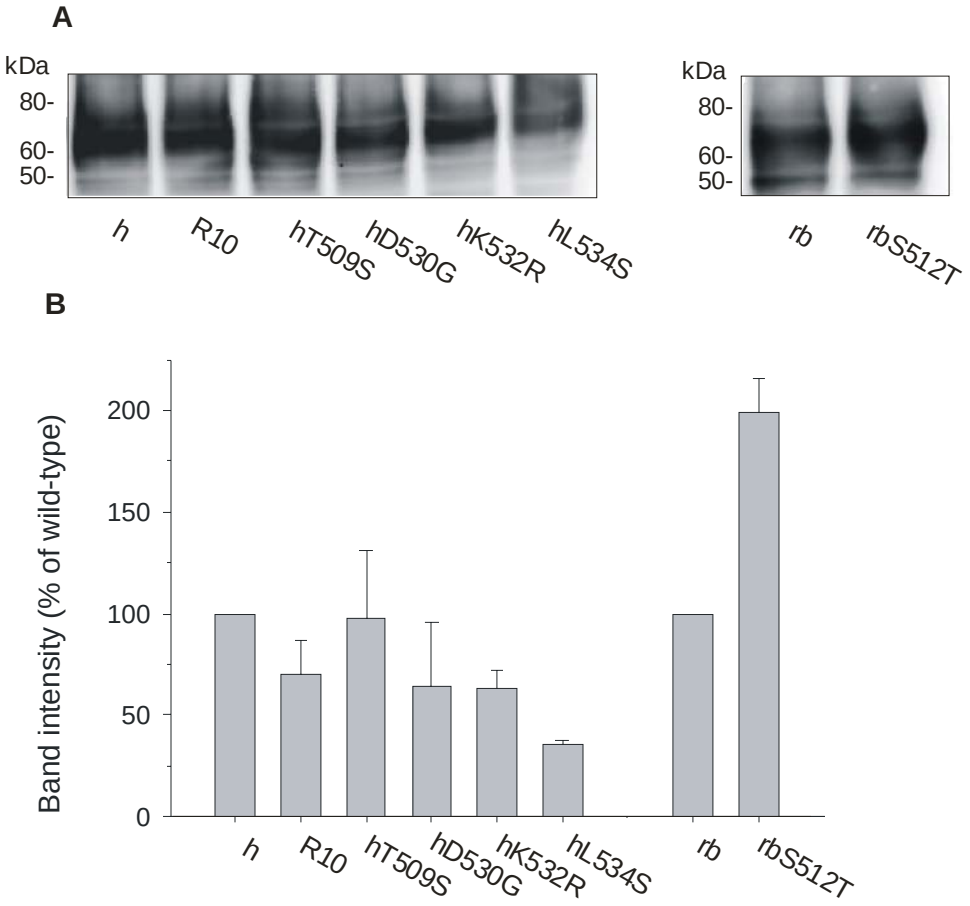

Figure 4.2 Cell surface protein expression of mutants. A, COS-7 cells expressing wild type and mutant transporters were treated with Sulfo-NHS-LC-biotin. Each blot includes an internal control of the parental transporter, either hNaDC1 (h) or rbNaDC1 (rb). R10 is a chimera containing transmembrane helix (TM) 10 from rbNaDC1 in hNaDC1 background. B, Western blots such as those shown in A were quantitated and expressed as a percentage of the parental transporter intensity from the same blot. The bars represent mean ± range (N = 2 blots, separate transfections).

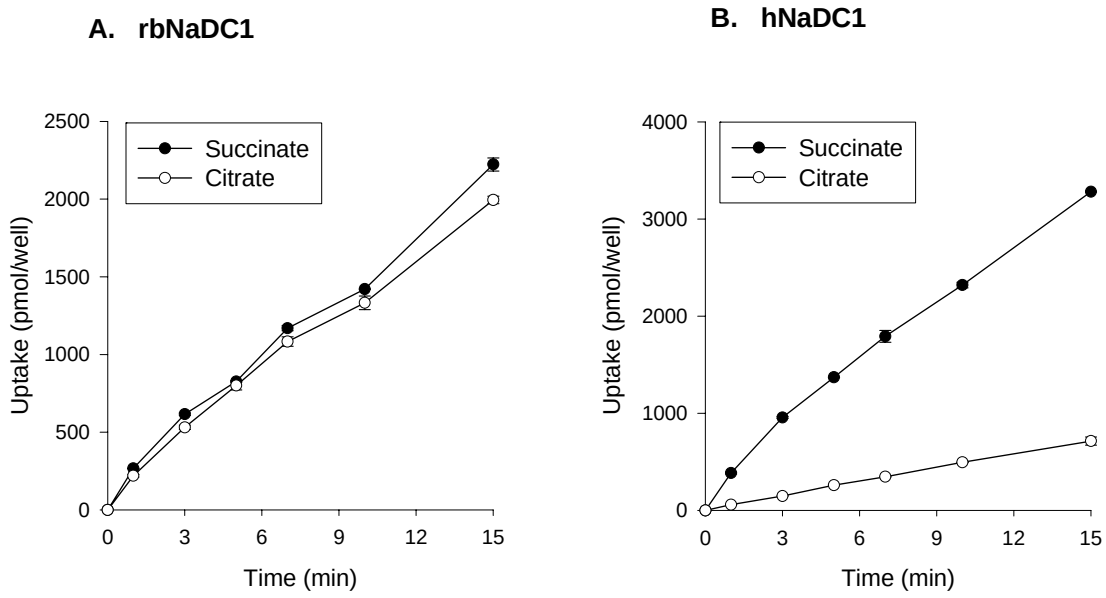

Figure 4.3 Time dependence of uptake of succinate and citrate by COS-7 cells expressing rbNaDC1 (panel A) and hNaDC1 (panel B). Monolayers were incubated with 100 μM [^{14}C]succinate or [^{14}C]citrate in sodium or choline buffer at different time point varying from 1 min to 15 min. Each value represents the mean ± range of two determinations from one typical experiment.

Succinate and Citrate Kinetics

The rbNaDC1 expressed in COS-7 cells had a mean K_m for citrate of about 270 μM, whereas hNaDC1 had a mean K_m for citrate of about 4000 μM (Table 4.1). The R10 chimera containing transmembrane helix 10 from rabbit in hNaDC1 background had an intermediate citrate K_m value of about 760 μM, significantly lower than the parental hNaDC1. The results are consistent with previous study comparing the properties of rb and hNaDC1 expressed in *Xenopus* oocytes, with citrate K_m values of 900 μM (rbNaDC1), 7200 μM (hNaDC1), and 3700 μM (R10 chimera)

(Kahn & Pajor, 1999). The succinate K_m values determined in the oocyte expression system were 500 μM (rabbit) and 800 μM (human) (Pajor & Sun, 1996b). In the present study, the K_m value for succinate was about 100 μM in rabbit and about 800 μM in hNaDC1. For some reason, the kinetic values for rbNaDC1 are lower when expressed in mammalian cells compared with *Xenopus* oocytes (Weerachayaphorn & Pajor, 2007). The R10 chimera had a succinate K_m of about 150 μM, similar to that of the rabbit NaDC1 although significantly higher. The most striking effect of single mutations on succinate and citrate kinetics was seen at position 509. The hT509S mutant had a shift in the K_m for both citrate and succinate from the characteristics of hNaDC1 to those of rbNaDC1 (the single experiments are shown in Figure 4.5 and Figure 4.6, and the mean of three experiments is in Table 4.1, 4.2). The K_m values for both citrate and succinate in hT509S were significantly higher than those of the R10 chimera. The hD530G and hL534S mutants exhibited intermediate phenotypes with K_m for citrate of 2300 μM and 1900 μM, respectively, but the K_m values for succinate were not significantly different from those of the parental hNaDC1. The hK532R mutant had no significant changes in citrate or succinate K_m. Because the hT509S mutant was different than chimera R10, the effects of double and triple mutations including T509S were tested. All of the double or triple mutants had no changes in cell surface expression (data not shown) and showed no functional differences compared with the hT509S mutant alone (Table 4.1, 4.2). To verify the importance of Thr-509 in determining differences in citrate and succinate affinity, the serine at the equivalent position in rbNaDC1 (Ser-512) was mutated to threonine. The rbS512T mutant exhibited increased K_m values for both citrate and succinate. The K_m for succinate of about 1300 μM was not significantly different from that of hNaDC1,

whereas the K_m for citrate of 1800 μM was intermediate between the rabbit and human values (the single experiments are shown in Figure 4.5 and Figure 4.6, and the mean of three experiments is in Table 4.1, 4.2. Therefore, the kinetic studies confirm that the serine or threonine at position 509 (h) or 512 (rb) is a determinant of citrate and succinate affinity in NaDC1.

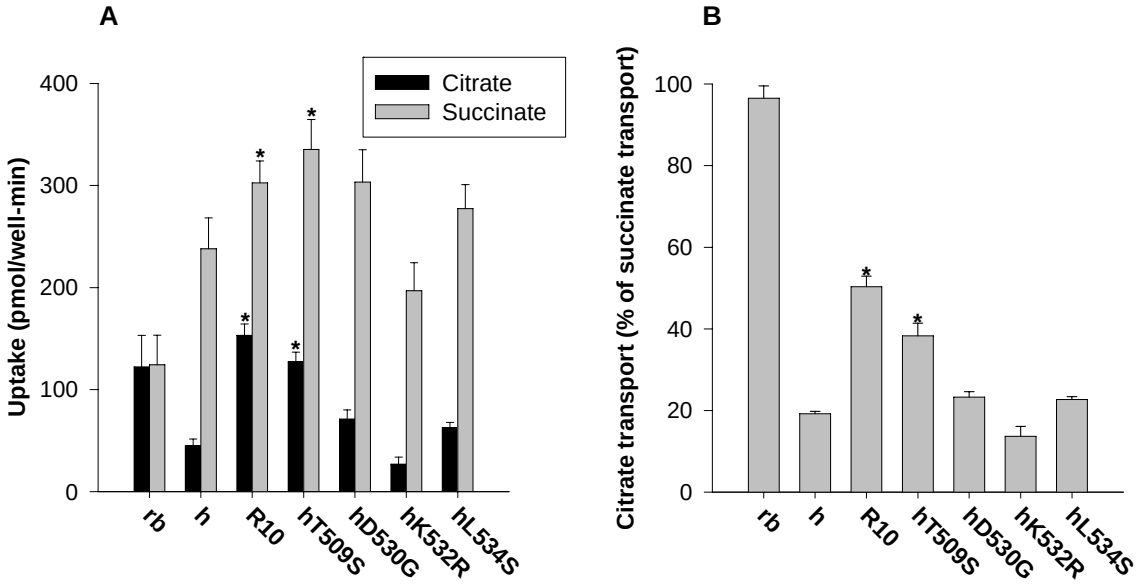

Figure 4.4 Transport activity of mutants. A, The transport of 1 mM [^{14}C]citrate or 1 mM [^{14}C]succinate was measured for 5 min in sodium containing buffer. B, The transport of citrate expressed as a percentage of succinate transport, calculated using the data shown in A. The bars represent mean ± S.E.M., N = 3 experiments. The * denotes significant difference compared with hNaDC1 ($p< 0.05$).

Table 4.1 Citrate kinetics in mutants. The kinetics of citrate transport were determined in COS-7 cells expressing rbNaDC1, hNaDC1, chimera R10 and mutants. Five minute uptakes were measured. Except for double and triple mutants, the kinetic values shown are the mean ± S.E.M. N is sample size. *, indicates significant difference compared with the parental hNaDC1 ($p< 0.05$). #, indicates significant difference compared with the parental rbNaDC1 ($p< 0.05$).

WT / Mutants	Citrate kinetics		N
	K_m (μM)	V_{max} (pmol/well-min)	
rbNaDC1	274 ± 14	131 ± 16	3
hNaDC1	3967 ± 377#	317 ± 59	3
R10 chimera	756 ± 112*	218 ± 38	4
hT509S	1325 ± 256*	373 ± 176	3
hD530G	2615 ± 298	527 ± 113	3
hK532R	3332 ± 284	488 ± 139	3
hL534S	2552 ± 691	390 ± 99	3
hT509S/D530G	919 ± 272	316 ± 196	2
hT509S/L534S	1928 ± 1130	368 ± 99	2
hT509S/D530G/L534S	1454 ± 404	552 ± 116	3
rbS512T	1791 ± 125#	125 ± 12	3

Table 4.2 Succinate kinetics in mutants. The kinetics of succinate transport were determined in COS-7 cells expressing rbNaDC1, hNaDC1, chimera R10 and mutants. Five minute uptakes were measured. Except for double and triple mutants, the kinetic values shown are the mean ± S.E.M. N is sample size. *, indicates significant difference compared with the parental hNaDC1 ($p< 0.05$). #, indicates significant difference compared with the parental rbNaDC1 ($p< 0.05$).

WT / Mutants	Succinate kinetics		N
	K_m (μM)	V_{max} (pmol/well-min)	
rbNaDC1	96 ± 13	104 ± 27	3
hNaDC1	782 ± 141#	188 ± 79	4
R10 chimera	149 ± 11*	378 ± 13	3
hT509S	217 ± 19*	510 ± 61	3
hD530G	836 ± 178	570 ± 37	3
hK532R	1041 ± 197	463 ± 127	3
hL534S	554 ± 129	452 ± 61	3
hT509S/D530G	289 ± 120	132 ± 101	2
hT509S/L534S	202 ± 71	331 ± 190	2
hT509S/D530G/L534S	138 ± 6	405 ± 171	3
rbS512T	1347 ± 421#	246 ± 43	3

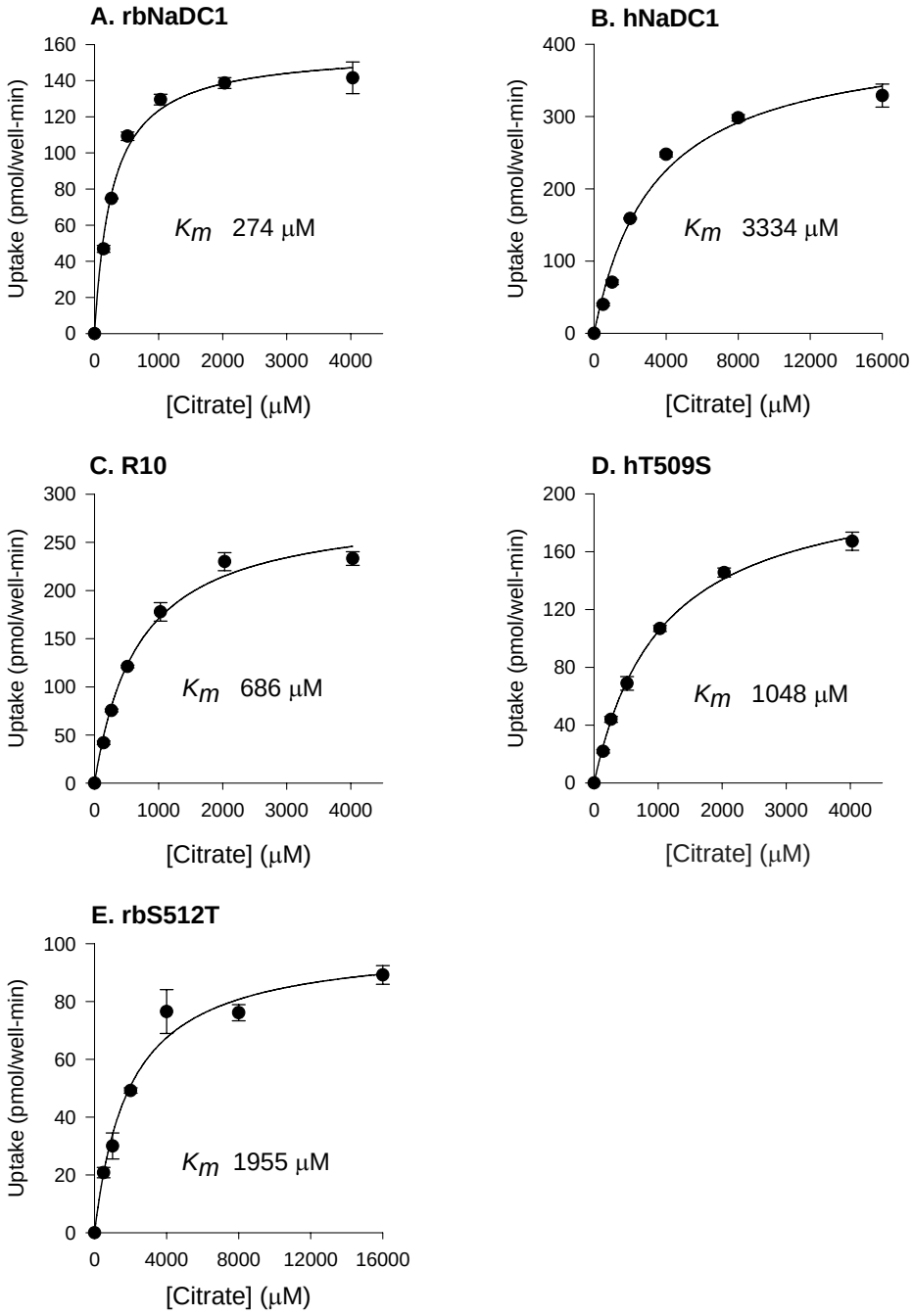

Figure 4.5 Citrate kinetics of hT509S and rbS512T mutants. Kinetic studies were determined in COS-7 cells expressing parental wild-types, the chimera R10, hT509S and rbS512T mutants. The uptake of [^{14}C]citrate was measured for 5 min. Each data point shows the mean ± range (N = 2) from a single experiment. The results of three separate experiments are shown in Table 4.1.

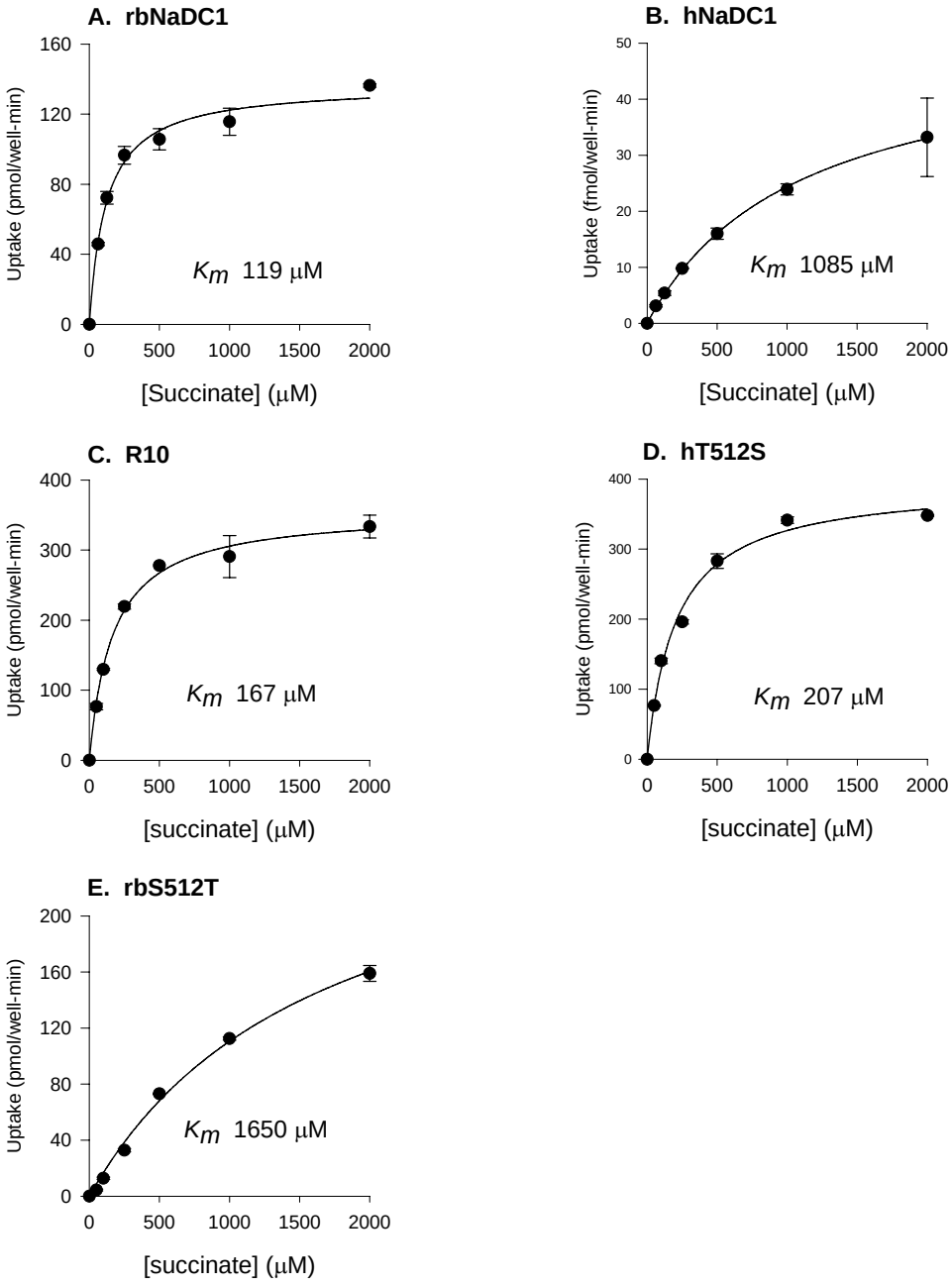

Figure 4.6 Succinate kinetics of hT509S and rbS512T mutants. Kinetic studies were determined in COS-7 cells expressing parental wild-types, the chimera R10, hT509S and rbS512T mutants. The uptake of [^{14}C]succinate was measured for 5 min. Each data point shows the mean ± range (N = 2) from a single experiment. The results of three separate experiments are shown in Table 4.2.

Differences in Substrate Specificity Are Also Determined by Amino Acid 509

The rabbit and human NaDC1 transporters also differ in their handling of four or five carbon dicarboxylate substrates, including fumarate, methylsuccinate, and malate (Pajor & Sun, 1996b; Pajor *et al.*, 1998a; Yao & Pajor, 2000). The substrate specificity of the wild-type and mutant transporters was tested by measuring the transport of succinate in the presence of test inhibitors (Figure 4.7).

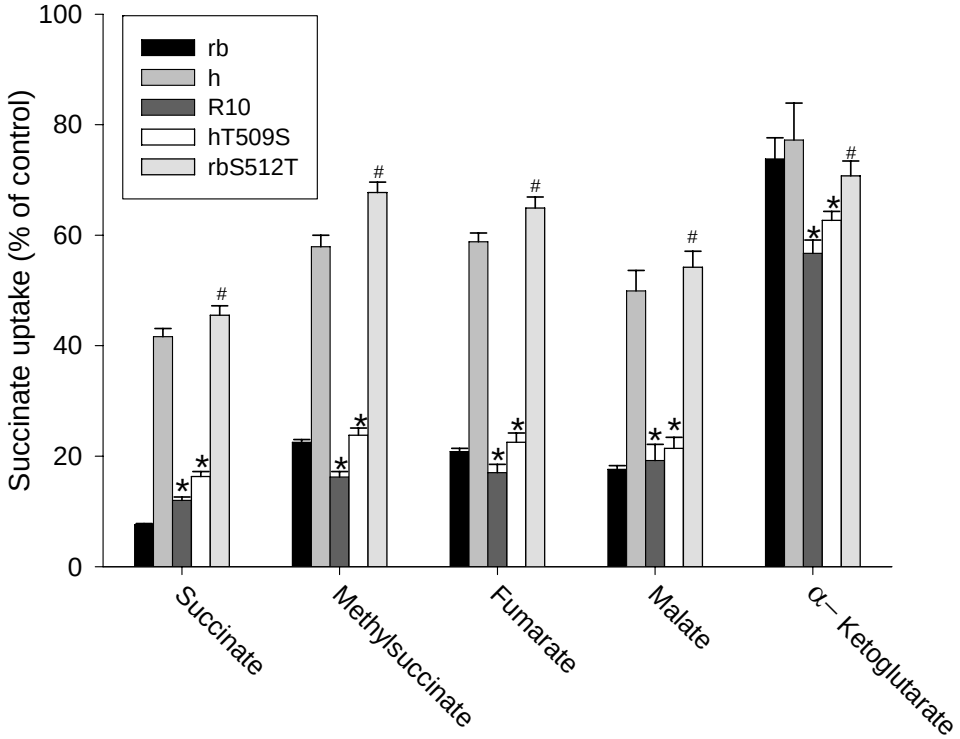

Figure 4.7 Substrate specificity of NaDC1 mutants. Transport of 10 μM [^{14}C]succinate was measured for 5 min in the presence or absence of 1mM test inhibitors. The transport in the presence of inhibitors is expressed as a percentage of control measured without inhibitors. The bars represent mean ± S.E.M., N = 3-4 experiments. The * denotes significant difference compared with the parental hNaDC1 and the # denotes significant difference compared with the parental rbNaDC1, ($p< 0.05$).

The inhibition by α-ketoglutarate was relatively low, suggesting that the affinity for this substrate is low in both human and rabbit NaDC1. The $K_{0.5}$ for α-ketoglutarate in hNaDC1 expressed in *Xenopus* oocytes is around 16 mM (Yao & Pajor, 2000). The sensitivity of rbNaDC1 to inhibition by succinate, methylsuccinate, fumarate, and malate was greater than hNaDC1 (Figure 4.7). The R10 chimera, with TM10 from rbNaDC1 in a hNaDC1 background, had the substrate specificity of rbNaDC1. The single mutation at position 509/512, hT509S and rbS512T, was sufficient to confer the substrate specificity of the donor. These results verify that the serine at position 509/512 is an important determinant of substrate specificity.

Thr-509 Determines Differences in Sodium Affinity

The activation of succinate transport by sodium was measured for wild-type and mutant transporters. There was a sigmoid relationship between sodium concentration and succinate transport rate, with apparent K_{Na} values of 30 mM for rbNaDC1 and 112 mM for hNaDC1 (Table 4.3), consistent with previous studies (Pajor & Sun, 1996b; Kahn & Pajor, 1999). Chimera R10 and the hT509S mutant had K_{Na} values that were not different from that of the rbNaDC1 and significantly different from that of the hNaDC1 (the single experiments are shown in Figure 4.8, and the mean of three experiments is in Table 4.3). The reverse mutation, rbS512T, produced a significant increase in K_{Na} although not as large as the threonine to serine mutation at position 509 in the human transporter (the single experiments are shown in Figure 4.8, and the mean of three experiments is in Table 4.3). The Hill coefficient (n_H) remained unchanged for parental transporters and mutants.

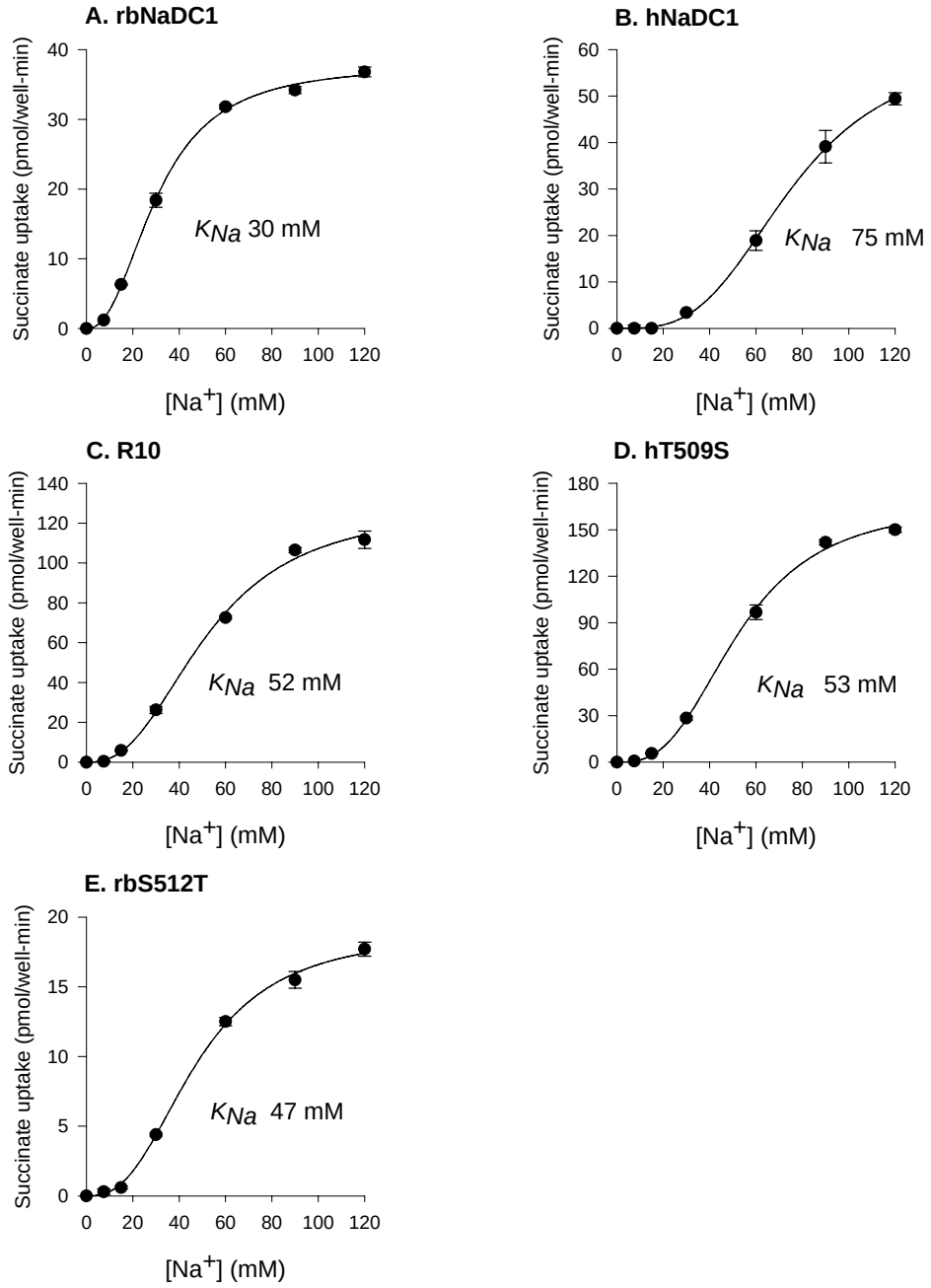

Figure 4.8 Sodium activation of succinate transport by COS-7 cells expressing the parental wild-type, the chimera R10, hT509S and rbS512T mutants. Five minute uptakes of 100 μM [^{14}C]succinate were measured in sodium concentrations up to 120 mM NaCl (NaCl was replaced by cholineCl). Each data point shows the mean ± range (N = 2) from a single experiment. The results of three separate experiments are shown in Table 4.3.

Table 4.3 Na^+ activation in mutants. Sodium activation of succinate transport in COS-7 cells expressing the wild type or mutant NaDC1 transporters. Five minute uptakes of 100 μM [^{14}C]succinate were measured in buffer containing sodium concentrations up to 120 mM. NaCl was replaced by choline chloride. The data represent the mean ± S.E.M, n = 3 experiments. Data were fitted to the Hill equation by nonlinear regression, the Hill coefficient is n_H. *, significant difference compared with the parental hNaDC1 ($p< 0.05$).

WT / Mutants	Na activation		
	K_{Na} (mM)	V_{max} (pmol/well-min)	(n_H)
rbNaDC1	30 ± 1*	65 ± 24	2.5 ± 0.3
hNaDC1	112 ± 25	55 ± 16	2.6 ± 0.4
R10 chimera	49 ± 3*	163 ± 19	2.6 ± 0.2
hT509S	51 ± 2*	153 ± 9	2.9 ± 0.2
rbS512T	46 ± 3*	21 ± 2	2.6 ± 0.1

DISCUSSION

The present study was based on previous observations that differences in substrate and cation affinity between the rabbit and human NaDC1 transporters are determined by residues located in transmembrane helices (TM) 7, 10 and 11 (Kahn & Pajor, 1999). Chimeras made between rb and hNaDC1 had the citrate affinity of the donor of TM 7, 10 and 11 and associated loops, whereas TM10 and 11 were sufficient to transfer cation affinity of the donor. The TM10 region used in the chimera study has only four amino acid differences between the human and rabbit sequences. To identify individual residues in this region that determine the functional differences, four mutants were made with the rabbit sequence substituted for that of the hNaDC1. The major finding of this study is that the residue at position 509 (human) or 512 (rabbit) is critical for determining both substrate and cation affinity in

NaDC1. When position 509/512 is occupied by a serine, as in the rbNaDC1, the affinity for substrates and sodium is higher than when a threonine is found at this position. Furthermore, the cation and substrate binding sites in NaDC1 are likely to be located in close proximity to one another.

The current secondary structure model of NaDC1 contains 11 TM, with an intracellular amino-terminus and an extracellular N-glycosylated carboxy-terminus (Zhang & Pajor, 2001). TM9 and the connecting loop to TM10 form part of the permeation pathway in NaDC1, and this region contains functionally important residues that are alternately accessible and inaccessible to the extracellular medium during the transport cycle (Pajor, 2001; Pajor & Randolph, 2005). The model places Thr-509 in the TM10 helix and Asp-530, Lys-532, and Leu-534 in the intracellular loop between TM10 and 11 (Figure 4.1). The relative position of Thr-509/Ser-512 within the middle of the transmembrane helix is consistent with the locations of substrate and cation binding sites within aqueous cavities formed by multiple helices of the known structural models of ion-coupled transport proteins, including the H^+-coupled lactose permease (Abramson *et al.*, 2003), Na^+-dependent leucine transporter, $LeuT_{Aa}$ (Yamashita *et al.*, 2005), and the Na^+-dependent aspartate transporter, Glt_{Ph} (Yernool *et al.*, 2004).

The substitution of Thr-509 by serine in hNaDC1 produces a change in succinate K_m to that of the rbNaDC1, which has a serine at position 512, the equivalent position (see alignment, Figure 4.1). The substrate specificity profile with other dicarboxylic acids including malate, fumarate and methylsuccinate, can also be converted between the human and rabbit phenotypes by the presence of serine or threonine at position 509/512. The difference in affinity for citrate, however,

probably requires additional amino acids. The hT509S mutant has an intermediate citrate K_m, indicating that additional amino acids, probably located in TM7 and 11, are required to determine differences in citrate affinity. In previous study of mouse NaDC1, Pajor and colleagues found that serine replacement of the equivalent position at Ala-504 produced a more rabbit-like phenotype with decreased affinity for succinate and adipate but the reverse mutation in rabbit (rbS512A) was not sufficient to increase affinity for adipate (Oshiro & Pajor, 2006). The S512C mutant of rbNaDC1 was not expressed on the cell surface, possibly because of protein misfolding (Pajor & Randolph, 2005). Cysteine was found at this position in the high affinity NaDC3 transporters.

The transport of dicarboxylates in NaDC1 is a sodium-dependent process that involves an ordered, cooperative binding of three sodium ions followed by substrate (Wright *et al.*, 1983; Yao & Pajor, 2000). An alteration in the Na^+ activation kinetics with an increase in sodium affinity was observed for hT509S, which was similar to chimera R10. Although the single mutation of hNaDC1 was sufficient to convert the K_{Na} to that of the rabbit, only a partial change in phenotype was seen in the reverse mutant, rbS512T. One possible explanation is that another residue, different in human and rabbit NaDC1, is also involved in determining the difference in cation affinity. In the human, the serine to threonine mutation is compatible with the endogenous second residue, but in the rabbit, the addition of threonine is not sufficient to overcome the properties of the endogenous second residue.

The involvement of a single residue in determining differences in both substrate and cation affinity could be explained by cation and substrate binding sites in close proximity to one another, similar to recent structures of sodium-coupled

transporters. For example, in the Na^+/aspartate transporter, $Glt_{Ph,}$ the substrate and cation binding sites are located close together. One residue, Ser-278, interacts with one of the sodium ions through the hydroxyl group, and also with the substrate through the backbone nitrogen of the same serine (Boudker *et al.*, 2007). In the Na^+/leucine cotransporter, $LeuT_{Aa}$, the substrate itself helps to coordinate one of the sodium ions (Yamashita *et al.*, 2005). Therefore, a mutation in the substrate binding site could alter cation affinity by either changing the position of the substrate within its binding site or changing the position of residues in the protein that interact with the cation. An alternate possibility is that Thr-509 (hNaDC1) or Ser-512 (rb) is not directly involved in substrate or cation binding, but rather is important in holding key residues in place. In the mitochondrial citrate transport protein (CTP), a sodium-independent transporter that is not related in sequence to NaDC1, mutation of Ser-123 to Cys increases the citrate K_m fivefold, although the structural model places this residue near (but not in direct contact with) the substrate (Ma *et al.*, 2005).

Since only the 509/512 residue of TM 10 is different between the human and rabbit NaDC1, the threonine-serine substitutions would not alter the structure of the helix with the exception of the side chain properties at the 509 or 512 position (Figure 4.9). The hydroxyl group of serine or threonine does not appear to be required for function since the mouse NaDC1 contains alanine at this position, and the S512A mutant of rbNaDC1 does not exhibit any change in functional properties (Oshiro & Pajor, 2006). Possibly the size or volume of the side chain at this position affects the substrate binding site in NaDC1. In the Na^+/Cl^--glycine transporters, GLYT1 and 2, substrate selectivity is determined by the presence of a glycine or serine in TM 6, and mutants containing the smaller glycine residue can accommodate larger substrates in

the binding site (Vandenberg *et al.*, 2007). It should be noted that Thr-509/Ser-512 of NaDC1 determines differences in function. There are likely to be multiple amino acids involved in coordinating each sodium ion and forming the substrate binding site, and these would probably be in common in the human and rabbit Na^+/dicarboxylate cotransporters.

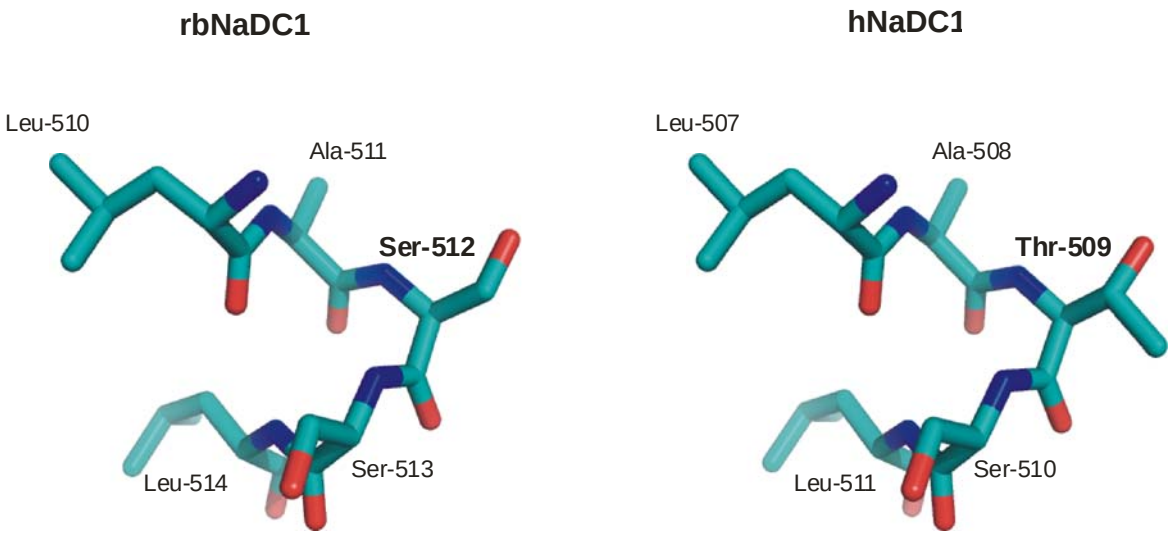

Figure 4.9 Models of part of TM 10 from wild-type rbNaDC1 with serine at position 512 (left) compared with hNaDC1 with threonine at the equivalent position, 509 (right). The model shows five amino acids from approximately the middle of TM10, with the N-terminal amino acids (Leu-510 (rb), or Leu-507, (h)) coming from the outside of the cell (top). The figure was prepared with the Pymol program (http://www.pymol.org).

In summary, this study identifies Thr-509 (h) or Ser-512 (rb) as a key residue that determines functional differences in substrate and cation affinity between rabbit and human NaDC1. This residue also determines differences in specificity for dicarboxylate substrates between the two transporters. The results confirm the important role of TM10 in forming part of the substrate and cation binding sites.

Since a single residue affects both transport properties, it is likely that NaDC1 resembles other sodium-coupled transporters in having substrate and cation binding sites in close proximity to one another.

CHAPTER 5: CONCLUSIONS AND FUTURE DIRECTIONS

The main discoveries of this dissertation are 1) di- and tricarboxylates are transported by Caco-2 cells through multiple transport pathways; 2) TM3 of NaDC1 contains residues involved in substrate recognition and Lys-84 originally predicted to be in intracellular loop is probably in the helix forming part of permeation transport pathway; 3) a serine or threonine at position 509 (or 512 in rbNaDC1) in TM10 partially determines differences in K_m for citrate, but is sufficient to confer affinity for succinate and cations, and substrate specificity for four-carbon dicarboxylates.

THE SUCCINATE AND CITRATE TRANSPORT PATHWAYS IN Caco-2 CELLS

As already discussed in Chapter 2, it has been known that citric acid cycle intermediates are absorbed from the gastrointestinal tract through carrier-mediated mechanisms. Di-and tricarboxylates are taken up from luminal side occurring by a sodium-coupled transport system; nevertheless, the detailed transport pathways have not been clearly identified. Here, the study in this dissertation first demonstrates the involvement of multiple transport pathways for the transport of di- and tricarboxylates by Caco-2 cells. It established that one of the intestinal transport pathways across apical membrane studied in Caco-2 is mediated by NaDC1. As a consequence of using Caco-2 as a model of enterocytes, which could reflect the cancerous state of the Caco-2 cells, the information provided may be different from the normal intestine. The Na^+-dependent transport of succinate and citrate in Caco-2 cells is mediated not only by NaDC1, but also by Na^+-coupled citrate transporter, NaCT, which is not expressed in human normal intestine. In addition,

characterization of di-and tricarboxylates transport in Caco-2 cells revealed the Na^+-independent transport of citrate that is likely mediated by an organic anion transporter, possibly organic anion transporter (OAT) 2 and OAT4. Again, the tissue distributions of any OATs have not been found in normal intestine. However, in order to firmly establish this conclusion, gene-specific silencing with siRNA might be needed to dissect the relative contribution of the different transports in the uptake of the different substrates.

Regarding transepithelial transport, as shown in Chapter 2, there is transepithelial transport of methylsuccinate across the basolateral membranes in both a Na^+-dependent and-independent transporter manner. The translocation of tricarboxylates across the basolateral compartment is believed to be mediated by an exchange mechanism (Wolffram *et al.*, 1994). At the moment, it is still unclear which transporter is responsible for di-and tricarboxylate transport across the basolateral membrane. Overall, these studies have revealed a novel and unique aspect of the transport mechanism of di-and tricarboxylates in Caco-2 cells. Some observations and transport systems for di-and tricarboxylates seen in Caco-2 cells are different from normal intestinal cells, implying that Caco-2 cells do not share the same transport system for di-and tricarboxylates. Caco-2 cells have proven a suitable model for studying carrier-mediated transport in human intestine (Sambuy *et al.*, 2005), nonetheless this cell line does not seem to be an appropriate model for studies of di- and tricarboxylate transport, especially citrate. Additionally, mannitol, an extracellular marker generally used to correct for residual extracellular volume, is unlikely to be a good marker for Caco-2 cells. Although the studies in Chapter 2

could not physiologically extrapolate to normal intestine, they could at least provide some insight into tri-and dicarboxylate transport in cancerous cells.

INVOLVEMENT OF TM3 IN FORMING PART OF THE PERMEATION PATHWAY IN NaDC1 AND CONTRIBUTING TO THE SUBSTRATE BINDING SITES

As written in the review of serotonin transporter by Rudnick (Rudnick, 2006), in order to understand the mechanism of a transporter in detail one requires knowledge of four key assets of the proteins. First, the nature of the binding site how the transporter can selectively transport one substrate and not another. Second, the pathways through which substrate and ions pass in their movement from one side of the membrane to the binding site and then from the binding site to the other side of the membrane. Third, conformational changes that close access from one side to the other side of the membrane and open access to the other, which are required for translocation to occur. Last, controls of conformational changes occur only when the appropriate ligands are bound at the binding sites.

Based on previous studies by Pajor and colleagues, NaDC1 contains functionally important residues in many helices. Amino acids in TM7, 8, 9 and the loop between 9 and 10, when are mutated to cysteine, are sensitive to inhibition by cysteine selective reagents (Pajor, 2001; Yao & Pajor, 2002; Pajor & Randolph, 2005). TM7 contains functionally important amino acids and seems to be essential for binding and translocation of succinate and citrate (Yao & Pajor, 2002). A minimum of ten amino acids in TM9 and 10 are likely to participate in the conformational changes seen during the transport cycle of NaDC1, and are part of the substrate permeation pathway in NaDC1 (Pajor, 2001; Pajor & Randolph, 2005).

Residues from multiple TMs, including 3, 7, 8, and 10 are involved in glutarate transport and evidence of functional interaction in the transition state between amino acid in TM3 and 4 was reported (Oshiro *et al.*, 2006). Overall, previous data from TM3, 7, 9 and the loop between 9 and 10 contain functionally important amino acid residues. From the known structural models of ion-coupled transport proteins, including the H^+-coupled lactose permease (Abramson *et al.*, 2003), Na^+-dependent leucine transporter, $LeuT_{Aa}$ (Yamashita *et al.*, 2005), and the Na^+-dependent aspartate transporter, Glt_{Ph} (Yernool *et al.*, 2004), the locations of the substrate and cation binding sites are shown to be within the aqueous cavities formed by multiple helices. Therefore, it is possible that TM3 and TM7 contribute as well as TM9 and TM10 to form a central pore being part of the permeation pathway.

The studies in Chapter 3 show that TM3 contains residues involved in substrate recognition, forms part of the permeation pathway in the transporter and contributes to the substrate binding sites. There is interesting information about Lys-84. The accessibility of K84C to MTSES seems to parallel the exposure of the substrate binding site. The accessibility of K84C to MTSES can be only seen in the presence of sodium. This is in accordance with the ordered binding mechanism of NaDC1, in which binding of sodium triggers a conformational change in NaDC1 in which the helices may tilt or rotate to allow exposure of the substrate-binding site and cause a subsequent increase in substrate affinity. The addition of succinate protected against cysteine modification at both 25^{o}C and 4^{o}C. This behavior suggests succinate binding produces steric hindrance of MTSES binding, and the binding of succinate seems occur at an early state in the transport cycle prior to translocation event. This is also in agreement with the transport process of NaDC1. Additionally, the

investigation of TM3 provides the new discovery. Lys-84 originally predicted to be in intracellular loop is probably in the helix forming part of permeation transport pathway as predicted. If Lys-84 is buried in TM3 more than halfway across the membrane, it can be accessible to the reagents on the extracellular side. Then it is compatible to the structure of LeuT, as having the shape of a shot glass, in which the cavity of the glass is the opening in the structure that leads from the extracellular side of the protein to the bound leucine (Yamashita *et al.*, 2005; Rudnick, 2006). It is also well-matched to the glutamate transporter which contains its substrate binding sites in a large bowl approximately 50 Å in diameter (Yernool *et al.*, 2004).

AMINO ACID RESIDUES THAT DETERMINE DIFFERENCES IN CITRATE K_m IN HUMAN AND RABBIT NaDC1

As mentioned earlier, to understand the mechanism of a transporter in more detail, it is important to know the nature of the binding site, which determines how the transporter can selectively transport one substrate and not another (Rudnick, 2006). As discussed in Chapter 4, there are some functional differences between rbNaDC1 and hNaDC1 with respect to high and low affinity for citrate and cations. A previous study by Pajor and Kahn's in which chimeric human and rabbit Na^+/dicarboxylate cotransporters were constructed to delineate the regions of the protein responsible for the functional differences between rbNaDC1 and hNaDC1 revealed interactions between transmembrane helices TM7, 10, and 11. These interactions contribute to the differences in apparent citrate affinities (Kahn & Pajor, 1999). The differences in apparent sodium affinities between the hNaDC1 and rbNaDC1 are determined primarily by residues in TM10 and 11 (Kahn & Pajor, 1999). The studies in Chapter 4, by construction of mutants in TM10 and

examination the effects of the four amino acids differences between hNaDC1 and rbNaDC1 in this region. One of the key residues in TM10 can be firstly identified. Serine or threonine at position 509 (in hNaDC1) or at position 512 (in rbNaDC1) determines functional differences between NaDC1 orthologs in both substrate and cation transport. As discovered the involvement of a single residue in determining differences in both substrate and cation affinity, thus indicating that the substrate and cation binding sites in NaDC1 are likely to be located in close proximity to one another. This property is quite similar to Na^+/aspartate transporter, Glt_{Ph} (Yernool *et al.*, 2004). In addition, the fact that the size or volume of the side chain affects the substrate binding sites rather than the side chain itself. However, it should be noted that multiple amino acids are involved in coordinating each sodium ion and form the substrate binding site.

FUTURE DIRECTIONS

To date, the vast majority of knowledge about the SLC13 gene family, including physiological function, tissue distribution and substrate specificity has been thoroughly known. Nonetheless, the information of the structure-function relationship that helps to understand the molecular mechanism and structural dynamics of membrane transporters in members of this gene family is still limited.

The current secondary structure models of members of the SLC13 family are based upon hydropathy analysis and contain between 11 and 14 predicted transmembrane helices (see review (Pajor, 2006)). Recently, evidence for a topology of human NaDC3 was disclosed for the first time using a combination of confocal immunofluorescence microscopy, membrane biotinylation of epitope-tagged N- and

C- termini, antibodies against the loop domains and cysteine accessibility method (Bai *et al.*, 2007). The result shows 11 transmembrane domains with an extracellular C-terminus and intracellular N-terminus. Even though the secondary structure model of hNaDC3 has been revealed, the models of other members of the SLC13 family are largely untested. The actual membrane topological structure of NaDC1 remains unknown. There is experimental evidence showing N- and C- termini are on the opposite sites of the membrane and supporting an odd number of TMs, which are can be either 11 or 13 (Pajor, 2006). Hydropathy analysis predicts the secondary structure model of NaDC1 that contains 11 hydrophobic transmembrane helices. However, modeling studies suggest that 13 TMs could also be possible (Joshi & Pajor, 2007). Thus, the membrane topological structure of NaDC1 should be further verified by site-directed mutagenesis to introduce cysteines in predicted loops of NaDC1 and topology will can be determined using cysteine specific sulfhydryl reagents.

As part of interest in the structure and function of NaDC1, it has become apparent that the part of the transporter that faces the cytoplasm undergoes important conformational changes during transport. In order to accommodate the dicarboxylates and sodium that are also transported during one turnover of the transporter, it is predicted changes in transmembrane helical packing during the transport cycle. To translocate all three sodiums and one dicarboxylate into the inside of the cells, the translocation pathway for NaDC1 should be formed in part, by loops as well as transmembrane domains.

Data from previous and present studies showed that TM3 and TM10 are parts of the permeation pathway. By placing some residues such as Lys-84 and Ser-512,

that affect substrate and cation binding, in the helix rather than in the loop, it is possible that the binding site for the substrate and cations is formed, at least in part by TM3 and TM10. Based on earlier evidence, TM7 contains conserved prolines (Pro-327 and Pro-351) which are important for structure and function as well as Phe-347 also affects the K_m for succinate (Joshi & Pajor, 2006). If TM3, 7, and 10 indeed form the central pore and it allows substrates to bind and permeate, then cysteine scans of TM7 needs to be further investigated to test the hypothesis that TM7 forms part of the permeation pore of NaDC1.

If TM3, 7, and 10 form the permeation pathway and substrate binding pocket to hold the substrate and cation, then it seems that there should be specific interactions directly between side chains with each other or among TM3, 7 and 10 to form the permeation pathway in NaDC1. Therefore, the interaction of these TMs will have to be tested by using an application employed from methods developed for studying the interaction between TM3 and TM4 (Oshiro *et al.*, 2006). A previous chimera study between mNaDC1 and rbNaDC1 took advantage from TSR analysis to show that there is functionally interaction in the transition state complex between TM3 and 4. Hence, TSR analysis can be applied to assess whether TM3, 7, and 10 interact or not. If there are interactions among TM3, 7 and 10 to form the permeation pore and allow the substrate to bind and permeate, then these interactions should be formed directly between amino acids located in TM3, 7 and 10. Consequently, these amino acids which interact among TM3, 7 and 10, or possibly other helices should be further elucidated.

In addition, since there is a series of ordered ligand induced conformational changes, it should further examine which helices move, the order in which they move,

the distances they move during partial reactions of the transport cycle how far they move as the transporter is moved from one conformation to another. Determination of proximities of different TM helices can be carried out by site-directed thiol cross-linking studies either cross-linking with cadmium or cross-linking with MTS reagents. As studied in serotonin (SERT), γ-aminobutyric acid transporter (GABA) (Wolin & Kaback, 2000; Kniazeff *et al.*, 2005; Zomot *et al.*, 2005). Cysteine double mutant pairs close to each other will coordinate cadmium binding, cross-linking can block transporter activity with Cd^{2+}. Studied in the *Vibrio parahaemolyticsus* Na^{+}/glucose transporter (vSGLT) by Wright EM *et al.* (Xie *et al.*, 2000). A split vSGLT was generated by co-expression of the N- and C-terminal seven-transmembrane helical proteins. Two single cysteine mutations in the split N- and C-terminal halves of vSGLT were introduced. The double cysteine-substituted split vSGLTs, L149C/A423C, showed Na^{+}/glucose transport activity comparable with that of a wild-type split vSGLT. This pair of cysteine residues, L149C/A423C, was then subjected to chemical cross-linking analysis using sulfhydryl-reactive cross-linkers with flexible spacer arm lengths of 16 Å (BMH), 11 Å (BMB), and 8.0 Å (BMOE). Application of BMH, BMB, or BMOE to membranes containing double cysteine-substituted split vSGLT L149C/A423C induced the cross-linking of these N_7 and C_7 fragments. Since BMOE has the shortest spacer arm (8 Å) among these three cross-linkers, Wright EM *et al.* concluded that residues L149C and A423C are in close proximity and the distance between residues L149C and A423C is within 8 Å (Xie *et al.*, 2000). Determination of proximities of different TM helices can also be conducted using cysteine scanning mutagenesis along with labeled with fluorescent thiol reagents and using double cysteine mutants and fluorescence and luminescence

energy transfer (FRET & LRET) to measure the distance between the probes on the two cysteines as seen in the study of the structure of Shaker potassium channel (S3-S4) (Selvin, 2002).

As in Chapter 4, it was known that the interactions between TM3, 7, and 10 which contribute to the differences in apparent substrate and sodium affinities between the hNaDC1 and rbNaDC1. While in this dissertation focused solely on TM10, the rest of the key residues in TM7 and TM11 are still unidentified and should be elucidated to test the hypothesis.

The important goal of research in this area is to understand how the conformational changes within NaDC1 leads to alternate accessibility of the binding site from the outside and inside of membrane at different conformational states of NaDC1. So far, the studies have examined the accessibility of cysteine-substituted amino acids from the outside of the cells (Pajor, 2001; Pajor & Randolph, 2005; Weerachayaphorn & Pajor, 2007). Only half of the transport cycle which is accessible from the outside of NaDC1 is known. Many interesting mechanistic questions remain to be answered. So far, a complete picture of the movements during the transport cycle is still missing. Currently, no information on the accessibility of amino acids from the inside of the cells and on what happens once the fully loaded transporter reorients are known. However, to study the structure and transport mechanism of sodium-couple transporters is limited in working with the mammalian proteins. The current knowledge about ion-coupled transporters has derived from studies with homolog from prokaryotic organisms. As reviewed in serotonin transporter (Rudnick, 2006), the recent structure of the bacterial Na^+/leucine

transporter, $LeuT_{Aa}$, provides information about the substrate-and cation-binding sites of the mammalian serotonin transporter.

Recently, Pajor and colleagues have isolated the homolog of Na^+/dicarboxylate symporter from *Staphylococcus aureus*, called SdcS, which is 35% identitical to NaDC1 and has a similar predicted secondary structure (Hall & Pajor, 2005). SdcS shares many functional properties with NaDC1, including sodium-driven transport with ordered binding. Its substrates are four carbon dicarboxylates, which are transported with high affinity *Km* ~ 12 μM (Hall & Pajor, 2007). Therefore, SdcS may serve as a model of NaDC1 for structural studies and allow experiments that are not possible with the mammalian transporters. At the moment, Dr. Pajor has been attempting to make membrane vesicle with different orientations: right-side-out (RSO) and inside-out (ISO) vesicles to explore the reverse transport mode and functional characteristics of cytoplasmic side of NaDC1 as studied hSGLT1 in bacterial membrane vesicles (Quick *et al.*, 2003). However, because there are some properties of SdcS different from those of NaDC1, for example, SdcS is not electrogenic but electro-neutral and it also transport protons, SdcS could reflect differences in accessibility and binding sites.

Recent evidence revealing I550V polymorphism of hNaDC1 may be associated with a reduction in urinary citrate excretion and contribute to hypocitraturia in recurrent calcium stone patients (Okamoto *et al.*, 2007). However, the underlying mechanism of how a mutation at this position causes the abnormality in citrate reabsorption is questioned. The abnormality may be due to a change in the functional properties of I550V (increase an affinity of NaDC1) or a defect in the membrane protein trafficking pathway either up-or down- regulation. Both of these

possiblities could result in an increase the number of NaDC1 proteins on the plasma membrane, thus accelerating the reabsorption of citrate from renal tubular cell. Therefore, identifying the possibilities of the molecular mechanism of NaDC1 mutant, I550V should be further studied. Further investigation of the way that these processes are disrupted in the NaDC1 mutant should be also elucidated.

At present, there is little information available on NaDC1 regulation and other aspects, such as protein-protein interaction, protein- lipid interaction, which are related to govern the NaDC1 subcellular trafficking, targeting and function. In recent years, several PDZ domain proteins, such as Na^+/H^+ exchanger regulatory factor (NHERF)-1, NHERF-2, PDZK1 (NHERF-3) and intestinal and kidney-enriched PDZ protein IKEPP (NHERF-4), have been identified (see review (Anzai *et al.*, 2005b)). The PDZ domain proteins have been suggested to be involved in the stabilization, targeting, and regulation of their binding partner (Biber, 2001;Levi, 2003;Moe, 2003;Anzai *et al.*, 2005b). The PDZ (PSD-95, DglA, and ZO-1)-binding domains have been identified in many proteins and have been known to be modular protein-protein recognition domains that play roles in targeting and protein complex assembly (Fanning & Anderson, 1999;Hung & Sheng, 2002).

It has been demonstrated that PEPT2, URAT1 and OAT4, which are localized on the apical membrane of proximal tubular cells, have a PDZ motif (S/T-X-Ø (X: any residue and Ø: a hydrophobic residue)) at their C-terminus (Anzai *et al.*, 2004; Miyazaki *et al.*, 2005; Noshiro *et al.*, 2006). Noshiro *et al*., Anzai *et al*., and Miyazaki *et al*. revealed that PEPT2, URAT1 and OAT4 interact with the PDZK1 via their C-terminal PDZ motif (Anzai *et al.*, 2004; Miyazaki *et al.*, 2005; Noshiro *et al.*, 2006). The coexpression of PEPT2/URAT1/OAT4 and PDZK1 increases

PEPT2/URAT1/OAT4 transport activity, suggesting PDZK1 regulates transport activities via an interaction with the PDZ motif. NaDC1, which is localized on the apical membrane, has a C-terminal amino-acid sequence that matches the PDZ-binding motif (T-T-P), in a manner similar to that of other apical organic anion transporters, such as PEPT2 (T-K-L) (Noshiro *et al.*, 2006), URAT1 (T-Q-F) (Anzai *et al.*, 2004), OAT4 (T-S-L) (Miyazaki *et al.*, 2005), thus indicating that NaDC1 most likely binds to certain PDZ domain proteins. In kidney there are four PDZ proteins have been identified: NHERF-1, NHERF-2, PDZK1 (NHERF-3), and IKEPP (NHERF-4) (see review (Anzai *et al.*, 2006)). Based on a previous finding that NHERF-2 is involved in the regulation of NaDC1 (Boehmer *et al.*, 2004), it is possible that NaDC1 binds with NHERF-2 or other PDZ protein(s) via its PDZ-motif. A functional regulator of NaDC1 that acts through direct interaction between PDZ domains and the C terminus of NaDC1 should be studied.

Moreover, since NaDC1 is responsible for the reabsorption of citrate from renal tubular cells, it is likely the activation of NaDC1 is correlated to hypocitraturia. There is interest in NaDC1 as a target for the treatment of kidney stones. One of the therapeutic approaches is that inhibition of NaDC1 function alleviates or prevents kidney stones resulting from hypocitraturia. At the moment, inhibitors for NaDC1 have not been reported yet. It is important to search for promising inhibitors of NaDC1 and to identify the location of inhibitor binding to NaDC1 and the mechanism of action.

These present and future studies will reveal a wealth of information and enable us to further understand more structural details of NaDC1: what the structure of NaDC1 is; where the substrate binding site is; how the transporter senses and

responds to cations and substrates; how TM3, 7 and 10 move in response to substrate binding; how NaDC1 moves substrates and ions from the extracellular to the binding site and then to the cytoplasm; how dynamic conformational changes occurring during the transport cycle of NaDC1 both forward and reverse orientations. In addition, these studies will provide insight for the development of targeted drugs for treatment and prevention of kidney stones.

BIBLIOGRAPHY

Abramson J, Smirnova I, Kasho V, Verner G, Kaback HR, & Iwata S (2003). Structure and mechanism of the lactose permease of Escherichia coli. *Science* **301**, 610-615.

Anderle P, Rakhmanova V, Woodford K, Zerangue N, & Sadee W (2003). Messenger RNA expression of transporter and ion channel genes in undifferentiated and differentiated Caco-2 cells compared to human intestines. *Pharm Res* **20**, 3-15.

Anzai N, Jutabha P, Enomoto A, Yokoyama H, Nonoguchi H, Hirata T, Shiraya K, He X, Cha SH, Takeda M, Miyazaki H, Sakata T, Tomita K, Igarashi T, Kanai Y, & Endou H (2005a). Functional characterization of rat organic anion transporter 5 (Slc22a19) at the apical membrane of renal proximal tubules. *J Pharmacol Exp Ther* **315**, 534-544.

Anzai N, Jutabha P, Kanai Y, & Endou H (2005b). Integrated physiology of proximal tubular organic anion transport. *Curr Opin Nephrol Hypertens* **14**, 472-479.

Anzai N, Kanai Y, & Endou H (2006). Organic anion transporter family: current knowledge. *J Pharmacol Sci* **100**, 411-426.

Anzai N, Miyazaki H, Noshiro R, Khamdang S, Chairoungdua A, Shin HJ, Enomoto A, Sakamoto S, Hirata T, Tomita K, Kanai Y, & Endou H (2004). The multivalent PDZ domain-containing protein PDZK1 regulates transport activity of renal urate-anion exchanger URAT1 via its C terminus. *J Biol Chem* **279**, 45942-45950.

Aruga S, Pajor AM, Nakamura K, Liu L, Moe OW, Preisig PA, & Alpern RJ (2004). OKP cells express the Na-dicarboxylate cotransporter NaDC-1. *Am J Physiol Cell Physiol* **287**, C64-C72.

Aruga S, Wehrli S, Kaissling B, Moe OW, Preisig PA, Pajor AM, & Alpern RJ (2000). Chronic metabolic acidosis increases NaDC-1 mRNA and protein abundance in rat kidney. *Kidney Int* **58**, 206-215.

Bai L & Pajor AM (1997). Expression cloning of NaDC-2, an intestinal Na^+- or Li^+-dependent dicarboxylate transporter. *Am J Physiol* **273**, G267-G274.

Bai XY, Chen X, Sun AQ, Feng Z, Hou K, & Fu B (2007). Membrane topology structure of human high-affinity, sodium-dependent dicarboxylate transporter. *FASEB J* **21**, 1-9.

Beck L & Markovich D (2000). The mouse Na^+-sulfate cotransporter gene Nas1. Cloning, tissue distribution, gene structure, chromosomal assignment, and transcriptional regulation by vitamin D. *J Biol Chem* **275**, 11880-11890.

Benyajati S and Pritchard JB (2005). Taurine efflux is mediated by renal luminal organic anion transporter, hOAT4 (SLC22A11). *FASEB J* **19**, A150 (Abstr.).

Biber J (2001). Emerging roles of transporter-PDZ complexes in renal proximal tubular reabsorption. *Pflugers Arch* **443**, 3-5.

Boehmer C, Embark HM, Bauer A, Palmada M, Yun CH, Weinman EJ, Endou H, Cohen P, Lahme S, Bichler KH, & Lang F (2004). Stimulation of renal Na^+ dicarboxylate cotransporter 1 by Na^+/H^+ exchanger regulating factor 2, serum and glucocorticoid inducible kinase isoforms, and protein kinase B. *Biochem Biophys Res Commun* **313**, 998-1003.

Boudker O, Ryan RM, Yernool D, Shimamoto K, & Gouaux E (2007). Coupling substrate and ion binding to extracellular gate of a sodium-dependent aspartate transporter. *Nature* **445**, 387-393.

Browne JL, Sanford PA, & Smyth DH (1978). Transfer and metabolism of citrate, succinate, alpha-ketoglutarate and pyruvate by hamster small intestine. *Proc R Soc Lond B Biol Sci* **200**, 117-135.

Burckhardt BC, Steffgen J, Langheit D, Muller GA, & Burckhardt G (2000). Potential-dependent steady-state kinetics of a dicarboxylate transporter cloned from winter flounder kidney. *Pflugers Arch* **441**, 323-330.

Burckhardt BC, Drinkuth B, Menzel C, Konig A, Steffgen J, Wright SH, & Burckhardt G (2002). The renal Na^+-dependent dicarboxylate transporter, NaDC-3, translocates dimethyl- and disulfhydryl-compounds and contributes to renal heavy metal detoxification. *J Am Soc Nephrol* **13**, 2628-2638.

Burckhardt BC, Lorenz J, Burckhardt G, & Steffgen J (2004). Interactions of benzylpenicillin and non-steroidal anti-inflammatory drugs with the sodium-dependent dicarboxylate transporter NaDC-3. *Cell Physiol Biochem* **14**, 415-424.

Busch W & Saier MH, Jr. (2002). The transporter classification (TC) system, 2002. *Crit Rev Biochem Mol Biol* **37**, 287-337.

Cha SH, Sekine T, Kusuhara H, Yu E, Kim JY, Kim DK, Sugiyama Y, Kanai Y, & Endou H (2000). Molecular cloning and characterization of multispecific organic anion transporter 4 expressed in the placenta. *J Biol Chem* **275**, 4507-4512.

Cha SH, Sekine T, Fukushima JI, Kanai Y, Kobayashi Y, Goya T, & Endou H (2001). Identification and characterization of human organic anion transporter 3 expressing predominantly in the kidney. *Mol Pharmacol* **59**, 1277-1286.

Chen X, Tsukaguchi H, Chen XZ, Berger UV, & Hediger MA (1999). Molecular and functional analysis of SDCT2, a novel rat sodium-dependent dicarboxylate transporter. *J Clin Invest* **103**, 1159-1168.

Chen XZ, Shayakul C, Berger UV, Tian W, & Hediger MA (1998). Characterization of a rat Na^+-dicarboxylate cotransporter. *J Biol Chem* **273**, 20972-20981.

Decoursey TE (2003). Voltage-gated proton channels and other proton transfer pathways. *Physiol Rev* **83**, 475-579.

Doyle DA, Morais CJ, Pfuetzner RA, Kuo A, Gulbis JM, Cohen SL, Chait BT, & MacKinnon R (1998). The structure of the potassium channel: molecular basis of K^+ conduction and selectivity. *Science* **280**, 69-77.

Dutzler R, Campbell EB, Cadene M, Chait BT, & MacKinnon R (2002). X-ray structure of a ClC chloride channel at 3.0 A reveals the molecular basis of anion selectivity. *Nature* **415**, 287-294.

Ekaratanawong S, Anzai N, Jutabha P, Miyazaki H, Noshiro R, Takeda M, Kanai Y, Sophasan S, & Endou H (2004). Human organic anion transporter 4 is a renal apical organic anion/dicarboxylate exchanger in the proximal tubules. *J Pharmacol Sci* **94**, 297-304.

Fanning AS & Anderson JM (1999). Protein modules as organizers of membrane structure. *Curr Opin Cell Biol* **11**, 432-439.

Fei YJ, Inoue K, & Ganapathy V (2003). Structural and functional characteristics of two sodium-coupled dicarboxylate transporters (ceNaDC1 and ceNaDC2) from Caenorhabditis elegans and their relevance to life span. *J Biol Chem* **278**, 6136-6144.

Garthwaite J (1979). Discrepancies in the extracellular space of sympathetic ganglia measured using different isotopes of mannitol and sucrose. *J Neurosci Methods* **1**, 185-193.

Garvey WT, Maianu L, Zhu JH, Brechtel-Hook G, Wallace P, & Baron AD (1998). Evidence for defects in the trafficking and translocation of GLUT4 glucose transporters in skeletal muscle as a cause of human insulin resistance. *J Clin Invest* **101**, 2377-2386.

Girard JP, Baekkevold ES, Feliu J, Brandtzaeg P, & Amalric F (1999). Molecular cloning and functional analysis of SUT-1, a sulfate transporter from human high endothelial venules. *Proc Natl Acad Sci U S A* **96**, 12772-12777.

Griffith DA & Pajor AM (1999). Acidic residues involved in cation and substrate interactions in the Na^+/dicarboxylate cotransporter, NaDC-1. *Biochemistry* **38**, 7524-7531.

Hagenbuch B & Meier PJ (2004). Organic anion transporting polypeptides of the OATP/ SLC21 family: phylogenetic classification as OATP/ SLCO superfamily, new nomenclature and molecular/functional properties. *Pflugers Arch* **447**, 653-665.

Hagos Y, Stein D, Ugele B, Burckhardt G, & Bahn A (2007). Human renal organic anion transporter 4 operates as an asymmetric urate transporter. *J Am Soc Nephrol* **18**, 430-439.

Hall JA & Pajor AM (2005). Functional characterization of a Na^+-coupled dicarboxylate carrier protein from Staphylococcus aureus. *J Bacteriol* **187**, 5189-5194.

Hall JA & Pajor AM (2007). Functional reconstitution of SdcS, a Na^+-coupled dicarboxylate carrier protein from Staphylococcus aureus. *J Bacteriol* **189**, 880-885.

Harries WE, Akhavan D, Miercke LJ, Khademi S, & Stroud RM (2004). The channel architecture of aquaporin 0 at a 2.2-Å resolution. *Proc Natl Acad Sci U S A* **101**, 14045-14050.

Hasannejad H, Takeda M, Taki K, Shin HJ, Babu E, Jutabha P, Khamdang S, Aleboyeh M, Onozato ML, Tojo A, Enomoto A, Anzai N, Narikawa S, Huang XL, Niwa T, & Endou H (2004). Interactions of human organic anion transporters with diuretics. *J Pharmacol Exp Ther* **308**, 1021-1029.

He W, Miao FJ, Lin DC, Schwandner RT, Wang Z, Gao J, Chen JL, Tian H, & Ling L (2004). Citric acid cycle intermediates as ligands for orphan G-protein-coupled receptors. *Nature* **429**, 188-193.

Hediger MA, Romero MF, Peng JB, Rolfs A, Takanaga H, & Bruford EA (2004). The ABCs of solute carriers: physiological, pathological and therapeutic implications of human membrane transport proteinsIntroduction. *Pflugers Arch* **447**, 465-468.

Hentschel H, Burckhardt BC, Scholermann B, Kuhne L, Burckhardt G, & Steffgen J (2003). Basolateral localization of flounder Na^+-dicarboxylate cotransporter (fNaDC-3) in the kidney of Pleuronectes americanus. *Pflugers Arch* **446**, 578-584.

Hille B (1986). Ionic channels: molecular pores of excitable membranes. *Harvey Lect* **82**, 47-69.

Hillgren KM, Kato A, & Borchardt RT (1995). In vitro systems for studying intestinal drug absorption. *Med Res Rev* **15**, 83-109.

Ho HT, Ko BC, Cheung AK, Lam AK, Tam S, Chung SK, & Chung SS (2007). Generation and characterization of sodium-dicarboxylate cotransporter-deficient mice. *Kidney Int* **72**,63-71.

Hosoyamada M, Sekine T, Kanai Y, & Endou H (1999). Molecular cloning and functional expression of a multispecific organic anion transporter from human kidney. *Am J Physiol* **276**, F122-F128.

Hung AY & Sheng M (2002). PDZ domains: structural modules for protein complex assembly. *J Biol Chem* **277**, 5699-5702.

Hunte C, Screpanti E, Venturi M, Rimon A, Padan E, & Michel H (2005). Structure of a Na^+/H^+ antiporter and insights into mechanism of action and regulation by pH. *Nature* **435**, 1197-1202.

Inoue K, Zhuang L, & Ganapathy V (2002a). Human Na^+ -coupled citrate transporter: primary structure, genomic organization, and transport function. *Biochem Biophys Res Commun* **299**, 465-471.

Inoue K, Zhuang L, Maddox DM, Smith SB, & Ganapathy V (2002b). Structure, function, and expression pattern of a novel sodium-coupled citrate transporter (NaCT) cloned from mammalian brain. *J Biol Chem* **277**, 39469-39476.

Inoue K, Zhuang L, Maddox DM, Smith SB, & Ganapathy V (2003). Human sodium-coupled citrate transporter, the orthologue of *Drosophila Indy*, as a novel target for lithium action. *Biochem J* **374**, 21-26.

Inoue K, Fei YJ, Zhuang L, Gopal E, Miyauchi S, & Ganapathy V (2004). Functional features and genomic organization of mouse NaCT, a sodium-coupled transporter for tricarboxylic acid cycle intermediates. *Biochem J* **378**, 949-957.

Iwata S, Ostermeier C, Ludwig B, & Michel H (1995). Structure at 2.8 Å resolution of cytochrome c oxidase from Paracoccus denitrificans. *Nature* **376**, 660-669.

Javitch JA (1998). Probing structure of neurotransmitter transporters by substituted-cysteine accessibility method. *Methods Enzymol* **296**, 331-346.

Joshi AD & Pajor AM (2006). Role of conserved prolines in the structure and function of the Na^+/dicarboxylate cotransporter 1, NaDC1. *Biochemistry* **45**, 4231-4239.

Joshi AD & Pajor AM (2007). Topology model of the Na^+/dicarboxylate cotransporter 1. *FASEB J* **21**, A530 (Abstr.).

Kaback HR, Dunten R, Frillingos S, Venkatesan P, Kwaw I, Zhang W, & Ermolova N (2007). Site-directed alkylation and the alternating access model for LacY. *Proc Natl Acad Sci U S A* **104**, 491-494.

Kahn ES & Pajor AM (1999). Determinants of substrate and cation affinities in the Na^+/dicarboxylate cotransporter. *Biochemistry* **38**, 6151-6156.

Karlin A & Akabas MH (1998). Substituted-cysteine accessibility method. *Methods Enzymol* **293**, 123-145.

Kekuda R, Wang H, Huang W, Pajor AM, Leibach FH, Devoe LD, Prasad PD, & Ganapathy V (1999). Primary structure and functional characteristics of a mammalian sodium-coupled high affinity dicarboxylate transporter. *J Biol Chem* **274**, 3422-3429.

Kimelberg HK, O'Connor ER, Sankar P, & Keese C (1992). Methods for determination of cell volume in tissue culture. *Can J Physiol Pharmacol* **70 Suppl**, S323-S333.

King SC (2004). The "Transport Specificity Ratio": a structure-function tool to search the protein fold for loci that control transition state stability in membrane transport catalysis. *BMC Biochem* **5**, 16.

Kittanakom S, Cordat E, Akkarapatumwong V, Yenchitsomanus PT, & Reithmeier RA (2004). Trafficking defects of a novel autosomal recessive distal renal tubular acidosis mutant (S773P) of the human kidney anion exchanger (kAE1). *J Biol Chem* **279**, 40960-40971.

Kniazeff J, Loland CJ, Goldberg N, Quick M, Das S, Sitte HH, Javitch JA, & Gether U (2005). Intramolecular cross-linking in a bacterial homolog of mammalian SLC6 neurotransmitter transporters suggests an evolutionary conserved role of transmembrane segments 7 and 8. *Neuropharmacology* **49**, 715-723.

Kobayashi Y, Ohshiro N, Sakai R, Ohbayashi M, Kohyama N, & Yamamoto T (2005). Transport mechanism and substrate specificity of human organic anion transporter 2 (hOat2 [SLC22A7]). *J Pharm Pharmacol* **57**, 573-578.

Koepsell H & Endou H (2004). The SLC22 drug transporter family. *Pflugers Arch* **447**, 666-676.

Lakowski B & Hekimi S (1998). The genetics of caloric restriction in Caenorhabditis elegans. *Proc Natl Acad Sci U S A* **95**, 13091-13096.

Lee A, Beck L, & Markovich D (2000). The human renal sodium sulfate cotransporter (SLC13A1; hNaSi-1) cDNA and gene: organization, chromosomal localization, and functional characterization. *Genomics* **70**, 354-363.

Leighton BH, Seal RP, Watts SD, Skyba MO, & Amara SG (2006). Structural rearrangements at the translocation pore of the human glutamate transporter, EAAT1. *J Biol Chem* **281**, 29788-29796.

Levi M (2003). Role of PDZ domain-containing proteins and ERM proteins in regulation of renal function and dysfunction. *J Am Soc Nephrol* **14**, 1949-1951.

Levi M, McDonald LA, Preisig PA, & Alpern RJ (1991). Chronic K depletion stimulates rat renal brush-border membrane Na-citrate cotransporter. *Am J Physiol* **261**, F767-F773.

Li H & Pajor AM (2003). Mutagenesis of the N-glycosylation site of hNaSi-1 reduces transport activity. *Am J Physiol Cell Physiol* **285**, C1188-C1196.

Luecke H, Richter HT, & Lanyi JK (1998). Proton transfer pathways in bacteriorhodopsin at 2.3 angstrom resolution. *Science* **280**, 1934-1937.

Ma C, Kotaria R, Mayor JA, Remani S, Walters DE, & Kaplan RS (2005). The yeast mitochondrial citrate transport protein: characterization of transmembrane domain III residue involvement in substrate translocation. *J Biol Chem* **280**, 2331-2340.

Mann SS, Hart TC, Pettenati MJ, Von Kap-Herr C, & Holmes RP (1999). Assignment of the sodium-dependent dicarboxylate transporter gene (SLC13A2 alias NaDC-1) to human chromosome region 17p11.1-->q11.1 by radiation hybrid mapping and fluorescence in situ hybridization. *Cytogenet Cell Genet* **84**, 89-90.

Markovich D, Forgo J, Stange G, Biber J, & Murer H (1993). Expression cloning of rat renal Na^+/SO_4^{2-} cotransport. *Proc Natl Acad Sci U S A* **90**, 8073-8077.

Markovich D & Murer H (2004). The SLC13 gene family of sodium sulphate/carboxylate cotransporters. *Pflugers Arch* **447**, 594-602.

Markovich D, Regeer RR, Kunzelmann K, & Dawson PA (2005). Functional characterization and genomic organization of the human Na^+-sulfate cotransporter hNaS2 gene (SLC13A4). *Biochem Biophys Res Commun* **326**, 729-734.

Masoro EJ (2000). Caloric restriction and aging: an update. *Exp Gerontol* **35**, 299-305.

Miyazaki H, Anzai N, Ekaratanawong S, Sakata T, Shin HJ, Jutabha P, Hirata T, He X, Nonoguchi H, Tomita K, Kanai Y, & Endou H (2005). Modulation of renal apical organic anion transporter 4 function by two PDZ domain-containing proteins. *J Am Soc Nephrol* **16**, 3498-3506.

Moe OW (2003). Scaffolds: Orchestrating proteins to achieve concerted function. *Kidney Int* **64**, 1916-1917.

Mohana Rao JK & Argos P (1986). A conformational preference parameter to predict helices in integral membrane proteins. *Biochim Biophys Acta* **869**, 197-214.

Murakami S, Nakashima R, Yamashita E, & Yamaguchi A (2002). Crystal structure of bacterial multidrug efflux transporter AcrB. *Nature* **419**, 587-593.

Nakada T, Zandi-Nejad K, Kurita Y, Kudo H, Broumand V, Kwon CY, Mercado A, Mount DB, & Hirose S (2005). Roles of Slc13a1 and Slc26a1 sulfate transporters of eel kidney in sulfate homeostasis and osmoregulation in freshwater. *Am J Physiol Regul Integr Comp Physiol* **289**, R575-R585.

Nielsen S, Terris J, Andersen D, Ecelbarger C, Frokiaer J, Jonassen T, Marples D, Knepper MA, & Petersen JS (1997). Congestive heart failure in rats is associated with increased expression and targeting of aquaporin-2 water channel in collecting duct. *Proc Natl Acad Sci U S A* **94**, 5450-5455.

Nieth H & Schollmeyer P (1966). Substrate-utilization of the human kidney. *Nature* **209**, 1244-1245.

Noshiro R, Anzai N, Sakata T, Miyazaki H, Terada T, Shin HJ, He X, Miura D, Inui K, Kanai Y, & Endou H (2006). The PDZ domain protein PDZK1 interacts with human peptide transporter PEPT2 and enhances its transport activity. *Kidney Int* **70**, 275-282.

Oh DM & Amidon GL (1999). Overview of membrane transport. *Pharm Biotechnol* **12**, 1-27.

Okamoto N, Aruga S, Matsuzaki S, Takahashi S, Matsushita K, & Kitamura T (2007). Associations between renal sodium-citrate cotransporter (hNaDC-1) gene polymorphism and urinary citrate excretion in recurrent renal calcium stone formers and normal controls. *Int J Urol* **14**, 344-349.

Oshiro N & Pajor AM (2005). Functional characterization of high-affinity Na^+/dicarboxylate cotransporter found in Xenopus laevis kidney and heart. *Am J Physiol Cell Physiol* **289**, C1159-C1168.

Oshiro N & Pajor AM (2006). Ala-504 is a determinant of substrate binding affinity in the mouse Na^+/dicarboxylate cotransporter. *Biochim Biophys Acta* **1758**, 781-788.

Oshiro N, King SC, & Pajor AM (2006). Transmembrane helices 3 and 4 are involved in substrate recognition by the Na^+/dicarboxylate cotransporter, NaDC1. *Biochemistry* **45**, 2302-2310.

Pajor AM (1995). Sequence and functional characterization of a renal sodium/dicarboxylate cotransporter. *J Biol Chem* **270**, 5779-5785.

Pajor AM (1996). Molecular cloning and functional expression of a sodium-dicarboxylate cotransporter from human kidney. *Am J Physiol* **270**, F642-F648.

Pajor AM (1999b). Citrate transport by the kidney and intestine. *Seminars in Nephrology* **19**, 195-200.

Pajor AM (1999a). Sodium-coupled transporters for Krebs cycle intermediates. *Annu Rev Physiol* **61**, 663-682.

Pajor AM (2001). Conformationally sensitive residues in transmembrane domain 9 of the Na^+/dicarboxylate co-transporter. *J Biol Chem* **276**, 29961-29968.

Pajor AM (2006). Molecular properties of the SLC13 family of dicarboxylate and sulfate transporters. *Pflugers Arch* **451**, 597-605.

Pajor AM & Sun N (1996a). Characterization of the rabbit renal Na^+-dicarboxylate cotransporter using antifusion protein antibodies. *Am J Physiol* **271**, C1808-C1816.

Pajor AM & Sun N (1996b). Functional differences between rabbit and human Na^+-dicarboxylate cotransporters, NaDC-1 and hNaDC-1. *Am J Physiol* **271**, F1093-F1099.

Pajor AM, Hirayama BA, & Loo DD (1998a). Sodium and lithium interactions with the Na^+/Dicarboxylate cotransporter. *J Biol Chem* **273**, 18923-18929.

Pajor AM, Sun N, Bai L, Markovich D, & Sule P (1998b). The substrate recognition domain in the Na^+/dicarboxylate and Na^+/sulfate cotransporters is located in the carboxy-terminal portion of the protein. *Biochim Biophys Acta* **1370**, 98-106.

Pajor AM, Sun N, & Valmonte HG (1998c). Mutational analysis of histidine residues in the rabbit Na^+/dicarboxylate co-transporter NaDC-1. *Biochem J* **331**, 257-264.

Pajor AM & Sun N (1999). Protein kinase C-mediated regulation of the renal Na^+/dicarboxylate cotransporter, NaDC-1. *Biochim Biophys Acta* **1420**, 223-230.

Pajor AM, Krajewski SJ, Sun N, & Gangula R (1999). Cysteine residues in the Na^+/dicarboxylate co-transporter, NaDC-1. *Biochem J* **344**, 205-209.

Pajor AM & Sun NN (2000). Molecular cloning, chromosomal organization, and functional characterization of a sodium-dicarboxylate cotransporter from mouse kidney. *Am J Physiol Renal Physiol* **279**, F482-F490.

Pajor AM, Kahn ES, & Gangula R (2000). Role of cationic amino acids in the Na^+/dicarboxylate co-transporter NaDC-1. *Biochem J* **350**, 677-683.

Pajor AM, Gangula R, & Yao X (2001). Cloning and functional characterization of a high-affinity Na^+/dicarboxylate cotransporter from mouse brain. *Am J Physiol Cell Physiol* **280**, C1215-C1223.

Pajor AM & Randolph KM (2005). Conformationally sensitive residues in extracellular loop 5 of the Na^+/dicarboxylate co-transporter. *J Biol Chem* **280**, 18728-18735.

Pak CY (1991). Etiology and treatment of urolithiasis. *Am J Kidney Dis* **18**, 624-637.

Palczewski K, Kumasaka T, Hori T, Behnke CA, Motoshima H, Fox BA, Le T, I, Teller DC, Okada T, Stenkamp RE, Yamamoto M, & Miyano M (2000). Crystal structure of rhodopsin: A G protein-coupled receptor. *Science* **289**, 739-745.

Parent L, Supplisson S, Loo DD, & Wright EM (1992). Electrogenic properties of the cloned Na^+/glucose cotransporter: II. A transport model under nonrapid equilibrium conditions. *J Membr Biol* **125**, 63-79.

Persson B & Argos P (1996). Topology prediction of membrane proteins. *Protein Sci* **5**, 363-371.

Petzinger E & Geyer J (2006). Drug transporters in pharmacokinetics. *Naunyn Schmiedebergs Arch Pharmacol* **372**, 465-475.

Pritchard JB & Miller DS (1993). Mechanisms mediating renal secretion of organic anions and cations. *Physiol Rev* **73**, 765-796.

Pritchard JB, Sweet DH, Miller DS, & Walden R (1999). Mechanism of organic anion transport across the apical membrane of choroid plexus. *J Biol Chem* **274**, 33382-33387.

Quick M, Tomasevic J, & Wright EM (2003). Functional asymmetry of the human Na^+/glucose transporter (hSGLT1) in bacterial membrane vesicles. *Biochemistry* **42**, 9147-9152.

Ramond MJ, Martinot-Peignoux M, & Erlinger S (1985). Dome formation in the human colon carcinoma cell line Caco-2 in culture. Influence of ouabain and permeable supports. *Biol Cell* **54**, 89-92.

Rogina B, Reenan RA, Nilsen SP, & Helfand SL (2000). Extended life-span conferred by cotransporter gene mutations in Drosophila. *Science* **290**, 2137-2140.

Rudnick G (2006). Serotonin transporters - structure and function. *J Membr Biol* **213**, 101-110.

Sadee W, Drubbisch V, & Amidon GL (1995). Biology of membrane transport proteins. *Pharm Res* **12**, 1823-1837.

Saier MH, Jr. (1999). A functional-phylogenetic system for the classification of transport proteins. *J Cell Biochem* **Suppl 32-33**, 84-94.

Saier MH, Jr. (2000). A functional-phylogenetic classification system for transmembrane solute transporters. *Microbiol Mol Biol Rev* **64**, 354-411.

Sakhaee K, Alpern R, Poindexter J, & Pak CY (1992). Citraturic response to oral citric acid load. *J Urol* **147**, 975-976.

Sambuy Y, de A, I, Ranaldi G, Scarino ML, Stammati A, & Zucco F (2005). The Caco-2 cell line as a model of the intestinal barrier: influence of cell and culture-related factors on Caco-2 cell functional characteristics. *Cell Biol Toxicol* **21**, 1-26.

Seithel A, Karlsson J, Hilgendorf C, Bjorquist A, & Ungell AL (2006). Variability in mRNA expression of ABC- and SLC-transporters in human intestinal cells: Comparison between human segments and Caco-2 cells. *Eur J Pharm Sci* **28**, 291-299.

Sekine T, Cha SH, Hosoyamada M, Kanai Y, Watanabe N, Furuta Y, Fukuda K, Igarashi T, & Endou H (1998a). Cloning, functional characterization, and localization of a rat renal Na^+-dicarboxylate transporter. *Am J Physiol* **275**, F298-F305.

Sekine T, Cha SH, Tsuda M, Apiwattanakul N, Nakajima N, Kanai Y, & Endou H (1998b). Identification of multispecific organic anion transporter 2 expressed predominantly in the liver. *FEBS Lett* **429**, 179-182.

Sekine T, Miyazaki H, & Endou H (2006). Molecular physiology of renal organic anion transporters. *Am J Physiol Renal Physiol* **290**, F251-F261.

Selvin PR (2002). Principles and biophysical applications of lanthanide-based probes. *Annu Rev Biophys Biomol Struct* **31**, 275-302.

Shank RP & Bennett DJ (1993). 2-Oxoglutarate transport: a potential mechanism for regulating glutamate and tricarboxylic acid cycle intermediates in neurons. *Neurochem Res* **18**, 401-410.

Sheridan E, Rumrich G, & Ullrich KJ (1983). Reabsorption of dicarboxylic acids from the proximal convolution of rat kidney. *Pflugers Arch* **399**, 18-28.

Shlaifer I & Kanner BI (2007). Conformationally sensitive reactivity to permeant sulfhydryl reagents of cysteine residues engineered into helical hairpin 1 of the glutamate transporter GLT-1. *Mol Pharmacol* **71**, 1341-1348.

Steffgen J, Burckhardt BC, Langenberg C, Kuhne L, Muller GA, Burckhardt G, & Wolff NA (1999). Expression cloning and characterization of a novel sodium-dicarboxylate cotransporter from winter flounder kidney. *J Biol Chem* **274**, 20191-20196.

Stoll B, McNelly S, Buscher HP, & Haussinger D (1991). Functional hepatocyte heterogeneity in glutamate, aspartate and alpha-ketoglutarate uptake: a histoautoradiographical study. *Hepatology* **13**, 247-253.

Sun W, Wu RR, van Poelje PD, & Erion MD (2001). Isolation of a family of organic anion transporters from human liver and kidney. *Biochem Biophys Res Commun* **283**, 417-422.

Sweet DH, Chan LM, Walden R, Yang XP, Miller DS, & Pritchard JB (2003). Organic anion transporter 3 (Slc22a8) is a dicarboxylate exchanger indirectly coupled to the Na^+ gradient. *Am J Physiol Renal Physiol* **284**, F763-F769.

Toyoshima C, Nakasako M, Nomura H, & Ogawa H (2000). Crystal structure of the calcium pump of sarcoplasmic reticulum at 2.6 Å resolution. *Nature* **405**, 647-655.

Trauner M, Meier PJ, & Boyer JL (1998). Molecular pathogenesis of cholestasis. *N Engl J Med* **339**, 1217-1227.

Van Winkle LJ, Bussolati O, Gazzola G, McGiven J, Mackenzie B, Saier MH, Jr, Taylor PM, Rennie MJ, Low SY (1999). *Biomembrane Transport*. San Diego, CA, Academic Press.

Vandenberg RJ, Shaddick K, & Ju P (2007). Molecular basis for substrate discrimination by glycine transporters. *J Biol Chem* **282**,14447-14453.

Wadiche JI & Kavanaugh MP (1998). Macroscopic and microscopic properties of a cloned glutamate transporter/chloride channel. *J Neurosci* **18**, 7650-7661.

Wang H, Fei YJ, Kekuda R, Yang-Feng TL, Devoe LD, Leibach FH, Prasad PD, & Ganapathy V (2000). Structure, function, and genomic organization of human Na^+-dependent high-affinity dicarboxylate transporter. *Am J Physiol Cell Physiol* **278**, C1019-C1030.

Weerachayaphorn J & Pajor AM (2007). Sodium-dependent extracellular accessibility of LYS-84 in the sodium/dicarboxylate cotransporter. *J Biol Chem* **282**, 20213-20222.

Welsh MJ & Smith AE (1993). Molecular mechanisms of CFTR chloride channel dysfunction in cystic fibrosis. *Cell* **73**, 1251-1254.

Windus DW, Cohn DE, & Heifets M (1986). Effects of fasting on citrate transport by the brush-border membrane of rat kidney. *Am J Physiol* **251**, F678-F682.

Wolffram S, Bisang B, Grenacher B, & Scharrer E (1990). Transport of tri- and dicarboxylic acids across the intestinal brush border membrane of calves. *J Nutr* **120**, 767-774.

Wolffram S, Hagemann C, Grenacher B, & Scharrer E (1992). Characterization of the transport of tri- and dicarboxylates by pig intestinal brush-border membrane vesicles. *Comp Biochem Physiol Comp Physiol* **101**, 759-767.

Wolffram S, Zimmermann W, & Scharrer E (1993). Transport of tricarballylate by intestinal brush-border membrane vesicles from steers. *Exp Physiol* **78**, 473-484.

Wolffram S, Unternahrer R, Grenacher B, & Scharrer E (1994). Transport of citrate across the brush border and basolateral membrane of rat small intestine. *Comp Biochem Physiol* **109A**, 39-52.

Wolin CD & Kaback HR (2000). Thiol cross-linking of transmembrane domains IV and V in the lactose permease of *Escherichia coli*. *Biochemistry* **39**, 6130-6135.

Wong KF, Selzer T, Benkovic SJ, & Hammes-Schiffer S (2005). Impact of distal mutations on the network of coupled motions correlated to hydride transfer in dihydrofolate reductase. *Proc Natl Acad Sci U S A* **102**, 6807-6812.

Wright EM, Wright SH, Hirayama B, & Kippen I (1982). Interactions between lithium and renal transport of Krebs cycle intermediates. *Proc Natl Acad Sci U S A* **79**, 7514-7517.

Wright SH & Dantzler WH (2004). Molecular and cellular physiology of renal organic cation and anion transport. *Physiol Rev* **84**, 987-1049.

Wright SH, Hirayama B, Kaunitz JD, Kippen I, & Wright EM (1983). Kinetics of sodium succinate cotransport across renal brush-border membranes. *J Biol Chem* **258**, 5456-5462.

Xie Z, Turk E, & Wright EM (2000). Characterization of the Vibrio parahaemolyticus Na^+/Glucose cotransporter. A bacterial member of the sodium/glucose transporter (SGLT) family. *J Biol Chem* **275**, 25959-25964.

Yamashita A, Singh SK, Kawate T, Jin Y, & Gouaux E (2005). Crystal structure of a bacterial homologue of Na^+/Cl^--dependent neurotransmitter transporters. *Nature* **437**, 215-223.

Yao X & Pajor AM (2000). The transport properties of the human renal Na^+-dicarboxylate cotransporter under voltage-clamp conditions. *Am J Physiol Renal Physiol* **279**, F54-F64.

Yao X & Pajor AM (2002). Arginine-349 and aspartate-373 of the Na^+/dicarboxylate cotransporter are conformationally sensitive residues. *Biochemistry* **41**, 1083-1090.

Yernool D, Boudker O, Jin Y, & Gouaux E (2004). Structure of a glutamate transporter homologue from Pyrococcus horikoshii. *Nature* **431**, 811-818.

Zhang FF & Pajor AM (2001). Topology of the Na^+/dicarboxylate cotransporter: the N-terminus and hydrophilic loop 4 are located intracellularly. *Biochim Biophys Acta* **1511**, 80-89.

Zhang YW & Rudnick G (2006). The cytoplasmic substrate permeation pathway of serotonin transporter. *J Biol Chem* **281**, 36213-36220.

Zimmerli B, O'Neill B, & Meier PJ (1992). Identification of sodium-dependent and sodium-independent dicarboxylate transport systems in rat liver basolateral membrane vesicles. *Pflugers Arch* **421**, 329-335.

Zomot E, Zhou Y, & Kanner BI (2005). Proximity of transmembrane domains 1 and 3 of the gamma-aminobutyric acid transporter GAT-1 inferred from paired cysteine mutagenesis. *J Biol Chem* **280**, 25512-25516.

VITA

Jittima Weerachayaphorn was born to Kamol and Wanna Weerachayaphorn in Bangkok, Thailand on October 6th, 1972. She graduated from Mahidol University at Bangkok, Thailand in 1995 with the first class honor Bachelor's degree in Nursing Science. After graduating and working in the medical intensive care unit at Ramathibodi hospital, Bangkok for three years, she continued to join the Master program in Physiology at Mahidol University. In 2003, she subsequently matriculated in the Cellular Physiology and Molecular Biophysics graduate program at the University of Texas Medical Branch. During her graduate training at UTMB, Jittima was awarded the student Travel Award for Gordon Research Conference in 2004 and Student Award for the American Physiological Society in 2007.

Jittima can be contacted through her parents at 31 Indamara 16, Sutthisarn Rd. Samsennai, Phayathai, Bangkok, 10400, Thailand.

Education

B.Sc. (Nursing), February 1995, Mahidol University, Bangkok, Thailand
M.Sc. (Physiology), December 2001, the Mahidol University, Bangkok, Thailand

Publications

Weerachayaphorn J and Pajor AM (2007). Sodium-dependent extracellular accessibility of Lys-84 in the sodium/dicarboxylate cotransporter. *J Biol Chem* **282**, 20213-20222.

Weerachayaphorn J and Pajor A.M. Threonine-509 is a determinant of both substrate and cation affinity in the human Na^+/dicarboxylate cotransporter. (Submitted to *Biochemistry*)

Weerachayaphorn J and Pajor AM. Identification of transport pathway for citric acid cycle intermediates in the human colon carcinoma cell line, Caco-2 cells. (Manuscript in preparation)

Abstracts

Weerachayaphorn J and Pajor AM (2007). Substituted Cysteine Accessibility of the External Half of Transmembrane Helix 3 of the Na^+/dicarboxylate Cotransporter. *FASEB J* **21** (5): A530. Experimental Biology 2005 and 37th International Congress of Physiological Sciences, Washington DC, 2007

Weerachayaphorn J and Pajor AM (2005). Na^+-dependent and -independent transport of succinate and citrate in the Caco-2 cell line. *FASEB J* **19** (4) Part 1 Suppl.: A748. Experimental Biology 2005 and 35th International Congress of Physiological Sciences, San Diego, 2005

Weerachayaphorn J and Pajor AM (2004). Identification of transport pathway for citric acid cycle intermediates in the human colon carcinoma cell line, Caco-2 cells. Gordon Research Conference on Membrane Transport Proteins, Les Diablerets, Switzerland, 2004

Weerachayaphorn J, Chuncharunee A, Suksamrarn A, and Piyachaturawat P (2002). Anti-hepatotoxic activity of *Curcuma comosa* against CCl_4-induced hepatotoxicity in mice. The 31st Annual meeting of The Physiological Society of Thailand, Petchaburi, Thailand, 2002

Weerachayaphorn J, Chuncharunee A, Suksamrarn A, and Piyachaturawat P (2001). Effect of *Curcuma comosa* Roxb. on bone mineral content in osteopenic mice. The 30th Annual meeting of The Physiological Society of Thailand, Songkla, Thailand, 2001